Quantum Chemical Studies of Radical-Containing Enzymes

Fahmi Himo*,† and Per E. M. Siegbahn*,‡

Theoretical Chemistry, Department of Biotechnology, Royal Institute of Technology, SCFAB, SE-106 91 Stockholm, Sweden, and Department of Physics, Stockholm University, SCFAB, SE-106 91 Stockholm, Sweden

Received September 3, 2002

Contents

Fahmi Himo was born in 1973. He did his undergraduate studies in physics at Stockholm University, where he also received his Ph.D. degree in 2000 (with Leif A. Eriksson and Per E. M. Siegbahn). He then spent two years as a Wenner-Gren postdoctoral fellow at The Scripps Research Institute in La Jolla working with Louis Noodleman and David A. Case. Currently, he is assistant professor at the Royal Institute of Technology in Stockholm. His main research interests are in the areas of enzymatic and organometallic catalysis.

Per E. M. Siegbahn was born in Stockholm, Sweden. He did his undergraduate studies at Uppsala University and received his Ph.D. degree at Stockholm University, in 1973 (with Björn Roos). He was a postdoctoral fellow at the University of California, Berkeley (with Henry F. Schaefer III) and at IBM, San Jose (with Bowen Liu). He returned to Stockholm University, where he became full professor in quantum chemistry (1983) and has remained ever since. His interests have varied over the years from the development of ab initio quantum chemical methods, to the applications on gas-phase reactions of small molecules, to models of heterogeneous catalysts, to the present interest in mechanisms for redox-active enzymes.

I. Introduction

For at least 20 years, high-accuracy quantum chemistry has been an indispensable tool for analyzing mechanisms of chemical reactions. The calculated energetics can often be enough to rule out or allow a suggested mechanism. For small- and medium-sized systems, where the accuracy achievable is very high, mechanisms are now seldom accepted without support from calculations. One of the most useful aspects of quantum chemical methods is that short-lived

† Royal Institute of Technology.
‡ Stockholm University.

10.1021/cr020436s CCC: $44.00
Published on Web 04/12/2003

species are treated with equal ease and accuracy as long-lived ones. This means, for example, that it is possible to obtain structures and energies for transition states for chemical reactions. It is also possible to obtain information about radicals, which is the theme of this review. The main drawback is that the systems studied experimentally may be too large for a quantum chemical treatment. There are two ways to attack this problem. First, the methods are improved to treat larger and larger systems. Second, and perhaps even more important, useful small models are developed for the large real systems. However, models are never exact, and a very important part of a quantum chemical study is therefore not only to select a good chemical model but also to understand the limitations of it. Since the area of high-accuracy quantum chemical applications for redox-active systems in biology is not much more than 5 years old, there are still large improvements to be made. The best way to obtain progress is to match experimental observations with results from quantum chemical model studies, which will be beneficial both for the understanding of the enzymatic reactions and for the improved use of quantum chemistry in this area. In the present review, examples will be given where the chemical models have had to be revised in the confrontation with experimental facts, but also examples where the initial experimental suggestions have had to be abandoned because they do not fulfill the energetic criteria provided by the calculations.

In the quantum chemical studies discussed in this review, density functional theory (DFT) methods are used throughout.[1] The reason for this is the high efficiency of these methods for large systems. The insufficient accuracy for treating chemical reactions was for a long time a problem with these methods, but a breakthrough came about a decade ago.[2] The key to the increased accuracy of these methods was the incorporation of terms in the functionals that depend on the gradient of the density. This was primarily important for the description of the exchange energy,[3] much less so for the correlation energy.[4] Incorporation of exact exchange and a few semiempirical parameters were also significant in this context.[5] Benchmark calculations showed that when these so-called hybrid functionals, particularly the B3LYP functional, were used, results almost as accurate as those obtained from the most accurate ab initio methods could be obtained at a fraction of the cost. For benchmark tests, which have gradually included more and more systems, the hybrid DFT methods have been shown to give energies normally within a few kilocalories/mole of essentially exact experiments. Even though this accuracy is surprisingly high, it must still be remembered that it cannot be expected that the error in a calculated barrier for an enzyme-catalyzed reaction should be less than 3−5 kcal/mol. Essentially all calculations discussed here for radical enzyme reactions have used the B3LYP functional. In many of the calculations, the enzyme environment has been described by a continuum dielectric medium with a dielectric constant equal to 4. In some models, some atoms have furthermore been fixed from their positions in X-ray structures. This will be pointed out explicitly in the text. Recent reviews give more details on these methods in the context of applications on enzymes.[6−9]

Scheme 1. Reaction Catalyzed by Ribonucleotide Reductase

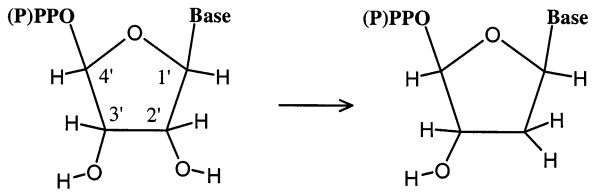

Ribonucleotide Deoxyribonucleotide

The present review will attempt to cover most of what has been done using accurate quantum chemical methods on mechanisms of radical enzymes. The radical enzymes reviewed here are those in which amino acid or cofactor radicals have been found. Only the most essential experimental background is given, since this can be found in other papers of this issue. The first enzyme discussed is ribonucleotide reductase (RNR), since this was the first enzyme where an amino acid derived radical was found, a tyrosyl radical in class I RNR.[10] It is also one of the enzymes most studied by quantum chemical methods. In class III RNR, a glycyl radical has been found. Other glycyl radical enzymes are discussed in the following section. In prostaglandin H synthase, discussed after that, a tyrosyl radical is essential for catalysis. B_{12}-dependent enzymes, which work by an adenosyl radical, are discussed next. In photosystem II, two different tyrosyl radicals have been found. An oxygen-derived ligand radical on the water-oxidizing complex has also been suggested. Galactose oxidase has a tyrosyl radical covalently linked to a cysteine, while in copper-dependent amine oxidases a radical form of the topa quinone cofactor has been implicated. The last three enzymes discussed, cytochrome *c* peroxidase, cytochrome P450, and cytochrome *c* oxidase, all contain a heme cofactor, which by reaction with dioxygen forms compound I, which has an Fe(IV) and an organic radical. In cytochrome *c* peroxidase this radical is a tryptophan cation and in P450 it is a porphyrin cation, while in cytochrome *c* oxidase it has been suggested to be a tyrosyl.

II. Ribonucleotide Reductase

The first functionally important amino acid radical found in an enzyme was the tyrosyl radical in class I ribonucleotide reductase (RNR),[10] which catalyzes the transformation shown in Scheme 1, in which a ribonucleotide is converted into a 2′-deoxyribonucleotide.[11] There are three classes of RNR with the common property that they function via a free radical mechanism but differ in the way this radical is generated.[12−15] Class I RNR requires iron and oxygen for its tyrosyl radical generation. Class II RNR has adenosylcobalamin as its radical generator and functions independently of oxygen. The class III enzyme has an iron−sulfur cluster that is required for the

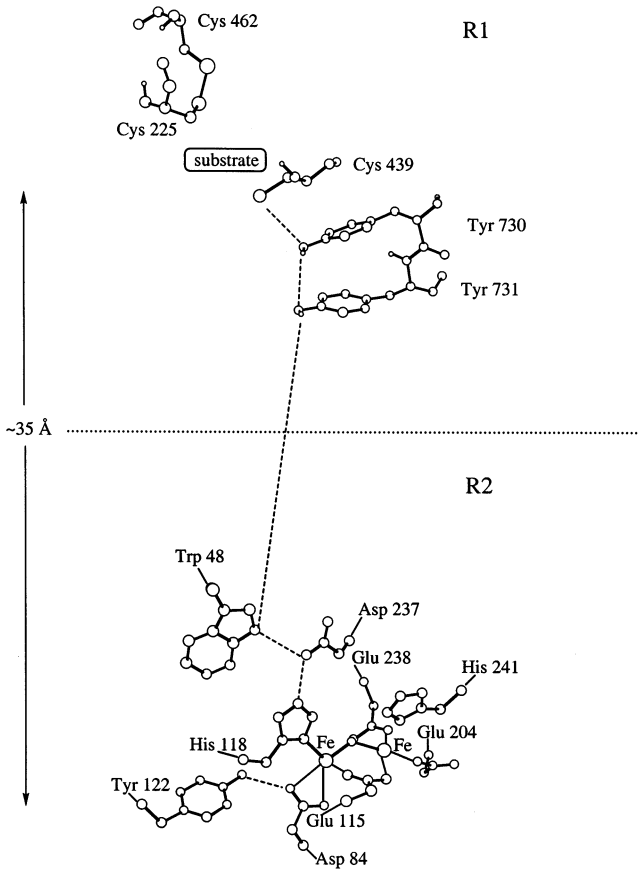

Figure 1. Conserved residues participating in the proposed hydrogen-bonded long-range transfer chain between the substrate site in protein R1 and the tyrosyl radical in protein R2 of *E. coli* ribonucleotide reductase (RNR). The dashed lines indicate possible hydrogen bonds in the crystal structures of the proteins.

generation of its glycyl radical and does not function under aerobic conditions.

A. Class I RNR

The class I RNR is composed of two proteins, R1 and R2, for which X-ray structures have been determined. R2 was determined by Nordlund et al.[16] and R1 by Uhlin and Eklund.[17] More recently, the structure of R1 including a substrate was also determined, by Eriksson et al.[18] A tentatively combined R1 and R2 structure, showing a suggested hydrogen-bonded chain[14,19] connecting the tyrosyl radical in R2 with the active site in R1, is shown in Figure 1.

The mechanism for the class I RNR can be briefly described in the following way. The O−O bond of an oxygen molecule is cleaved by the Fe_2(II,II) dimer complex in R2. The first intermediate observed after the O−O cleavage is termed **X**, which has been spectroscopically characterized as an Fe_2(IV,III) dimer.[20] In the next step, a proton and an electron are abstracted from a tyrosine, Tyr122, close to the iron dimer to create a neutral tyrosyl radical[10] and a resting Fe(III,III) dimer. The enzyme is now prepared for catalysis, which starts by a docking of the R1 and R2 proteins and a binding of the ribonucleotide at the substrate site in R1. The distance between the tyrosyl radical in R2 and the substrate site in R1 is more than 30 Å (see Figure 1). The substrate reac-

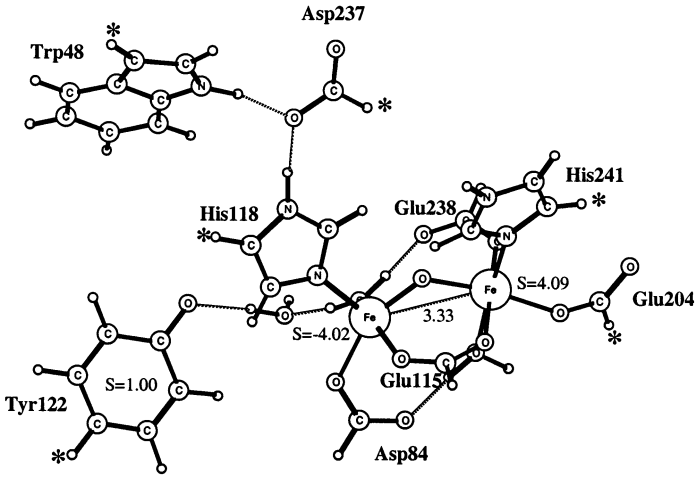

Figure 2. Optimized structure for the resting diferric state of RNR. Important spins are marked. The atoms marked with ∗ are fixed from the X-ray structure.

tions at R1 are initiated by a radical transfer from Tyr122 to Cys439 at the substrate site. The reduction of the ribonucleotide is then catalyzed by the Cys439 radical in five to seven steps. When the deoxyribonucleotide has been formed, there is a radical transfer back from Cys439 to Tyr122, and the catalytic cycle is closed. One tyrosyl radical can be active in a few hundred cycles.

All the different steps in the class I RNR mechanism have been studied using the B3LYP functional.[21−27] Some of these results, the ones involving the iron dimer, have been reviewed recently[9] and will therefore be only briefly described here. Instead, the present review will focus on the substrate reactions in R1.

In recent studies of the iron dimer region of RNR, the model in Figure 2 of about 80 atoms was used. Close to 100 different structures were optimized in order to investigate both tyrosyl radical formation and initiation of radical transfer. A preliminary analysis of the energies of the different structures optimized so far suggests the following mechanism for tyrosyl radical formation. The first part of this mechanism is the cleavage of the O−O bond. Dioxygen binds to the diferrous iron dimer to form a diferric peroxide state. As the O−O bond is cleaved, an electron is transferred from Trp48 and an Fe_2(III,IV) product is formed. At this stage an electron comes in from the outside to the Trp48 cationic radical and a proton is simultaneously drawn to the iron dimer complex. The proton is suggested to end up at a bridging μ-oxo ligand. The product formed is proposed to be compound **X** (see above). To create the Tyr122 radical from this structure requires an electron and a proton transfer from the tyrosine. To obtain a reasonably low barrier for this process, a water molecule was suggested to enter between Tyr122 and the iron-bound water ligand. By two concerted proton transfers, Tyr122 becomes deprotonated and Asp84 protonated. The proton is finally transferred to a bridging hydroxide through a relatively large motion of Asp84. Simultaneously, an electron is transferred from tyrosine to iron. The creation of the tyrosyl radical from compound **X** is strongly exothermic by

15 kcal/mol, which can explain how it can be stable over very long periods.[10] The structure of the product is in good agreement with the X-ray structure of the resting diferric state.[16]

From the energies of the optimized structures, a pathway can also be suggested for the initiation of the radical transfer. As mentioned above, the radical transfer should occur between Tyr122 in R2 and Cys439 in R1. The first step in this transfer is probably the transfer between Tyr122 and another tyrosine, in the region above Asp237 and Trp48 (see Figure 2). This region is not resolved in the X-ray structure, but a plausible candidate for this tyrosine is Tyr356. In the preliminary suggested mechanism a proton is first added to the iron dimer before the radical is transferred, placed at the bridging μ-oxo ligand, which is the most stable position of the complex. A possibility is that this proton enters the iron dimer region as R1 and R2 docks. Sending in a proton to the iron dimer at this stage transforms the Tyr122 from a very stable radical, as is observed for the resting diferric state, into a quite unstable radical, which is needed to initiate catalysis. Once the added proton is in place, a proton from the iron-bound water, and an electron from Trp48 can be transferred to Tyr122 at a low cost of only 3.9 kcal/mol. From this point, a proton and an electron are transferred from Tyr356 to the nearby Asp237 and Trp48 in a fast and almost thermoneutral step. A minor rearrangement of the iron complex is then all what is needed to complete the radical transfer initiation.

After the radical has been transferred from Tyr122 to Tyr356, B3LYP studies have suggested that the Cys439 radical formation occurs by a sequence of hydrogen atom transfer steps.[23] To move the radical over such a long distance as 30 Å, intermediates are required. A key point for the radical transfer is that these intermediates must be energetically accessible by the neutral Tyr122 radical. This limits the possible intermediates in RNR to neutral tyrosyl radicals, neutral cysteinyl radicals, and tryptophan radicals. Cationic tyrosyl radicals are not accessible, which means that electron transfer between tyrosines has to be accompanied by deprotonations of the donating groups and protonations of the accepting radicals. The simplest way to achieve this is to use a hydrogen atom transfer mechanism, where both an electron and a proton are transferred (see Figure 3). The alternative would be to accompany the electron transfer by a deprotonation to a local base, but there are no indications from the X-ray structure that such bases exist. In the B3LYP study, hydrogen atom transfer transition states between tyrosyl and tyrosine and between tyrosyl and cysteine were located. The barriers were found to be very low with 4.9 and 8.1 kcal/mol, respectively, corresponding to rates of 10^9 and 10^7 s^{-1}. Hydrogen atom transfer is therefore certainly a feasible radical transfer mechanism in RNR.

A detailed picture of the substrate region in R1 is shown in Figure 4. As seen in this figure, the ribonucleotide is bound by hydrogen bonds to its hydroxyl oxygen atoms. These hydrogen bonds are

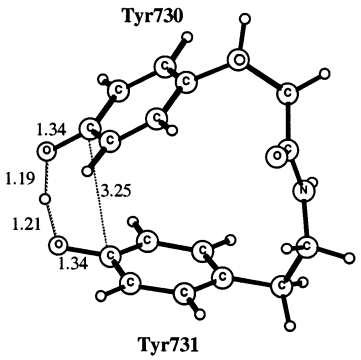

Figure 3. Optimized transition state structure for hydrogen atom transfer between a tyrosine and a neutral tyrosyl radical.

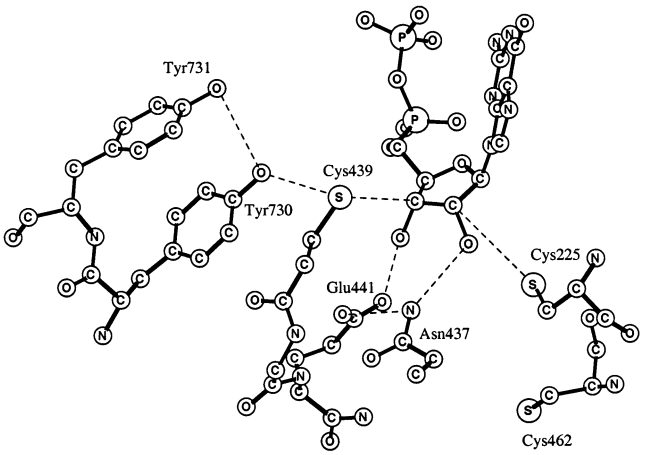

Figure 4. X-ray structure of the substrate region of the R1 subunit of *E. coli* RNR.

formed to Glu441 at the C3′-oxygen and to a combination of Glu441 and Asn437 at the C2′-oxygen. The binding of the substrate ribonucleotide and the creation of the Cys439 radical[15] constitute the starting point for the substrate reactions, which end by the formation of the deoxyribonucleotide and the recreation of the Cys439 radical. In this process a water molecule is lost and a disulfide bond is formed between two other essential cysteines, Cys225 and Cys462.

In recent years there has been substantial experimental progress in the understanding at a molecular level of the different steps of the substrate reactions of RNR. From isotopic labeling, kinetic, spectroscopic, and site-directed mutagenesis experiments, and also theoretical calculations, a reaction mechanism has been suggested by Stubbe et al.[15,28,29] Successively new findings have revised the mechanism several times and the most recent version is shown in Scheme 2.

In the first step a hydrogen atom from C3′ of the ribonucleotide substrate is abstracted by the Cys439 radical. In the second step, a proton is abstracted by the C2′-hydroxyl of the substrate from a cysteine, plausibly from Cys225, leading to formation of a water molecule. Simultaneously, suggested by theoretical studies,[30] the initial carboxylate anion of Glu441 abstracts a proton from the C3′-hydroxyl group. This leaves the substrate as a neutral radical species and the cysteine as an anion after step 2.

Scheme 2. Reaction Mechanism for Class I RNR Suggested on the Basis of Experiments and Calculations

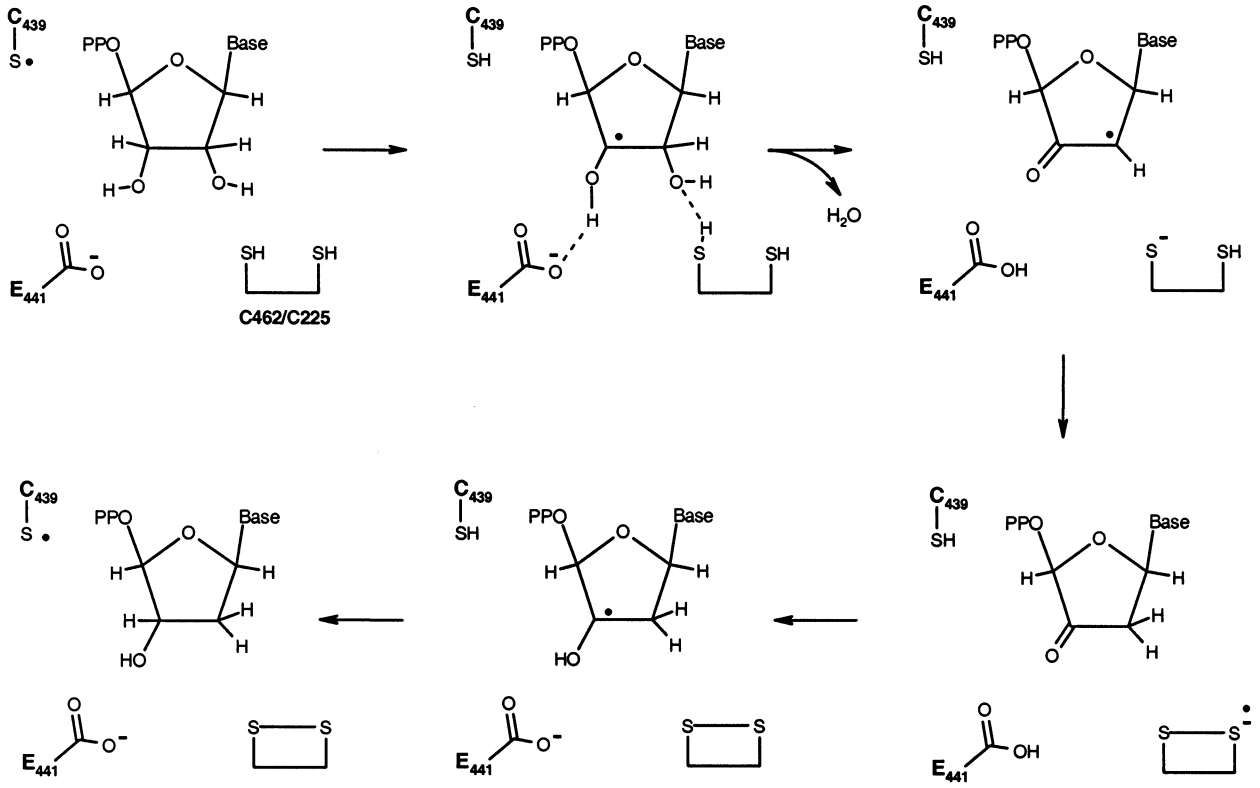

Alternatively, mechanisms involving either a radical cation or radical anion have been invoked for this step, suggested by results for model systems.[31,32] In the third step, a hydrogen atom is abstracted by C2′ of the substrate from a cysteine, and the two cysteines (Cys225 and Cys462) form a disulfide anion. In the fourth step, the substrate abstracts an electron from the disulfide anion and a proton from Glu441 to form a hydroxyl at C3′. Finally, the C3′-radical can in the fifth step reabstract a hydrogen atom from Cys439 to complete the formation of the deoxyribonucleotide product.

The substrate reaction mechanism of RNR has been studied theoretically using the B3LYP functional, initially leading to a somewhat different reaction sequence.[21] It was found that the most reasonable energetics was obtained if a protonated Glu441 was used as a starting point for the catalytic cycle. In the suggested first step, a hydrogen atom is abstracted by Cys439 from C3′, as in the experimentally suggested scheme. This abstraction is assisted by the presence of the Glu441 and Asn437 residues, which initiate the transfer of a hydrogen from the C3′-OH group to the C2′-OH. The completion of this transfer, leading to formation of a water molecule, occurs in the second step. Since the proton was assumed to be available at Glu441, this water formation was thus suggested to occur by a different mechanism than the one assumed in Scheme 2, where a cysteine residue was proposed to be involved. At the end of the second step, an oxaallylic radical is formed. In the third step, a hydrogen atom is abstracted by C2′ from Cys225, leading to a stable species with a keto group, which is the resting state for the remaining steps of the cycle. To find a mechanism with a reasonable barrier for the fourth step turned out to be very difficult. The mechanism with the lowest barrier found was one where the Cys225 group attacks the C3′ center of the ribose ring. This was suggested to occur by a simultaneous formation of a C−S and an O−H bond at the C3′ keto group. A cyclic transition state was proposed, including apart from Cys225 also Glu441 and a water molecule in a ring, and Asn437 outside the ring. In the fifth step, the disulfide bond between Cys225 and Cys462 is formed, assisted by the presence of Glu441 and Asn437. In the final sixth step, the deoxyribonucleotide should be formed in essentially the reverse of the first step, as proposed also in Scheme 2.

The suggested theoretical mechanism gives an energetic rationalization for the following experimental observations. First, and most importantly, the results show that the most probable rate-limiting step of the substrate steps is the reprotonation of the C3′ oxygen, which is also accompanied by an electron transfer. A key role of Glu441 in this step is demonstrated, which explains why the reaction is halted at this point if this amino acid is mutated into a glutamine.[33] A role of Glu441 is also given for the water-formation step, in agreement with the same mutation experiments. The picture given of the calculated energetics is furthermore in agreement with information from experiments concerning the overall rate and the presence of different intermediates. However, the suggested mechanism suffers from the drawback that Glu441 starts out protonated, which may not be very likely. With a reasonable pK_a of about 4 for Glu441, the cost to protonate this residue from the outside is not excessive (about 4 kcal/mol), but enzyme active sites are normally not

Scheme 3. Reaction Mechanism for Class I RNR Investigated by Recent B3LYP Calculations

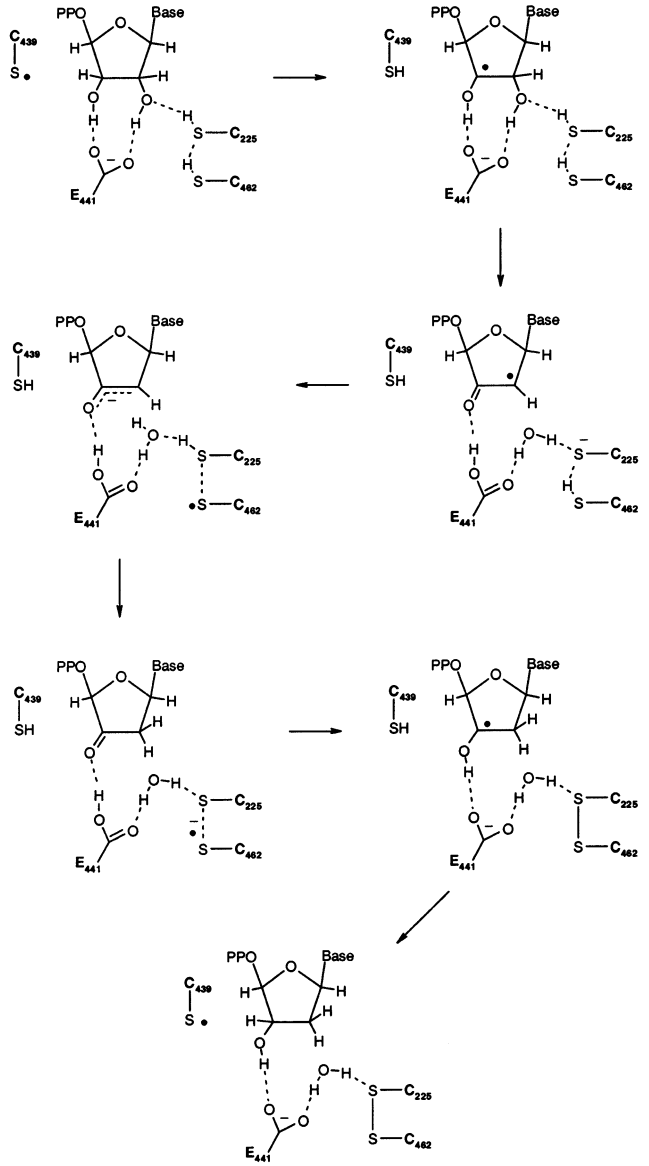

constructed in a way where a proton has to be fetched from a place outside the catalytic site. In a more recent study,[25] a more severe problem with the suggested mechanism was discovered. In the mechanism, Cys225 was given a very flexible role, being able to form a C−S bond to the C3′ carbon. If this flexibility of the enzyme peptide is allowed, it is difficult to rule out an attack also on the C4′ carbon by Cys225. However, calculations show that if the Cys225 radical is allowed to abstract the hydrogen at C4′, a very deep minimum is reached that would halt catalysis. It therefore had to be concluded that Cys225 must be held very firmly in its position by the peptide, and the formation of the C−S bond to C3′ is therefore quite unlikely.

Very recently, new calculations were performed by Pelmenschikov et al.[34] in order to investigate the above-mentioned problems. In the model used, Glu441 starts out unprotonated and the catalytic residues were restricted in their flexibility by fixing the position of one atom for each residue from the X-ray structure. The mechanism investigated by these

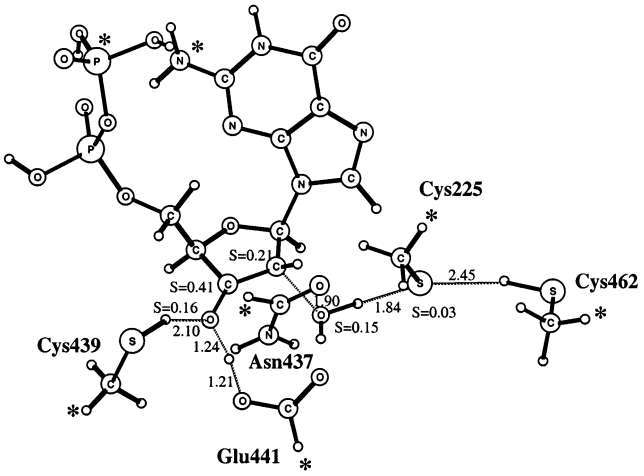

Figure 5. Transition state for water formation in class I RNR. Atoms marked with ∗ were fixed from the X-ray structure.

calculations is shown in Scheme 3 and the model used in Figure 5. As seen in Scheme 3, the mechanism is quite similar to the one in Scheme 2.

Two of the transition states in Scheme 3 will be described here. The first one of these is shown in Figure 5 and describes the water-formation step. When Glu441 is unprotonated, the proton needed to make water obviously has to be taken from another place and Cys225 appears most likely from the enzyme structure. However, Glu441 still plays a major role in this step by abstracting the hydroxyl proton at C3′. In fact, if the proton transfer to Glu441 was prevented, a very high barrier for proton abstraction from Cys225 was found. It is furthermore interesting to note that the computed barrier for water formation is actually higher than the one found for the older model where Glu441 was protonated from the beginning. However, this does not affect the overall rate, since this step is still not rate-limiting.

The second transition state discussed here was found for the rate-limiting step and is shown in Figure 6. This is a quite remarkable transition state that is not similar to any one obtained previously by model calculations. The most unusual aspect of this TS is that a quite long range electron transfer occurs. There are two processes structurally separated by 6−7 Å in the TS, proton transfer from Glu441 to the substrate and S−S bond formation, that require electron transfer from Cys225 to the substrate. It is far from obvious that the methods used would be capable of correctly describing this type of TS. In fact, long-range ET is commonly regarded as out of reach for normal quantum chemical methods requiring special methods where the coordinates of the transferred electron are treated separately.[35] Still, after a considerable effort the TS was located and the computed Hessian showed an imaginary frequency of 270 cm^{-1}. The most interesting electronic feature of this TS is a substantial spin delocalization with spin populations of 0.33 and 0.35 on the two sulfurs forming the bond and with 0.30 on the substrate, mostly located at C3′, even though these atoms are separated by 6−7 Å. The analysis of the mechanism for this step is still in progress and an interesting

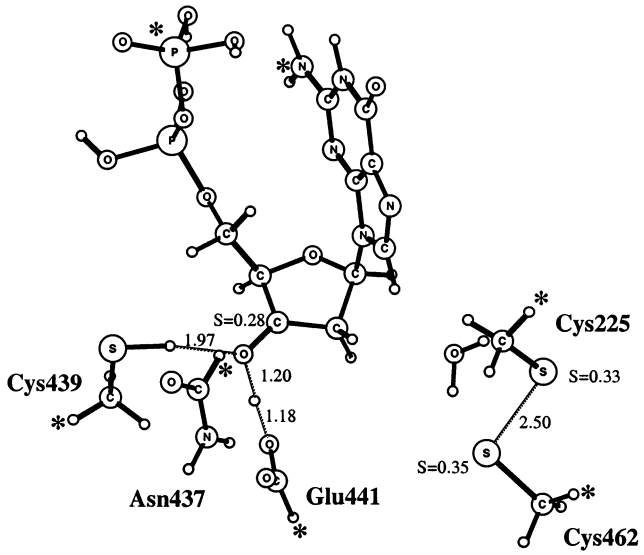

Figure 6. Transition state for the reprotonation of the C3′ oxygen and disulfide formation in class I RNR. Atoms marked with ∗ were fixed from the X-ray structure.

point to be investigated is, for example, whether the water molecule in the model plays a role in the electron transfer.

B. Class III RNR

The X-ray structure of the active site for the anaerobic class III RNR shows that there are only two active site cysteines, Cys290 and Cys79, corresponding to Cys439 and Cys225 of class I RNR.[36] Since there is no cysteine corresponding to Cys462, no disulfide bridge can be formed. The two electrons needed for catalysis are instead taken from a formate reductant, which leads to CO_2 production as the electrons are delivered to the substrate. Two additional residues proposed to be important for the catalytic mechanism in the class I RNR are missing in class III, Glu441 and Asn437, which are replaced by Met288 and Ser292 in class III. Clearly, the catalytic mechanisms in the two classes have to differ at some point. The glycyl radical produced by the iron−sulfur cluster is located close to Cys290 at the active site, and no long-range radical transfer is therefore needed as in class I RNR.

The substrate mechanism for anaerobic RNR has been studied using the B3LYP functional.[37] To use the experience gained from the class I study, the first approach was made as similar as possible to that one and the formate reductant was therefore placed at the position of the missing glutamate of class I RNR. Following the class I study, the formate was protonated. The choice of formic acid rather than formate as a model was also made because both a proton and a formate are needed in the mechanism at some stage. This makes the class III mechanism fundamentally different from the one of class I, where the protons needed can be supplied by the two cysteines forming the disulfide bond. The addition of a proton is therefore a requirement for any viable class III mechanism, such as the structure-based mechanism of Eklund and Fontecave.[38] The question is only where the required proton should be placed. Since it is also required that it is easily accessible by the 3′-keto group and since the formate is suggested to be in this region, a protonation of the formate appears as the simplest possibility. The role of the formate was therefore proposed to be 2-fold in class III RNR: it replaces the function of Glu441 as a hydrogen-bonding partner to the substrate, and it acts as a two-electron donor for the reaction. With a formic acid present, the first steps up to and including the step where the stable keto group has been formed (step 3) could be suggested to be essentially the same as the ones for the class I enzyme. The main difference is that the asparagine corresponding to Asn437 is missing in the anaerobic case, which only slightly modifies the energetics.

The suggested mechanisms for class I and III mainly differ after the substrate keto group has been formed. Since this form of the substrate is so stable, the rate-limiting steps of the substrate reactions of both classes are found when proceeding beyond this point. In the suggested class III mechanism the first step at this point is to create a formyl radical by removing the C-hydrogen. This was suggested to occur by a hydrogen atom abstraction by the Cys79 radical and was found to be endothermic by 9.7 kcal/mol. The computed barrier for this step was 14.2 kcal/mol. An important question in this context is how a formyl radical can exist in the enzyme without causing damage. This question is partly answered by the calculations, which show that the formyl radical only exists in an unstable state 10 kcal/mol above the stable Cys79 radical. This means that the formyl radical can only possibly cause damage if it is involved in reactions with higher exothermicities than 10 kcal/mol. As a further protection of the formyl radical, it is strongly hydrogen-bonded by about 10 kcal/mol. This bond has to be broken if the radical should migrate away to another region, which would thus require traversing an energy barrier about 20 kcal/mol above the Cys79 radical. This should prevent harmful reactions, since the rate-limiting barrier for the substrate reactions is only 17 kcal/mol.

When the formyl radical has been created, the next step is the attack by the radical on the stable keto form of the substrate. This reaction can be described as a hydrogen atom (proton and electron) transfer to the C3′ oxo group with a simultaneous formation of carbon dioxide. This was found to be the rate-limiting step of the mechanism with a TS that is calculated to be 19.9 kcal/mol above the resting state. The product is 2.5 kcal/mol below the resting state. The only step remaining in the catalytic cycle is then the recreation of the Cys290 radical, which is found to be substantially exergonic by 8.2 kcal/mol, passing over a very small barrier of 1.5 kcal/mol.

The suggested mechanism is consistent with the site-directed mutagenesis work of Andersson et al.,[39] where they showed that Cys79 and Cys290 are essential for the reaction. In a study by Mulliez et al.,[40] the carbon in formate was labeled with ^{14}C and was found to end up in carbon dioxide, which is also consistent with the suggested mechanism. They furthermore replaced the C-bound hydrogen in for-

Scheme 4. Reaction Mechanism for Class III RNR Suggested on the Basis of Recent B3LYP Calculations

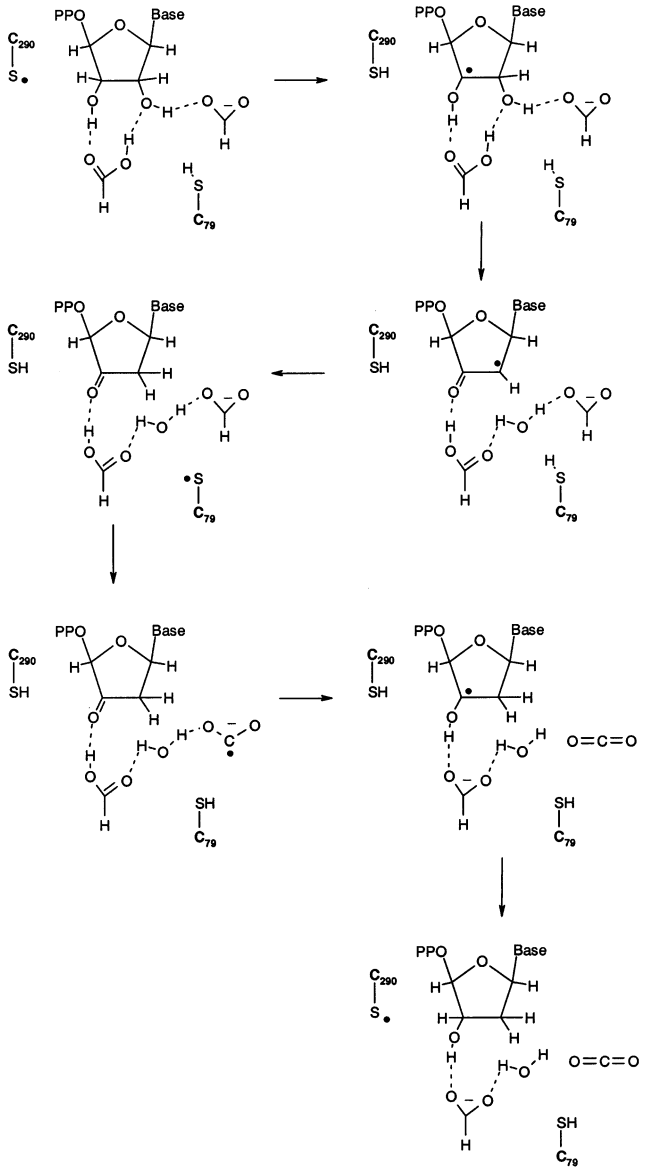

mate with tritium and found that tritium eventually ends up in water and not in the substrate. In the suggested mechanism, the C-bound hydrogen ends up in the protein at Cys79. The agreement between experiments and theory therefore depends on the rate of proton exchange between Cys79 and water and requires that this is faster than the rate-limiting step of the substrate reactions. The exchange of protons between water and the cysteine side chain has been studied experimentally for the isolated cysteine amino acid,[41] and a rate of 1400 s^{-1} was found, substantially faster than the rate-limiting step of anaerobic RNR.

Since the above mechanism assumes that the formate reductant is protonated and this may not be very likely, another possible mechanism was tested in a recent study by Cho et al. (Scheme 4).[42] This mechanism was suggested by Andersson et al.[43] and implies that two formates actually enter the catalytic cycle. It was found that the active site is actually very well set up to harbor these two formates by supplying

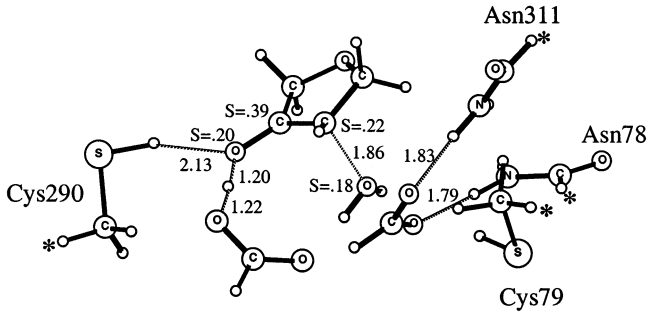

Figure 7. Transition state for water formation in class III RNR. Atoms marked with ∗ were fixed from the X-ray structure.

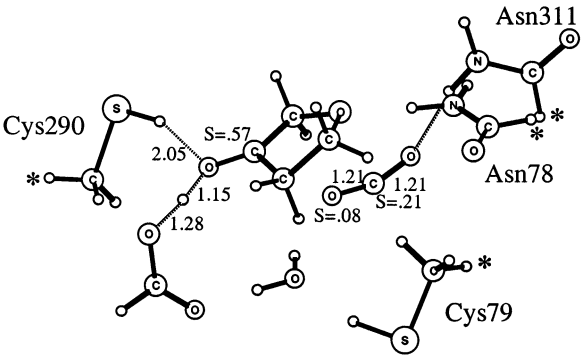

Figure 8. Transition state for the reprotonation of the C3′ oxygen and for carbon dioxide formation class III RNR. Atoms marked with ∗ were fixed from the X-ray structure.

important hydrogen bonds. If two formates are at the active site, the question of why an additional proton should enter the active site is answered. It is clear that the additional −2 charge of the two formates at the active site will automatically draw a proton into the site to compensate for the negative charge. This investigation is still in progress, but two tentative transition states will be described here.

There are two features of the water formation transition state in Figure 7 that are particularly noteworthy. First, it can be noted how the formic acid and the formate (two formates plus a proton) are held in position by hydrogen bonds, two of them from the conserved asparagines. The second point to note is that the proton which is used to form water is taken from the formic acid and not from the cysteine. The mechanism for water formation is thus suggested to be quite similar to the one for the previous model with one formic acid. It is also similar to the protonated Glu441 model for the class I enzyme but different from the more recent unprotonated model, where the proton is taken from a cysteine.

The transition state for CO_2 formation is shown in Figure 8. Just as in the unprotonated class I mechanism, there are two processes occurring simultaneously at a substantial distance of 5−6 Å from each other. One is the reprotonation of the C3′ oxygen, and the other one is an electron transfer from CO_2^- to the substrate. Again, it is remarkable that B3LYP is actually able to describe this type of reaction with a reasonable barrier of 12 kcal/mol. The spin at the transition state is strongly delocalized with a spin population on CO_2 of 0.32 and on the substrate of 0.60, mainly located at C3′. With these transition

states determined, in Figures 7 and 8, it should be possible to obtain new information about coupling of long-range electron transfer and chemical transformations that has not been accessible before. The analysis of these processes is still in progress.

III. Glycyl Radical Enzymes

Three enzymes are now known to utilize a glycyl radical in their catalytic processes.[44−46] The first enzyme discovered in this family was pyruvate formate lyase (PFL).[47,48] This was followed by the identification of the glycyl radical in class III anaerobic ribonucleotide reductase (ARNR)[49−52] and very recently in benzylsuccinate synthase (BSS).[53]

These enzymes are catalytically inactive when synthesized and are activated by hydrogen atom abstraction from glycine, producing a glycyl radical. For this process, an iron−sulfur cluster is usually required. After activation, these enzymes function only anaerobically. Exposure to oxygen is known to irreversibly inactivate the enzymes by cleavage of the polypeptide chain at the glycyl radical site.

There has been a considerable interest to study the glycyl radical enzymes using quantum chemical methods. In this section we present these studies. First, the stability of the protein-bound glycyl radical and the various factors affecting that are discussed. Next, the theoretical study of the oxygen reactions leading to the cleavage of the protein backbone is presented. Calculations examining the substrate reactions of PFL and BSS are then reviewed. The mechanism of class III anaerobic RNR is discussed in the RNR section.

A. Stability of the Glycyl Radical

The stability of the glycyl radical is usually explained using the captodative effect,[54−57] which occurs when the radical center is located between an electron donor (the amino group) and an electron acceptor (the amide carbonyl). The cooperative effect of these two groups results in an enhanced radical resonance stability. Another effect that is believed to make the glycyl radical more stable than the corresponding radicals in other amino acids is the lack of side chain. Since the C_α center in the radical is perfectly planar, the nonbonding interactions between the side chain and the adjacent carbonyl will destabilize the radical compared to its parent molecule with tetrahedral C_α carbon. Absence of this nonbonding interaction in the glycyl radical would render it considerably more stable than other corresponding C_α-amino acid radicals. These issues have been examined using density functional methods.[58−64]

To identify and understand the important contributions to the stability of the protein-bound glycyl radical, the C_α–H bond dissociation energy (BDE) was calculated for a series of models, starting from the simplest tetrahedral carbon of methane and systematically adding one functional group at the time.[60] The energies are listed in Table 1.

In a clear confirmation of the captodative hypothesis, it is seen that while amino and carbonyl substitutions on methane separately (NH_2-CH_3 and CH_3-CHO) cause a lowering of the BDE by 13.1 and 10.7 kcal/mol, respectively, the combined effect of the two (NH_2-CH_2-CHO) is a decrease in the BDE by as much as 33.5 kcal/mol. Inclusion of the peptide bond on either side of the NH_2-CH_2-CHO model will diminish the electron-withdrawing (or electron-donating) power of the substituent, resulting in a weaker captodative effect. The BDE of the largest model, $CH_3-CO-NH-CH_2-CO-NH-CH_3$, is calculated to be 78.9 kcal/mol.

Table 1. B3LYP-Calculated $C_\alpha-H$ Bond Dissociation Energies (kcal/mol) and C_α-Spin Populations for Different Models of Protein-Bound Glycyl

model	$C_\alpha-H$ BDE	spin on C_α
CH_4	101.5	1.15
NH_2-CH_3	88.4	0.89
CH_3-CHO	90.8	0.86
NH_2-CH_2-CHO	68.0	0.48
NH_2-CH_2-COOH	73.8	0.59
$NH_2-CH_2-CONH_2$	74.4	0.62
$CHO-NH-CH_2-CHO$	74.5	0.60
$CHO-NH-CH_2-CO-NH_2$	79.3	0.70
$CH_3-CO-NH-CH_2-CO-NH-CH_3$	78.9	0.70

Scheme 5. Resonance Structures Identified in Protein-Bound Glycyl Radical

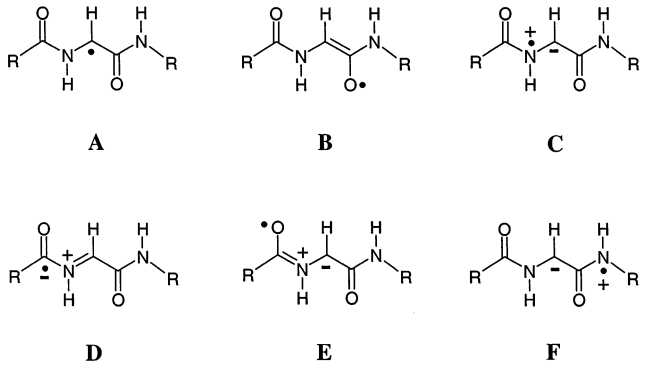

The glycine residue is believed to serve as a site for radical storage. The glycyl radical starts catalysis by abstracting a hydrogen atom from a neighboring cysteine, which then attacks the substrate. For its biological function, it was argued that protein-bound glycine has a well-tuned $C_\alpha-H$ BDE. Using the same theoretical method, the cysteine residue has a calculated S−H BDE of 81.7 kcal/mol, i.e., only a couple of kcal/mol higher than the glycine residue, hence making the thiyl radical readily accessible. A more stable glycyl radical would make it several orders of magnitude slower to create the transient thiyl radical and thus slow the whole catalytic process. On the other hand, a less stable glycyl radical would allow the radical to move around to unwanted sites and make the protein subject to damage and cleavage.

From the calculated bond lengths and spin populations, the resonances displayed in Scheme 5 were identified for the protein-bound glycyl radical.[60] Resonances A−C are the ones associated with the captodative effect, while resonances D−F are associated with the peptide bonds present in protein-bound glycyl.

The spin delocalization in the protein-bound glycyl radical is high. In the largest models, C_α has 0.70 of the spin, the carbonyl oxygen and carbon 0.10 and

Scheme 6. Mechanism of Protein Cleavage by Reaction with O_2[a]

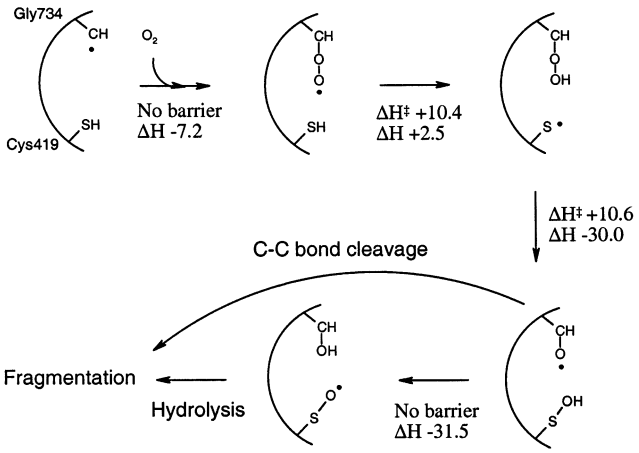

[a] Calculated reaction energies and barriers are indicated.

−0.04, respectively, and the nitrogen center 0.09. The spin is also delocalized over the peptide bonds. The oxygen and the carbon of the carbonyl of the peptide bond have 0.09 and 0.03 of the unpaired spin, respectively, and the nitrogen on the opposite side has 0.07.

B. Oxidative Degradation of Glycyl Radical Enzymes

Exposure to oxygen leads to irreversible inactivation of the enzymes by cleavage of the polypeptide chain at the glycyl radical site. Manual and rapid-quench EPR studies of the mechanism of inactivation and cleavage of wild-type and mutant PFL enzymes showed that two transient protein-based radical species are formed in the process.[65,66] The first is a carbon-based peroxyl radical (ROO•) and the second is a sulfinyl radical (RSO•). Gauld and Eriksson used density functional methods to examine different mechanisms of this reaction[67] and proposed the reaction sequence displayed in Scheme 6. The first step involves addition of molecular oxygen to the glycyl radical to give the observed peroxyl radical. Next, the peroxyl radical abstracts a hydrogen atom from the neighboring Cys419, to yield a thiyl radical. The rate-limiting step is the rebound reaction in which the thiyl radical abstracts back a hydroxyl group from the glycine. The calculated barrier is 13.1 kcal/mol relative the starting point. Finally, the resulting glycyl-alkoxy radical (Gly-O•) abstracts a hydrogen atom from the cysteine-hydroxyl moiety to give the observed sulfinyl radical.

Fragmentation is then achieved either by hydrolysis of the hydroxyglycine moiety or by C−C bond cleavage of the Gly-alkoxy radical.

C. Substrate Mechanism of Pyruvate Formate Lyase

PFL catalyzes the reversible conversion of pyruvate and coenzyme A (CoA) into formate and acetyl-CoA (Scheme 7), which is a key component of the anaerobic carbon metabolism in *Escherichia coli* and other prokaryotes. In 1984, Knappe and co-workers de-

Scheme 7. Reaction Catalyzed by PFL

tected a free radical in PFL,[47] and in 1992 this radical was assigned to the Gly734 residue.[48] Two other residues are known to be essential for catalysis, Cys418 and Cys419.

Before the crystal structure of PFL became available in 1999,[68,69] the most compelling reaction mechanism was the one proposed by Kozarich and co-workers.[70,71] The first step in this mechanism is the creation of a transient thiyl radical formed by a hydrogen atom transfer from a cysteine residue (Cys419) to the glycyl radical. This step is now believed to be the common initial step in all glycyl radical enzymes. The cysteinyl radical then adds to the keto group of pyruvate to give a tetrahedral oxy-radical intermediate, which subsequently collapses into an acetylated cysteine and a formyl radical. The formyl radical then abstracts a hydrogen atom from the quenched glycine to regenerate the glycyl radical. A step of transesterification between Cys419 and Cys418 follows before the reaction is completed by the heterolytic transfer of the acetyl from Cys418 to CoA.

DFT calculations were performed (also prior to the crystal structure) to test this, at the time, controversial mechanism.[72] As discussed above, the C_α-H bond strength of protein-bound glycine is well-tuned to make the thiyl radical accessible. The barrier for the direct hydrogen transfer reaction between cysteine and glycyl was calculated to the very feasible 9.9 kcal/mol (the optimized transition state structure is displayed in Figure 9).

The next step, addition of the thiyl radical to the carbonyl carbon of pyruvate to give the tetrahedral oxy-radical intermediate, was shown indeed to be energetically very plausible. The barrier was calculated to 12.3 kcal/mol, and the intermediate was found to be only 9.9 kcal/mol higher than the free reactants (added to the 3.4 kcal/mol cost of creating the thiyl radical, these energies become 15.7 and 13.3 kcal/mol, respectively). The barrier for the dissociation of the radical intermediate into acetylated cysteine and formyl radical was calculated to be only 2.8 kcal/mol with an exothermicity of 3.9 kcal/mol,

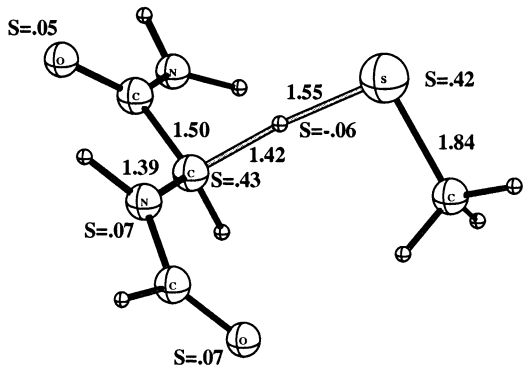

Figure 9. Optimized transition state structure for the direct hydrogen atom transfer from cysteine to glycyl radical.

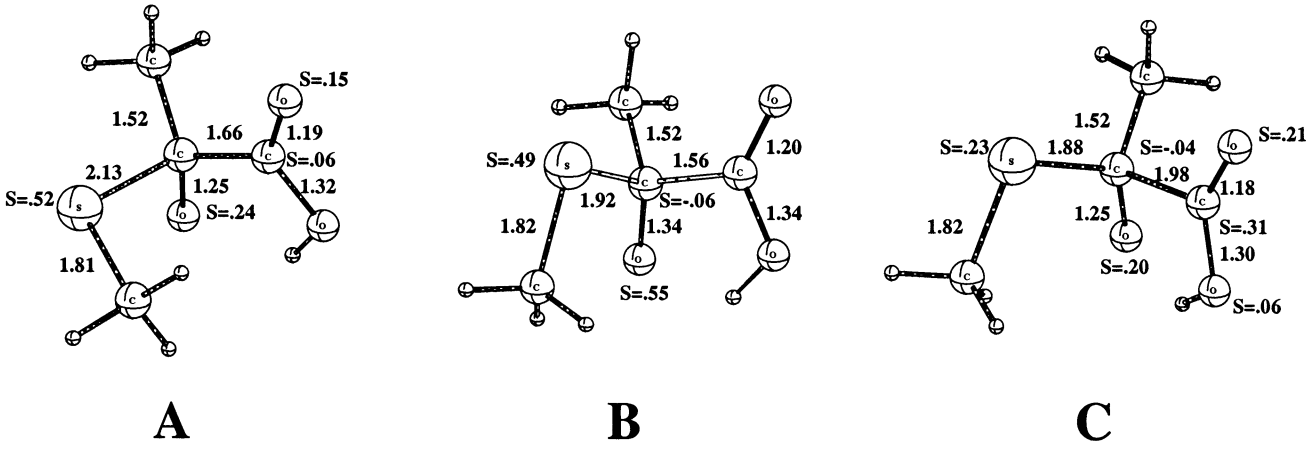

Figure 10. Optimized structures for (A) transition state of the thiyl radical addition to pyruvate (TS1), (B) tetrahedral oxy-radical intermediate, and (C) transition state of the dissociation of formyl radical (TS2).

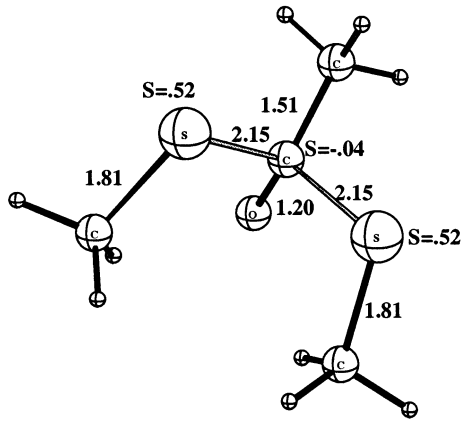

Figure 11. Optimized structure and spin-population distribution of the transition state of the homolytic acetyl transfer between cysteines.

giving an overall endothermicity of 6.0 kcal/mol for the reaction step:

$$\text{Cys}\bullet + \text{pyruvate} \rightarrow \text{Cys-acetyl} + \text{formyl}\bullet$$

The optimized structures of the intermediate and the transition states are shown in Figure 10.

The tetrahedral radical intermediate will thus readily dissociate and release formyl radical. This reactive radical was proposed by Kozarich to abstract a hydrogen atom from Gly734, regenerating hence the stable enzyme radical at that site. Although the calculations gave plausible energies for this step (a barrier of 4.9 kcal/mol and exothermicity of 17.5 kcal/mol), another pathway was preferred. The formyl radical was proposed to be quenched by a cysteine residue instead, to facilitate the acetyl transfer that takes place in the next step. The barrier for this formyl radical quenching by cysteine was calculated to be 1.1 kcal/mol and the exothermicity to be 14.1 kcal/mol.

Having created the radical at Cys419, the proposed acetyl group transfer between Cys419 and Cys418 is now facile, with a barrier of quite reasonable 11.6 kcal/mol (transition state structure in Figure 11).

For the next step, the calculations suggested that the transfer of the acetyl group from Cys418 to CoA occurs in two steps:

$$\text{CoA-SH} + \text{Cys419}\bullet \rightarrow \text{CoA-S}\bullet + \text{Cys419} \quad (1)$$

$$\text{CoA-S}\bullet + \text{Cys418-acetyl} \rightarrow \text{CoA-acetyl} + \text{Cys418}\bullet \quad (2)$$

The first step (1) is a simple hydrogen atom transfer, where the Cys419 radical abstracts a hydrogen from CoA-SH. This thermoneutral step has a calculated barrier of only 2.4 kcal/mol. Step 2 is also thermoneutral and involves the homolytic transfer of the acetyl group between the other cysteine and the CoA radical. Since the same model was used for CoA and cysteine (CH_3SH), this step is identical to the acetyl transfer between the two cysteines, with a computed barrier of 11.6 kcal/mol.

A direct nucleophilic attack by the thiol group of CoA on the carbonyl carbon of acetylated cysteine, yielding a tetrahedral intermediate, was also considered, but the barrier turned out to be very high (41.2 kcal/mol).

The final step is to regenerate the glycyl radical by hydrogen atom transfer from glycine to the cysteinyl radical. This step is the reverse of the first step with a barrier of 6.5 kcal/mol and exothermicity of 3.4 kcal/mol.

The recent X-ray crystal structure of Becker et al.[69] provided new insight into the mechanism. PFL was crystallized in complex with the substrate analogue oxamate, which differs from pyruvate in having an amino group instead of the methyl (the active site geometry is presented in Figure 12). The structure shows that the Gly734 and Cys419 are indeed in close proximity (3.7 Å), confirming the biochemical experiments. The position of the substrate in the structure implies that Cys418, and not Cys419, performs the radical attack on pyruvate. This would require two hydrogen atom transfers to create the radical at Cys418, first from Cys419 to the glycyl radical and then from Cys418 to Cys419. Since the two cysteines were modeled in exactly the same way in the calculations presented above, all the results found for the addition of Cys419 radical to pyruvate also apply to

Scheme 8. Reaction Mechanism for PFL Based on Biochemical Experiments, DFT Calculations, and Crystal Structure[a]

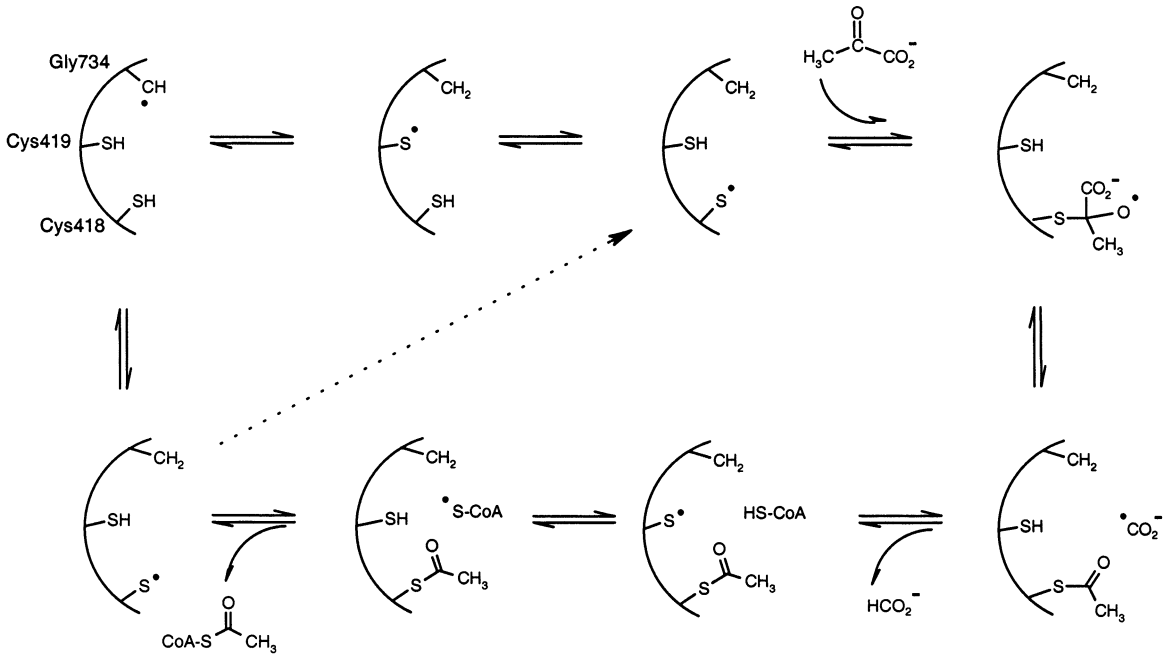

[a] Dashed arrow indicates a possible short cut.

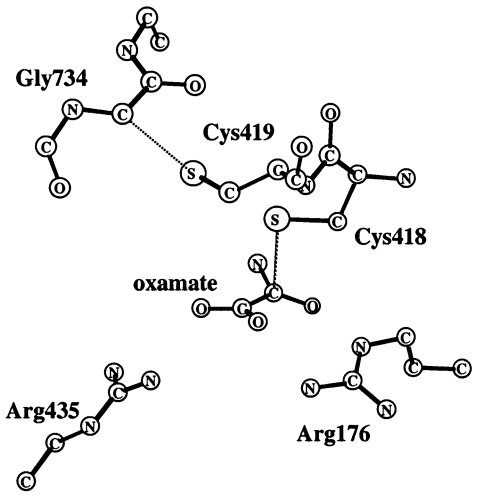

Figure 12. X-ray structure of the active site of PFL in complex with the substrate analogue oxamate.[69]

Cys418. The crystal structure proves also that the previously suggested acetyl transfer between Cys419 and Cys418 is redundant, since Cys418 is the residue involved in the attack.

On the basis of these structural findings, the biochemical experiments of Kozarich and co-workers and Knappe and co-workers, and the DFT calculations presented above, the currently accepted mechanism of PFL is summarized in Scheme 8.

D. Substrate Mechanism of Benzylsuccinate Synthase

Benzylsuccinate synthase initiates the anaerobic toluene degradation in denitrifying bacteria by catalyzing the addition of toluene to fumarate, forming benzylsuccinate (Scheme 9).

The enzyme was first suggested to contain a glycyl radical on the basis of the strong homology between

Scheme 9. Reaction Catalyzed by BSS

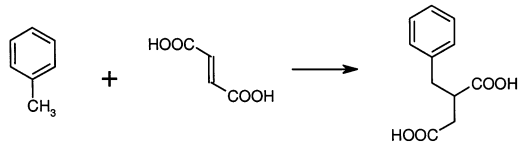

the α-subunit and PFL and ARNR.[73] Very recently, the existence of the glycyl radical in BSS was established by Krieger et al. using electron paramagnetic resonance spectroscopy.[53]

By analogy to the PFL reaction mechanism, and based on the spectroscopic and biochemical information available,[74−78] the mechanism displayed in Scheme 10 has been proposed for BSS.[53,73] First, the stable glycyl radical (presumably at position 828 in *Azoarcus* sp. Strain T numbering) abstracts a hydrogen atom from a neighboring cysteine residue (presumably Cys492), creating the transient thiyl radical. The thiyl radical in turn abstracts a hydrogen atom from the toluene methyl, creating a benzyl radical intermediate. This benzyl radical then attacks the double bond of the fumarate, yielding a benzylsuccinyl radical intermediate, which is subsequently quenched by hydrogen atom transfer from the cysteine, giving the benzylsuccinate product. The cysteinyl radical then either abstracts a hydrogen atom from the glycine residue, regenerating the stable glycyl radical, or starts a new catalytic cycle by abstracting a hydrogen atom from a new toluene substrate.

DFT calculations were performed to test this proposal.[79] Indeed, the calculations provided very strong support for this mechanism. All the steps were shown to have favorable reaction energies and activation barriers. The rate-limiting step was found to be the addition of benzyl radical to fumarate (step 3 of Scheme 10), with a total barrier of 15.0 kcal/mol.

Scheme 10. Proposed Reaction Mechanism of BSS[a]

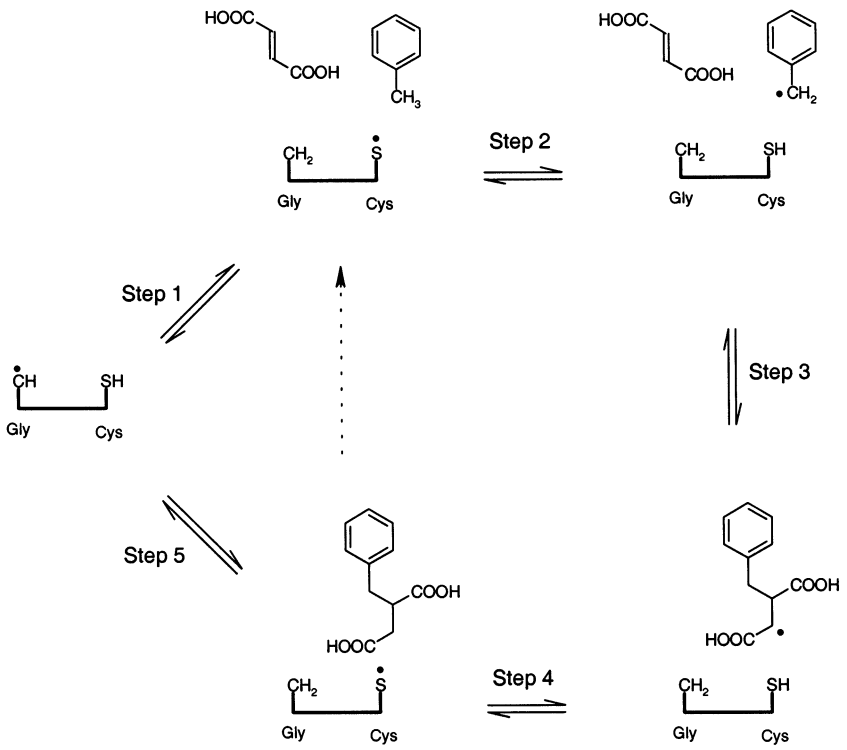

[a] Dashed arrow indicates a possible short cut.

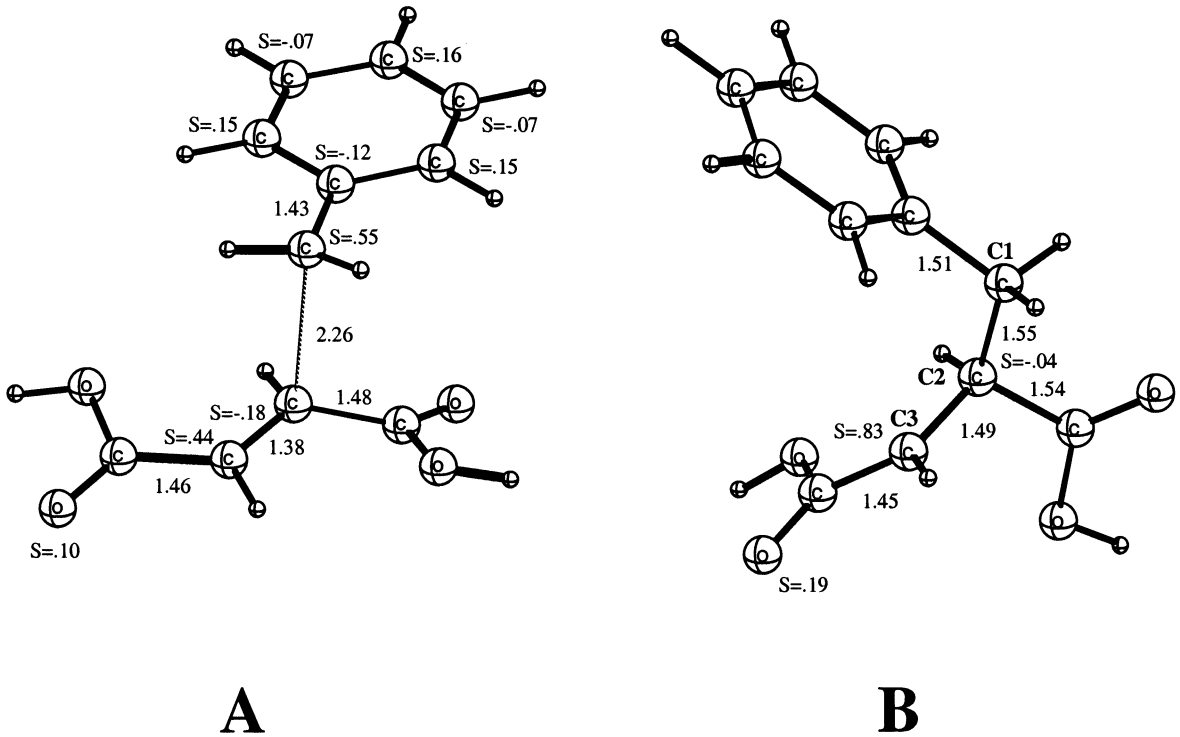

A **B**

Figure 13. Optimized structures for (A) the transition state for addition of benzyl radical to fumarate and (B) the resulting benzylsuccinyl radical.

Optimized structures of the C−C formation transition state and the resulting benzylsuccinate radical intermediate are shown in Figure 13. To create the benzyl radical involved in the addition, it was shown that the two hydrogen atom transfer steps, from cysteine to glycyl (initial step of glycyl radical enzymes) and from toluene to cysteinyl, occur with relatively low barriers (10.7 and 12.9 kcal/mol, respectively). The benzyl radical is stabilized by resonances similar to those in phenoxyl, lowering the toluene CH bond dissociation energy and hydrogen transfer barrier.

The step to quench the benzylsuccinyl radical by transferring a hydrogen atom from the cysteine (step 4 of Scheme 10) is calculated to be exothermic by 5.8 kcal/mol, with a quite low barrier of the 7.0 kcal/mol.

Scheme 11. Reactions Catalyzed by Prostaglandin H Synthase

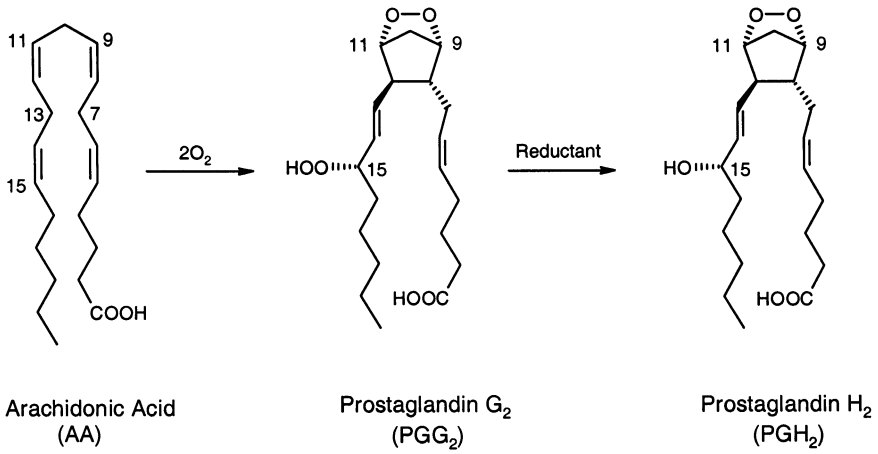

Finally, the glycyl radical is regenerated in a step that is the reverse of the first step.

IV. Prostaglandin H Synthase

A tyrosyl radical is believed to play a major role in catalysis for the key regulatory enzyme in prostaglandin biosynthesis, prostaglandin H synthase (PGHS). Two PGHS isozymes are known with different physiological roles and expression levels. The constitutive isozyme (PGHS-1) is ascribed housekeeping functions, whereas the inducible isozyme (PGHS-2) is associated with pathological processes.[80] Recently, the reaction mechanism of the conversion of arachidonic acid (AA) to prostaglandin H_2 (PGH_2) has been the subject of a DFT study by Blomberg et al. using the B3LYP functional.[81] PGHS is a single hemoprotein that exhibits two enzyme activities: a cyclooxygenase that catalyzes the dioxygenation of arachidonic acid to yield prostaglandin G_2 (PGG_2), and a peroxidase that converts PGG_2 to PGH_2 (Scheme 11).

The current hypothesis to account for the linkage between the PGHS activities is that a reaction of PGHS with hydrogen peroxide first forms peroxidase compound I (step 1), which then oxidizes a tyrosine residue in the protein to form a tyrosyl radical (step 2). Peroxide-induced tyrosyl radicals have been detected in both PGHS-1 and -2.[82−85] Precisely how the tyrosyl radical is formed by compound I is not known and there are some mysteries in this context. The main one is that an obvious base is missing in the neighborhood of the tyrosine. Since the tyrosyl radical is only sufficiently stable as neutral, the OH proton has to go somewhere when the electron is transferred to compound I, but where it goes is not known at present.

In the cyclooxygenase mechanism (Scheme 12) the tyrosyl radical is postulated to abstract a hydrogen atom from C13 of arachidonic acid to generate a protein-bound arachidonyl radical, which initiates a cascade of radical reactions that incorporate two molecules of O_2 and result in a PGG_2 radical. Finally, the tyrosyl radical is regenerated by abstraction of its phenoxyl hydrogen atom by the PGG_2 radical to generate the product of the cyclooxygenase reaction, PGG_2.

A detailed chemical mechanism for the transformation of arachidonic acid to PGG_2 was proposed by Hamberg and Samuelsson[86] (see Scheme 12). In this sequence, abstraction of the pro-*S* hydrogen atom from C13 of arachidonic acid first forms a C11−C15 pentadienyl radical. Under regular turnover conditions, this step is indicated to be rate-limiting.[86] Reaction of this radical with O_2 then leads to oxygen attachment at C11 and subsequent cyclization to form a 9,11-peroxo bridge, which leaves a radical at C8. Cyclization of the radical at C8 onto the diene at C12 generates an allyl radical spanning C13−15, which attacks a second O_2 to give a hydroperoxy (PGG_2) radical. The final step is reduction of the PGG_2 radical to PGG_2 by the tyrosine in the active site. Although this scheme provides an elegant explanation of the observed product, none of the proposed intermediates have been identified for 3 decades due to experimental difficulties.

The crystal structure of PGHS-1 with arachidonate (AA) bound in the active site pocket[87] was used as a starting point to set up a chemical model for the B3LYP study. Although there are structural differences between PGHS-1 and -2[88−90] the models used will not involve these. This means that the results should also be valid for PGHS-2. In PGHS, the substrate AA is the 20-carbon-long 4-fold-unsaturated acid [(*Z*,*Z*,*Z*,*Z*)-5,8,11,14-eicosatetraenoic acid] in an active site composed of around 20 amino acids. In the study two models were used, one smaller model (model 1) treated with the B3LYP functional and one larger model (model 2) treated with a two-layered ONIOM-model that incorporates some parts of the surroundings (see Figure 14). The conventional numbering of the carbons in AA, shown in the figure, is used here to describe the reactions.

Model 1 consists of the C7−C16 part of the AA substrate, which is where the radical chemistry is believed to occur. The carboxylate and ω-end of AA have no chemical properties affecting the radical reactions taking place on C8−C15, but they introduce pure steric effects when incorporated in the active site of PGHS. In model 1, (Z,Z,Z)-2,5,8-decatriene, no steric effects were taken into account, i.e., all degrees of freedom were optimized. Since all species in the system are uncharged and no strong hydrogen bonds

Scheme 12. Mechanistic Model of the Cyclooxygenase Reaction

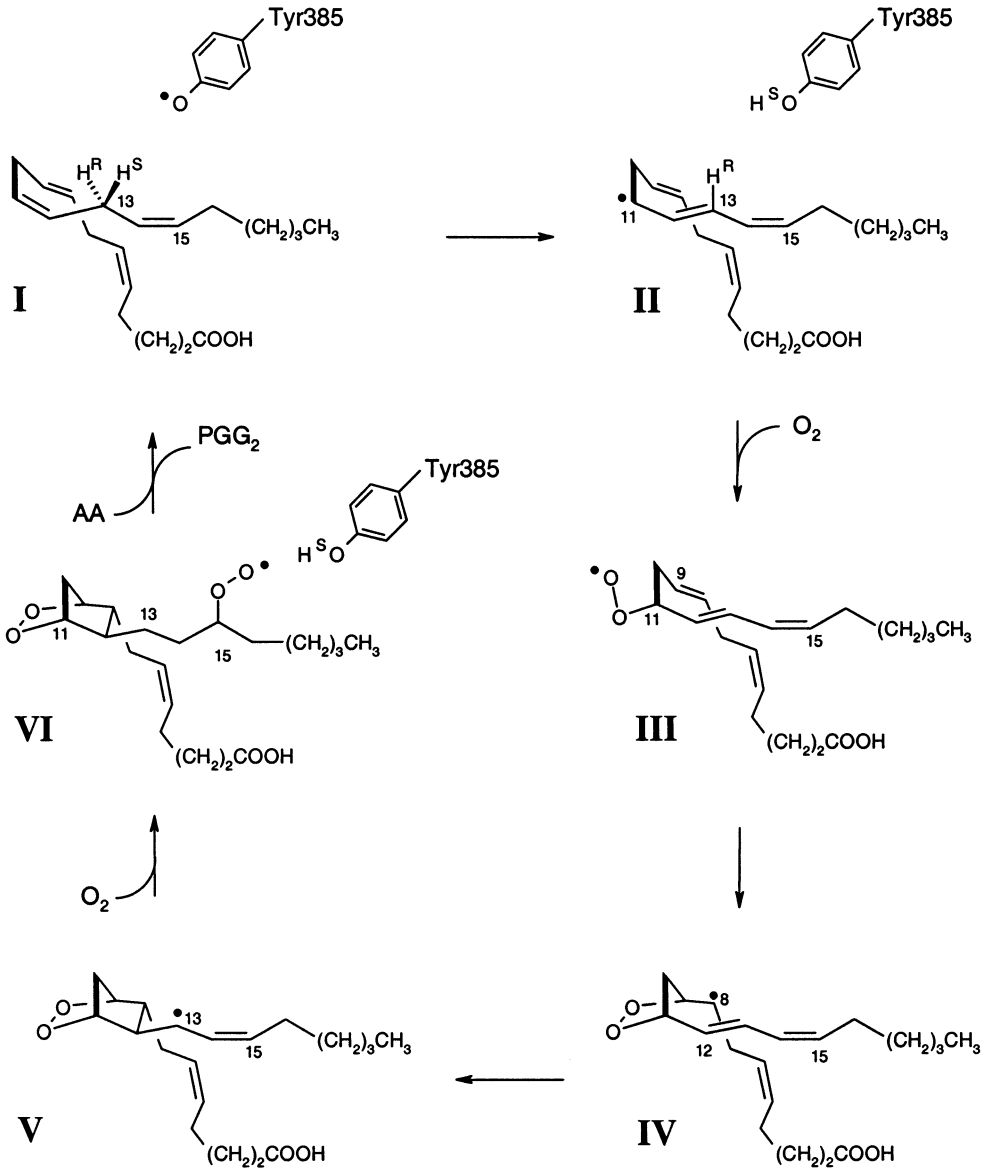

are present, the interaction between the intermediates and the surrounding should be small and not vary much between the different stationary points. The active site pocket surrounding the active part of AA consists of amino acids only giving rise to hydrophobic interactions. Since the polarity of the amino acids surrounding the active site is quite uniform, these interactions should be rather well described by a polarizable continuum model.

In model 2, the full substrate and the amino acids Tyr385, Tyr355, and Arg120 are incorporated, and in Figure 14 the parts of the model that were treated at the B3LYP level and those treated at the semiempirical AM1 level are indicated. The distances between the β-carbons of Tyr385, Tyr355, Arg120 and the ω-end (C20) of the substrate were frozen relative to each other with the coordinates taken from the crystal structure[87] (see Figure 14). This was done to keep the shape of the substrate in the active site of PGHS. Arg120 and Tyr355 were incorporated in the model, since they position the carboxylic end of AA through a salt bridge and a hydrogen bond, respectively. Arg120 has been shown to be crucial for binding AA in a reactive conformation in PGHS-1.[91] Some amino acids that were not incorporated in the model will have steric effects that are important for the stereochemistry in the production of PGG_2. These effects were therefore not fully described in the DFT study.

The results presented below are obtained using model 1 calculations. In general, models 1 and 2 yield energies within 1−2 kcal/mol from each other.

The energy diagram for the cyclooxygenase reaction, shown in Figure 15, was obtained in the following way. The geometries of all intermediates and transition states were fully optimized as usual. In the optimized geometries, large basis set calculations were performed to obtain refined energies. Zero-point, temperature, and dielectric effects were then added. Unlike most cases described in this review, these energies were finally corrected from known energies of similar reactions studied experimentally. For example, the reaction energy and barrier height for O_2 attack on the arachidonic acid radical was cor-

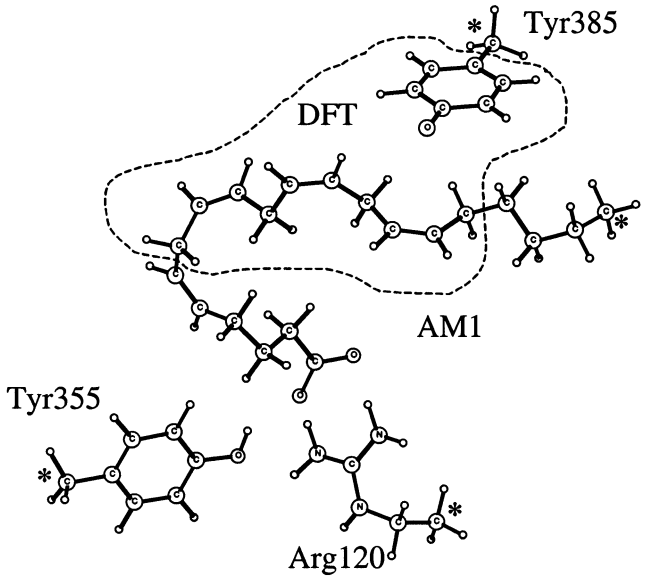

Figure 14. The two layers in the ONIOM model. The restricted carbons in the model are marked with an asterisk.

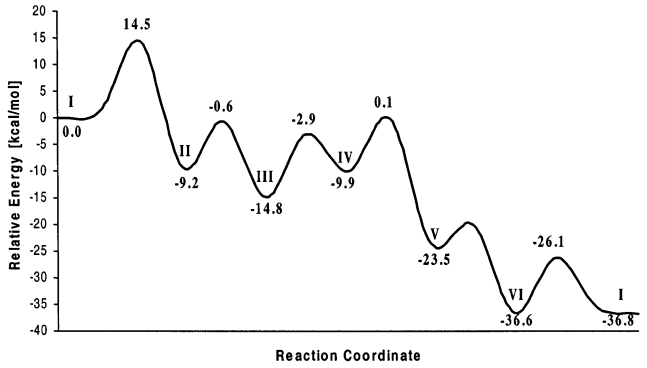

Figure 15. Free energy surface for the cyclooxygenase reaction of prostaglandin H synthase.

rected from experiments on the corresponding reaction for the pentadienyl radical. The difference between calculated and experimental results for the pentadienyl reaction was added to the calculated results for the arachidonic acid radical. These and similar corrections for the other states amount to a few kilocalories/mole at most. It is this corrected energy diagram that is shown in the figure.

Two optimized transition states are shown in Figure 16 as examples of the structures obtained. In the first of these, the C13 pro-*S* hydrogen is abstracted by the Tyr385 radical, the rate-limiting step of the cyclooxygenase cycle. Since this reaction is quite exothermic, there is an early transition state with an O−H distance of 1.37 Å. The calculated barrier height is 12.3 kcal/mol, which is corrected to 14.5 kcal/mol by experimental data from 1,4 pentadiene and phenol. The experimental rate-limiting barrier for the cyclooxygenase reaction corresponds to a free energy barrier of 14.8 kcal/mol.[82] The other transition state shown here is the final step of the catalytic cycle, where the tyrosine is recreated. This is a thermoneutral reaction, and the hydrogen is therefore rather close to the midpoint between the oxygens involved, with a distance to the Tyr385 oxygen of 1.19 Å. The spin distributions of the two transition states are quite similar and typical for this type of radical reaction involving tyrosine.

The calculated energetics could finally be used to draw some conclusions concerning the stereo- and enantioselectivity of the cyclooxygenase reaction. As a comparison, the energetics for competing reactions leading to products with different stereosymmetry were also calculated. It should be remembered that the most common explanation for the selectivity concerns a special binding pocket of dioxygen in the enzyme, and this effect was not included in the model used. However, from the calculated energies for the model used it could, for example, be concluded that the 13-HPETE formation following an attack by the first O_2 on C13 is unfavorable and will therefore not occur, in agreement with experimental observations. Furthermore, the attack by the second O_2 on C13 leads to the most stable product, also in agreement with experiments. The calculations also indicated that the rate for reverse reactions compared to the rate of dissociation of products in some cases can be decisive for the selectivity.

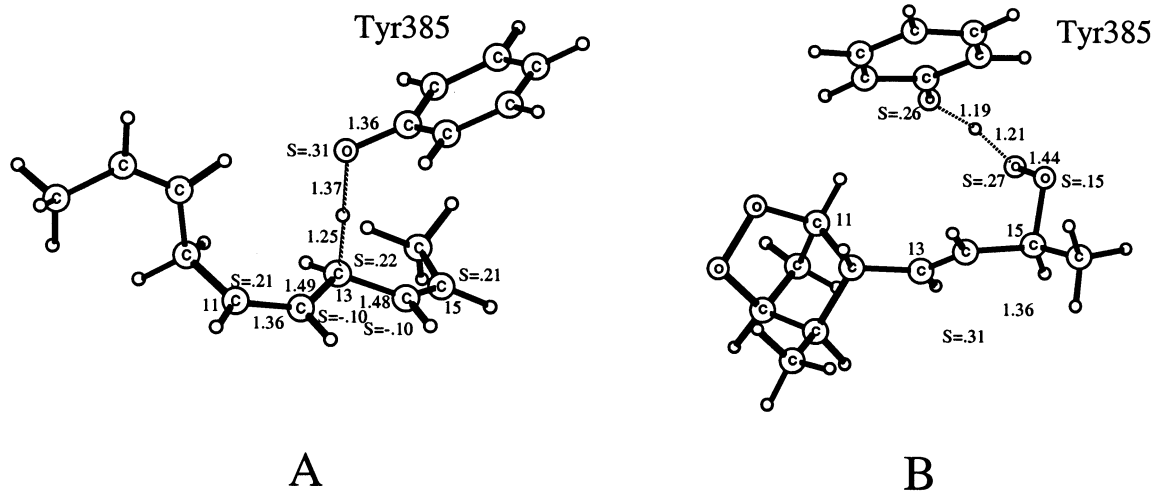

Figure 16. Optimized transition state structures for (A) the abstraction of the pro-*S*-hydrogen (step 1 of Scheme 12) and (B) the hydrogen abstraction back by the peroxyl radical (step 6 of Scheme 12).

Scheme 13. Schematic Structure of the B_{12} Cofactor

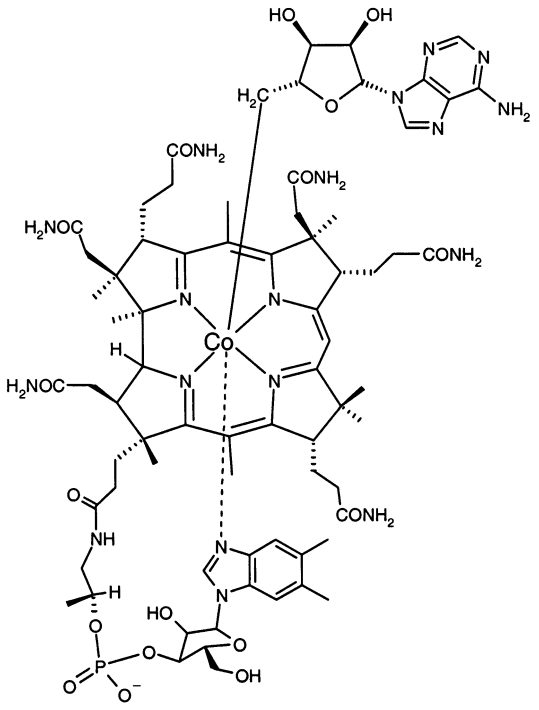

Scheme 14. Rearrangement Reaction Catalyzed by B_{12} Enzymes

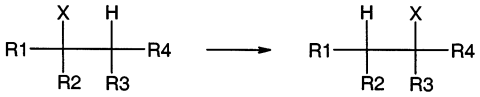

Scheme 15. Generally Accepted Mechanism for B_{12}-Dependent Rearrangement Reactions

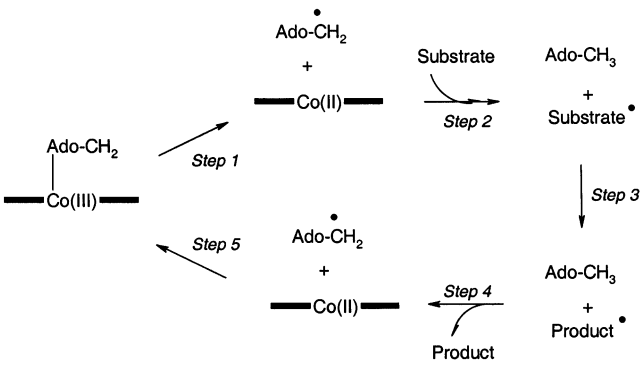

V. Coenzyme B_{12}-Dependent Enzymes

Coenzyme B_{12} (Scheme 13) assists many enzymatic reactions, a class of which involves the rearrangement reaction displayed in Scheme 14, where a functional group X swaps places with a hydrogen atom on an adjacent carbon.[92,93]

It is generally accepted that the reactions of these enzymes proceed through the generic mechanism shown in Scheme 15.[94−100] Catalysis is initiated by the homolysis of the Co−C bond to give Co(II) and 5′-deoxyadenosyl radical (Ado-CH_2•, step 1), which then abstracts a hydrogen atom from the substrate, creating a substrate-based radical (step 2). The substrate radical subsequently rearranges to yield a product-based radical (step 3), which then abstracts back the hydrogen atom from the 5′-deoxyadenosine, regenerating the Ado-CH_2• radical (step 4). Recombination of the Ado-CH_2• radical and Co(II) completes the catalytic cycle (step 5).

There have been a number of theoretical studies addressing different issues of this mechanism. In what follows, we first discuss briefly the energetics of the Co−C bond (step 1) and then the mechanisms of substrate rearrangement for the different enzymes (mainly step 3).

A. Co−C Bond Cleavage

The Co−C bond in the vitamin B_{12} is one of few metal−carbon bonds known in biology, and is the key to the reactivity of this species. The energy required to break this bond homolytically has been measured to the quite low, ∼31 kcal/mol in solution.[101] Although rather low, this bond strength must be substantially lowered in enzymatic catalysis, where kinetic measurements have indicated a reaction acceleration of ca. 12 orders of magnitude, i.e., the BDE is reduced by ca. 15 kcal/mol.[102−105] How in detail this destabilization is achieved has proven elusive. Effects such as corrin ring flexibility, displacement of the axial base ligand, or the angular distortion of the alkyl group have been suggested to play an important role in the Co−C bond destabilization. However, no single factor has yet emerged as responsible for this huge BDE drop.

Several quantum chemical studies employing realistic models of the corrin ring have appeared during the past few years discussing this issue.[106−115] These were very recently reviewed by Kozlowski.[116] Here, we briefly mention some of the important results concerning the energetics of the Co−C bond.

Dölker et al. studied the importance of the axial trans Co−N bond on the BDE of Co−C bond.[113] It was seen that Co-Me BDE increases by a modest 1 kcal/mol for a change in the trans Co−N bond length by up to 0.5 Å in any direction, either shortening or lengthening. This result is related to the fact that the potential energy surface of the Co−N bond is very shallow. In fact, the total binding energy of the Co−N bond was calculated to very small, 2.2 kcal/mol. Similar conclusions were reached by Jensen and Ryde.[112]

BDE calculations by Andruniow et al. showed also that the Co−C bond strength is almost independent of the trans axial ligand.[109,110] Using water, imidazole, or dimethylbenzimidazole as trans ligands gave very similar BDEs. A series of R groups (ranging in size from methyl to *tert*-butyl) were used, and it was seen that the optimized Co−C_R bond length correlates with the bulkiness of the R group, with the *tert*-butyl giving a Co−C_R bond length 0.10−0.15 Å longer than that for methyl. Interestingly, the Co−C_R BDE was found to correlate linearly with the optimized Co−C_R bond length, with the BDE for *tert*-butyl being as much as 15 kcal/mol lower than that for Me. On the basis of these findings, the authors suggested that the Co−C bond labilization seen in enzyme-bound coenzyme B_{12} compared to solution is a result of the Co−C bond elongation. The basic question remains, however: How does the protein provide these 15 kcal/

Scheme 16. Summary of the Main B_{12}-Dependent Rearrangement Reactions Studied Theoretically

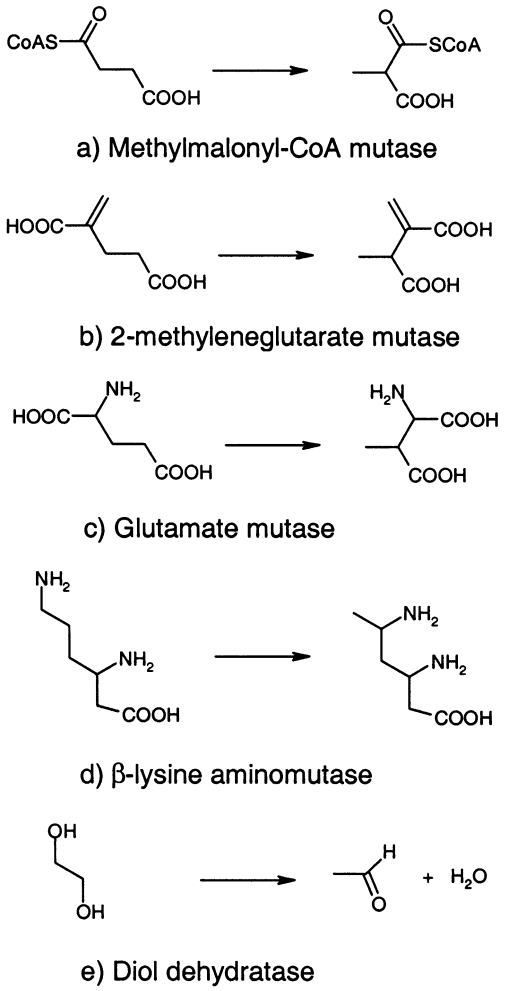

Scheme 17. Radical Rearrangement Step in B_{12}-Dependent Rearrangement Reactions (Corresponding to Step 3 of Scheme 15)

Scheme 18. Different Mechanism Considered for the Radical Rearrangement Step

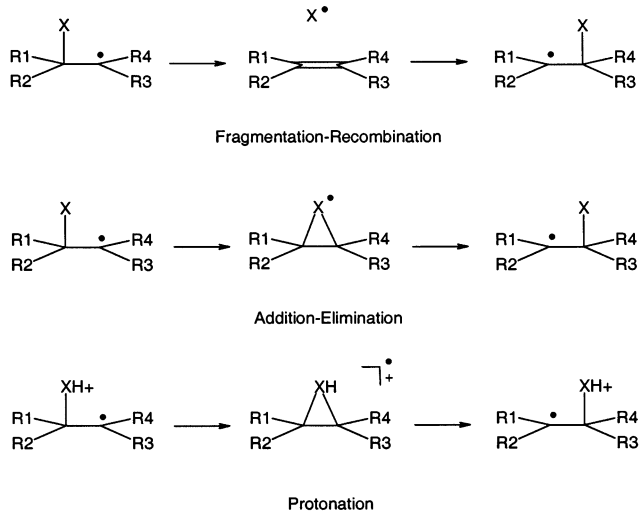

mol needed to elongate the Co−C bond? Andruniow et al. suggest that the electrostatic field generated by polar amino acids in the protein causes electronic reorganization in the Co−C and Co−N bonds, leading to destabilization of the Co−C bond. The evidence supporting this hypothesis are not satisfactory at the moment.

Interestingly, although the position of the axial base does not explain the acceleration in the enzyme, recent calculations indicate that it may have a role in preventing the competitive heterolytic catalysis process.[114]

As seen, the various effects influencing the Co−C bond are far from being fully understood. Many questions remain to be answered and we will undoubtedly see more theoretical studies addressing these issues in the coming few years.

B. Substrate Reactions

The main coenzyme B_{12}-dependent substrate rearrangement reactions that have been studied theoretically are summarized in Scheme 16.[117−130]

According to the mechanism outlined above (Scheme 15), the substrate radical is created by hydrogen atom transfer to the Ado-CH_2• radical (step 2 of Scheme 15). Radom and co-workers have calculated the barrier for the H-atom transfer between models of the substrate and the Ado-CH_2• radical to be ca. 10 kcal/mol,[117] which is quite feasible. It should, however, be remembered that this barrier is to be added to the total cost of the Co−C bond dissociation in order to properly account for the energetics of the system.

Assuming the radical mechanism, the next step is the rearrangement of the radical, as shown in Scheme 17. The various reactions studied computationally differ mainly in the nature of the migrating group X, and less importantly in the nature of the R substituents.

We now briefly present the most important results obtained theoretically on step 3 for each of the systems of Scheme 16.

1. Methylmalonyl-CoA Mutase

Methylmalonyl-CoA mutase catalyzes the transformation of methylmalonyl-CoA to succinyl-CoA (Scheme 16a). In the language of Scheme 17, the migrating group here is a thioformyl-CoA group. Radom an co-workers have performed quantum chemical calculations [G3(MP2)-Rad(p) and B3LYP] to probe the energetics of this transformation.[117−119]

Three different mechanisms for this transfer have been studied, as shown in Scheme 18. In the first, termed the fragmentation−recombination mechanism, a transient fragmentation to form a radical of the migrating group and an alkene takes place. Readdition of the radical to the adjacent carbon center yields the desired product-based radical. This mechanism has been suggested to be the unifying mechanism for all B_{12}-dependent radical rearrangements.[120] The second mechanism, termed the addition−elimination mechanism, involves an intramolecular migration of the group X, with the three-

Table 2. Effects of Hydrogen Bonding on the Barrier (kcal/mol) of the Formyl Group Migration in 3-Propanal Radical[119]

hydrogen-bond donor	gas-phase barrier
no donor	11.2
HF	9.9
NH_4^+	5.9
H_3O^+	2.5
full protonation	2.4

membered ring being either a transition state or a transient intermediate. Finally, the last possibility considered is to protonate the migrating group, thereby giving the transfer a cationic character that will lower the barrier. This proposal is based on very early studies by Golding and Radom, where protonation of the migrating group was shown to yield considerably lower barriers.[121]

Using a sufficiently large model of the substrate (including −COOH and −SH substituents), the energy barrier for the fragmentation−recombination pathway was found to be quite high, ca. 17 kcal/mol, and could hence be ruled out.[118] Next, the barrier for the one-step radical migration in the addition−elimination pathway was calculated to be somewhat lower, on the order of 15 kcal/mol.

Protonation of the migrating group was calculated to give the very low barrier of ca. 8 kcal/mol. The energetic cost of the protonation (effectively the pK_a difference between the proton donor and the substrate radical) should however be added to this value in order to get the true barrier.

The observation that protonation of the migrating group facilitates the reaction led Radom and co-workers to propose that also partial protonation (essentially hydrogen bonding with different strengths) can lead to reduced barriers. In a series of calculations, they let groups with varying acidities hydrogen bond to the migrating carbonyl group in the 3-propanal radical model.[119] The results are listed in Table 2.

The degree of protonation of the substrate (as measured by the acidity of the hydrogen-bonding donor) determines hence the activation of the migrating formyl group. However, as the calculations did not consider the effects of solvation, it is difficult to evaluate exactly how much hydrogen bonding can contribute to lowering the barrier.

2. 2-Methyleneglutarate Mutase

2-Methyleneglutarate mutase catalyzes the interconversion of 2-methyleneglutarate and (*R*)-3-methylitaconate (Scheme 16b). The migrating group here is a vinyl group. The conclusions obtained from the calculations for 2-methyleneglutarate mutase are quite similar to the reaction of methylmalonyl-CoA mutase.[122] That is, the fragmentation−recombination pathway has high barrier (ca 40 kcal/mol), and the addition−elimination pathway has a lower barrier (20.7 kcal/mol). Protonation lowers the barrier considerably (to 2.7 kcal/mol). The overall reaction is endothermic by 12.1 kcal/mol.

3. Glutamate Mutase

Glutamate mutase catalyzes the interconversion of (*S*)-glutamate and (2*S*,3*S*)-3-methylaspartate (Scheme 16c). In contrast to the above-mentioned systems, the migrating group here (aminomethyl) is saturated, which makes the bridged intermediate more difficult to obtain. The calculations by Radom and co-workers favor a fragmentation−recombination mechanism for this enzyme, with a highest calculated barrier of ca. 16 kcal/mol.[123]

4. Aminomutases

Aminomutases catalyze the 1,2-shift of an amino group (the migrating group is hence NH_2). In addition to coenzyme B_{12}, these enzymes require pyridoxal 5′-phosphate (PLP) for catalysis. The main conclusion from the calculations by Radom end co-workers[124,125] is that the PLP, by binding to the migrating amino group of the substrate, converts it to an imine group, which migrates much easier, in line with the results presented above for the other systems. Protonation of the PLP cofactor reduces the barrier further.

5. Diol Dehydratase

Diol dehydratase catalyzes the transformation of 1,2-ethanediol into acetaldehyde and water (Scheme 16e). At first glance, this appears to be considerably different from the other reactions discussed so far for this class of enzymes. However, the proposed mechanism for this enzyme (Scheme 19) involves a step of radical migration similar to the other enzymes. A step of water elimination follows the migration to complete the reactions.

Direct OH transfer in the second step has a high barrier of ca. 26 kcal/mol. Gas-phase protonation of the migrating OH group was found to lead to dissociation into substrate radical cation and water.[126] This led George et al. to propose that this decomposition, after a series of hydrogen atom (alternatively proton) donation and abstraction steps, leads to the desired product.[126] However, this "predissociation mechanism" does not appear to be consistent with ^{18}O-labeling experiments, which require the intermediacy of the 1,1-diol in the dehydration mechanism.

Radom and co-workers[127,128] proposed that a cooperative effect of hydrogen bonding on the migrating and spectator hydroxyl groups (see Scheme 20) lowers the migration barrier considerably. For instance, in the extreme case of A = NH_4^+ and B = NH_3, the barrier is reduced by as much as 25 kcal/mol, down to 1.8 kcal/mol. Again, these are all gas-phase calculations that need to be complemented by solvation effects in order to evaluate the hydrogen-bonding effects.

A very different alternative mechanism that does not involve radical rearrangement and that also accounts for the water elimination was suggested recently.[129] By analogy to a suggestion for the water-elimination step in ribonucleotide reductase,[21] George et al. proposed that water is eliminated without the need to go though the rearrangement step, as shown in Scheme 21.[129] The key component here is a carboxylic acid that facilitates the proton transfer from one hydroxyl group to the other, upon which the water is released. The calculated barrier for this concerted one step mechanism is ca. 10 kcal/mol.

Scheme 19. Proposed Mechanism for Diol Dehydratase

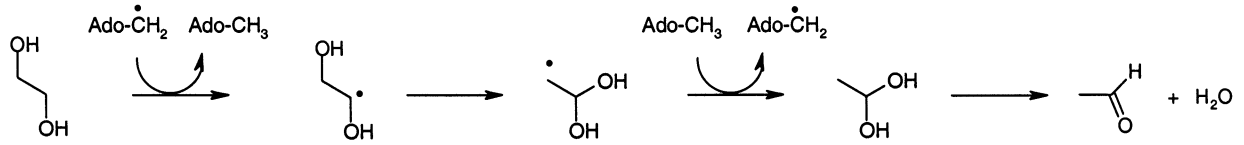

Scheme 20. Synergetic Retro-Push−Pull Mechanism Proposed To Facilitate Hydroxyl Transfer in Diol Dehydratase[128]

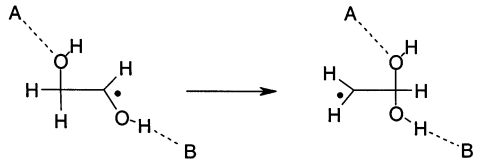

Scheme 21. Alternative Mechanism Proposed for the Rearrangement and Water Elimination Steps in Diol Dehydratase[129]

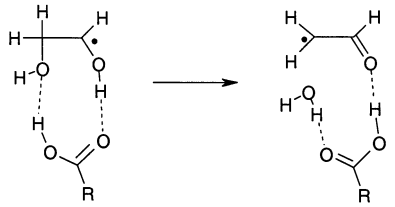

However, as in the case of the predissociation mechanism, this mechanism appears not to be consistent with the ^{18}O-labeling experiments, since it does not involve the 1,1-diol as an intermediate.

VI. Water Oxidation in Photosystem II

Two different tyrosyl radicals have been detected in photosystem II (PSII).[131] One of them, Tyr_Z, is located in the neighborhood of the water oxidizing complex (WOC) and has been suggested to have an important role in this process, while the other one, Tyr_D, is further away. There have also been suggestions of an oxygen-derived ligand radical at the WOC appearing at a critical stage in the dioxygen formation process,[132,133] but this is more debated. The structure of the WOC is still not known, although significant progress has recently been made when a crystal structure from *Synechoccus elongatus* at 3.8 Å resolution was obtained.[134] With this resolution, the electron density suggests a Y-shaped complex containing all four manganese centers previously known to be present in PSII. No Ca ion, which is also known to be essential for water oxidation, could be located at that resolution. Chloride should also be present but was not seen either.

In the water oxidation process, dioxygen is evolved after every four photons absorbed, suggesting at least four intermediates, termed S_0, S_1, S_2, and S_3. In each step, a photon is absorbed by the antenna pigments of the light-harvesting proteins and the energy is transferred to the photosynthetic reaction centers of photosystems I and II. At the reaction center of photosystem II a charge separation takes place, in which the chlorophyll P680 is ionized and the electron is transferred to the quinone Q_A. At this stage, $P680^+$ is rereduced by an electron coming from Tyr_Z located about 7 Å away from the water oxidizing complex. In this process Tyr_Z loses a proton to become a neutral tyrosyl radical.

Scheme 22. Schematic Picture of the Hydrogen Abstraction Scheme (A) and the Electron Transfer Scheme (B) for Tyrosyl Reduction in PSII

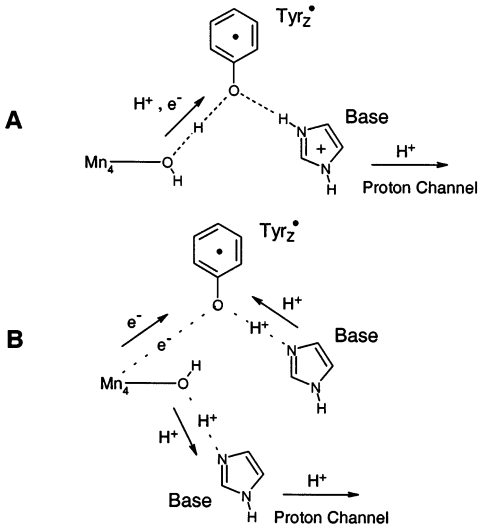

The oxidation and subsequent reduction of Tyr_Z are thus important parts in every S-state transition. A likely scenario for the oxidation of Tyr_Z is that as an electron is transferred to $P680^+$ in the reaction center, a simultaneous proton transfer occurs to a histidine (D1-H190) located next to Tyr_Z. The question of how Tyr_Z is rereduced has been a major issue in the water oxidizing mechanism for several years. There are two leading theories, illustrated schematically in Scheme 22. In the first one, termed the hydrogen atom transfer (HAT) model, both the electron and proton going to tyrosine come from the manganese complex in a concerted single step, and a neutral tyrosine is formed directly.[135−137] The proton transferred in the oxidation step from tyrosine to a nearby base (assumed to be a histidine) is postulated to leave this region through a proton channel toward the bulk (see Scheme 22A). This mechanism has been criticized in favor of the more conventional electron transfer (ET) mechanism,[138−141] as illustrated in Scheme 22B. In this latter case only the electron is transferred from the manganese complex to the tyrosyl radical. This could lead to either a tyrosinate or a neutral tyrosine in which case a proton is transferred to tyrosinate from the nearby base (see Scheme 22B), where it has stayed since the oxidation of the tyrosine. Simultaneously, a proton is transferred from another part of the manganese complex to another base (shown in the scheme as another histidine), for further transport to the bulk.[138−141] In a recent B3LYP study, model calculations were used to elucidate important parts of these mechanisms.[142]

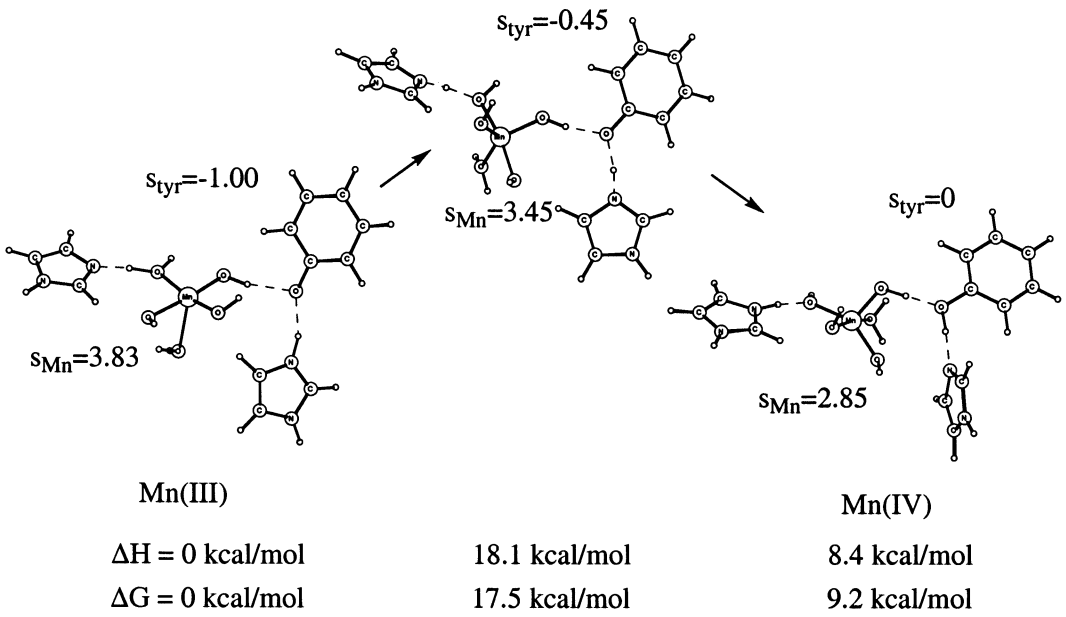

Figure 17. Electron-transfer mechanism in PSII using an imidazole as the extra base.

A mononuclear manganese model complex was used for simplicity in the B3LYP studies. The particular step modeled corresponds to the S_1 to S_2 step, where manganese is considered oxidized from Mn(III) to Mn(IV). The experimentally determined lifetime of the S_1 state, 75−95 μs, corresponds to a free energy of activation, $\Delta G^{\ddagger}$, of 11.8−12.0 kcal/mol for this reaction step, and from the temperature dependence of the reaction rate, an activation energy of only 3−4 kcal/mol has been determined,[138−141,143] indicative of a large tunneling effect. To compare the electron transfer with the hydrogen atom transfer mechanism at an equal level, a common model system with two bases was used. One base is the D1-H190 histidine, which abstracts the tyrosine proton in the oxidation step and which in the electron transfer mechanism is suggested to return the proton to tyrosine in the reduction step. The second base is only needed for the electron transfer mechanism, where it should abstract a proton from a water ligand on the manganese complex when an electron is transferred from manganese to the tyrosyl radical. Without a detailed structure for PSII, another imidazole was arbitrarily chosen for this base, leading to the model shown in Figure 17. An electron transfer transition state was located, having a structure of the manganese complex between the Mn(III) and the Mn(IV) structures, with a spin population of 0.45 on tyrosine. The free energy of activation for this type of mechanism was found to be very high, 17.5 kcal/mol, in rather poor agreement with experiment, with only a small entropy effect of 0.6 kcal/mol, actually decreasing the barrier.

One reason for the high barrier obtained for the electron transfer process is clearly that the reaction is endergonic by 9.2 kcal/mol. This is quite model dependent and the reaction could easily be made less endergonic using a different model of the manganese complex. However, the calculated activation enthalpy for the electron transfer process of 18.1 kcal/mol is still surprisingly high. The possibility that the B3LYP method cannot handle this type of process in an accurate way cannot immediately be ruled out. To test this possibility, Marcus theory for electron transfer was applied to the same model. For this purpose, the system was divided into two parts, the Tyr-His part, containing the phenoxyl radical, hydrogen bonded to a protonated imidazole, and the Mn−His part, containing the $Mn(OH)_3(H_2O)_2$ complex hydrogen bonding to the imidazole base. The activation energy according to Marcus theory is $E_a = (\lambda + E)^2/4\lambda$, where E is the reaction energy and λ is the reorganization energy. The reaction energy E = 8.4 kcal/mol, was taken from the combined system (see Figure 17), and the reorganization energy was calculated separately for the two parts of the system. For the Mn−His part a value of 29.0 kcal/mol for the reorganization energy was obtained using the Mn(III) structure for the Mn(IV) state, and a value of 31.2 kcal/mol was obtained when the Mn(IV) structure was used for the Mn(III) state. For the Tyr-His part a value of 17.9 kcal/mol was obtained for the reorganization energy when the radical structure was used and a value of 17.2 kcal/mol when the nonradical structure was used. Thus, for the forward reaction in Figure 17 the reorganization energy would be 29.0 + 17.9 = 46.9 kcal/mol. This led to a calculated value for E_a of 16.3 kcal/mol according to Marcus theory, in good agreement with the quantum chemical value of 18.5 kcal/mol. Assuming the reorganization energies are well-described, these results indicate that the B3LYP method appears adequate for this process and that there actually is a high barrier for electron transfer for the present model system.

For comparison, the hydrogen atom transfer mechanism was also investigated using the same model with two imidazoles present, and the results are given in Figure 18. The model reaction was found to be endergonic by 3.9 kcal/mol with a free energy of activation, of 10.6 kcal/mol, in good agreement with the experimental value of about 12 kcal/mol. However, the temperature dependence of the rate obtained from the calculations is much stronger than that obtained experimentally with a calculated acti-

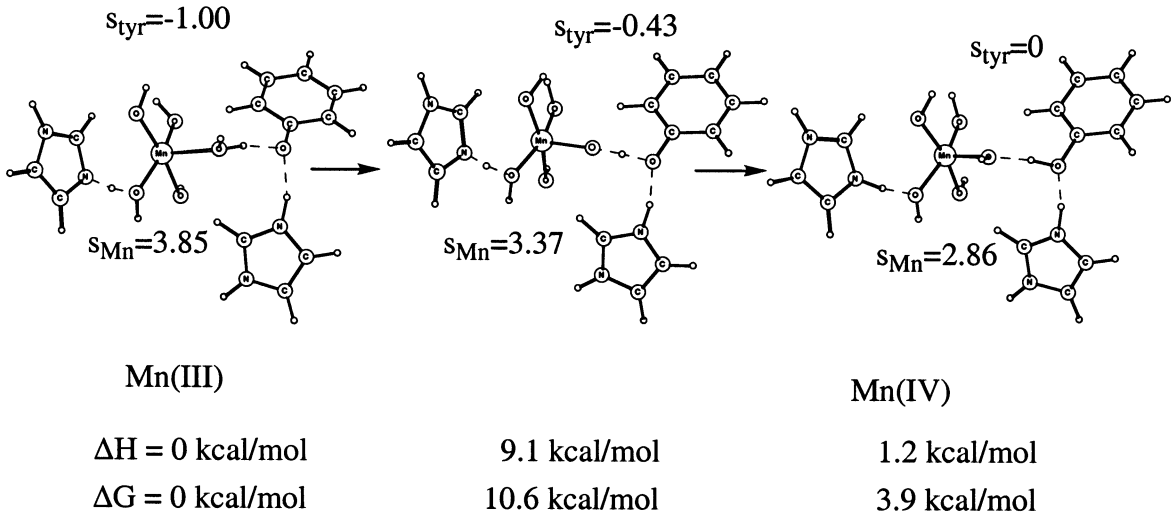

Figure 18. Hydrogen atom transfer mechanism in PSII using the same model as for the electron-transfer mechanism.

vation enthalpy of 9.1 kcal/mol, compared to the experimental value of 3 kcal/mol. Assuming the validity of transition state theory, this would be described as a much too small calculated entropy effect on the barrier. However, the low activation energy could also be due to a tunneling effect, which would require a different computational model. Another factor that could possibly affect the computed results is that the model used gave a slightly endothermic reaction, while in reality it should be slightly exothermic. However, even if such a difference in the reaction energy could affect the barrier height slightly, a large discrepancy between the calculated and experimental temperature dependence would still remain.

The model calculations described above should only be seen as a starting point for more realistic studies of the tyrosyl reduction mechanism. This is a very useful starting point, since transition state structures of this type are extremely difficult to locate but have a tendency not to change very much and can therefore be used for larger models in the future. From the results obtained it is tempting to draw the conclusion that hydrogen atom transfer should be favored over electron transfer also in the actual PSII. However, to draw this conclusion models leading to an exergonic reaction and with manganese clusters having much smaller reorganization energies would have to be used. It should also be remembered that the low-resolution X-ray structure of PSII at present indicates a distance between the manganese cluster and the tyrosyl radical as large as 7 Å,[134] compared to only 4 Å in the above models.

As mentioned above, some experimental and theoretical observations suggest that an oxygen radical ligand is formed in the critical S_3 state in water oxidation. If true, this would be even more central to water oxidation than the formation of a rather distant tyrosyl radical. Several experimental techniques have given results that have been interpreted as a lack of manganese oxidation in the S_2 to S_3 transition. This suggestion has been made using XANES,[132] EPR,[144] and NMR[145] experiments. When the XANES observation was connected with an observed increase of both the short Mn−Mn distances in the WOC, it was suggested that one of the μ-oxo ligands had been oxidized instead of manganese. However, different interpretations have been made using other XANES experiments,[146] which instead indicated that manganese is actually oxidized also in the S_2 to S_3 transition. The experimental situation is thus not clear at present.

The mechanism for water oxidation in PSII has been investigated in several B3LYP studies[133,142,147,148] and has recently been reviewed.[149] The present review will therefore be rather brief on this subject. In the most extensive of these studies,[147] an Mn_3 model including calcium and chloride was used. In setting up this model, information from EXAFS, in particular, and from EPR, NMR, and XANES were used. The recent low-resolution X-ray structure was not known at the time the model calculations were performed. EXAFS experiments[132] have been interpreted to show three Mn−Mn distances, two of them of 2.7 Å and one of 3.3 Å in the S_1 state.[132] A structure consisting of two μ-oxo bridged Mn-dimers linked in some way therefore appears likely. Information concerning the change of these distances from S state to S state is also available from EXAFS. For the Mn_3-Ca model constructed on the basis of these experiments, different O−H bond strengths were calculated, and the resulting structural information was compared to interpretations of EXAFS measurements.[132] Energetically, the most important question is whether there is an O−H bond strength of a coordinated water that is sufficiently similar to the O−H bond strength of tyrosine. This is a necessary condition for both mechanisms described in Scheme 22, since the starting and end points of the Mn cluster are the same in both cases and since each S state starts out with an oxidized tyrosyl radical and ends with a reduced tyrosine. This energetic criterion together with the detailed structural changes are very demanding requirements for a feasible mechanism, and are in fact enough to suggest an entire reaction scheme.

The main step of relevance for the possible oxygen radical formation is the S_2 to S_3 transition. In this critical transition an electron was taken away from the complex and a proton was removed from a water

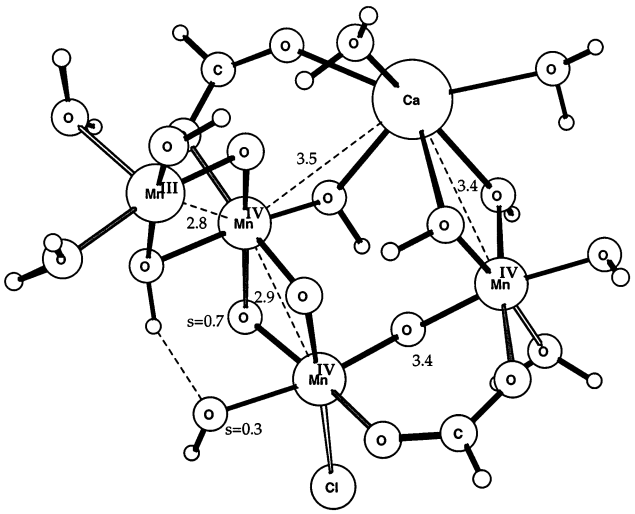

Figure 19. A suggested S_3 state Mn4 model for the water oxidizing complex in PSII. Distances in Å and the oxygen radical spin are marked, as well as manganese oxidation states.

ligand bridging calcium and an Mn(IV) center. A main result found is that a bridging oxygen becomes oxidized in this transition, and the mechanism is therefore termed the oxygen radical mechanism. This result is in line with B3LYP results obtained for a large number of manganese complexes, where it had been found that an oxidation of Mn(IV) to Mn(V) is far too costly in the present type of weak-field complexes. The calculated result thus supports those experiments mentioned above, which were interpreted in terms of a lack of manganese oxidation in this transition. Several different structures where also the fourth manganese center was included in the model have been investigated recently. The one that so far best fits the EXAFS data is shown in Figure 19 in its S_3 state. It can be noted that the radical character is not only located on the bridging oxygen but also to some extent on a terminal hydroxo ligand. However, some of the distance changes for the fourth manganese center do not match EXAFS and there are also minor problems with the energetics. Further investigations of structures of this type are in progress.

VII. Galactose Oxidase

Galactose oxidase (GO) is a mononuclear type 2 copper enzyme that catalyzes the two-electron oxidation of a large number of primary alcohols to their corresponding aldehydes, coupled with the reduction of dioxygen to hydrogen peroxide:

$$RCH_2OH + O_2 \rightarrow RCHO + H_2O_2$$

The protein is a single polypeptide with molecular mass of ca. 68 kDa. To perform the two-electron chemistry, the enzyme utilizes, in addition to the copper center, a protein radical cofactor, which has been assigned to the Tyr272 residue. The protein radical couples antiferromagnetically to the copper ion, resulting in an EPR-silent species.

The crystal structure[150] shows the copper site to be close to the surface with essentially square-pyramidal coordination with Tyr495 in the axial

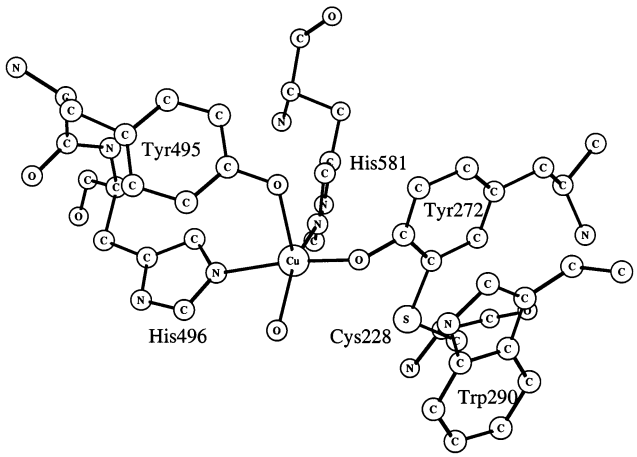

Figure 20. Crystal structure of the active site of galactose oxidase.

position and Tyr272, His581, His496 and a water or acetate to be replaced by substrate in equatorial positions (Figure 20). Furthermore, the Tyr272 residue (the radical site) was found to be cross-linked to a cysteine residue (Cys228) through a thioether bond at the ortho-position to the phenol OH. The Tyr-Cys moiety is π-stacked to a tryptophan residue (Trp290), which also controls entry to the active site. Another interesting feature of the active site is the direct backbone link between the consecutive amino acids Tyr495 in the axial position and His496 in the equatorial position.

The proposed catalytic mechanism for GO is shown in Scheme 23.[151−153] After the substrate binds to the equatorial copper position (occupied by water or acetate in the crystal structures), the first step is a proton transfer from the alcohol to the axial tyrosinate (Tyr495). Next, a hydrogen atom is transferred from the substrate to the modified tyrosyl radical. The resulting substrate-derived ketyl radical is then oxidized through electron transfer to the copper center, yielding Cu(I) and aldehyde product. The two latter steps have been suggested to occur simultaneously in a concerted manner.[154−156] The Cu(I) and tyrosine are, finally, reoxidized by molecular oxygen, regenerating Cu(II) and tyrosyl, and giving hydrogen peroxide as product.

This mechanism has been studied using B3LYP density functional calculations.[157] The two histidines were modeled using imidazoles, the equatorial tyrosine using SH-substituted phenol, whereas the somewhat smaller, but fully adequate, vinyl alcohol served as model for the axial tyrosine. Methanol was used as a substrate. The rest of the phenol ring of the axial tyrosine and the backbone link between it and the equatorial histidine (His496) were included as molecular mechanics atoms, using the IMOMM (integrated molecular orbital/molecular mechanics) hybrid method.[158−161]

It was found that the first step, the proton transfer from the substrate to Tyr495 (step 1 in Scheme 23), occurs with a very low barrier (less than 3 kcal/mol). The exothermicity was calculated to be 3.2 kcal/mol. An important result that came out from the calculations was that the radical site prior to the proton transfer (**1** in Scheme 23) is not the equatorial

Scheme 23. Proposed Reaction Mechanism for Galactose Oxidase

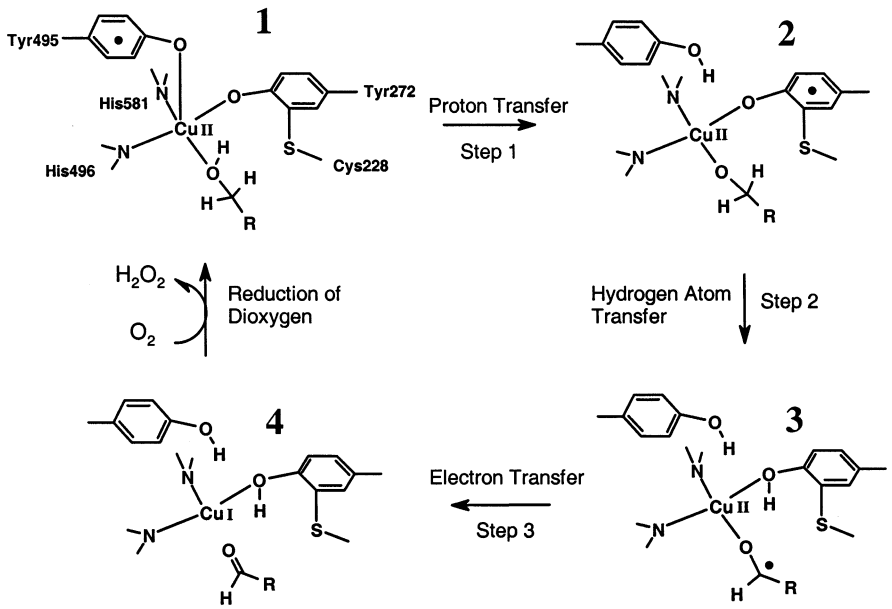

cysteine-substituted tyrosine residue, but rather the axial tyrosine. The axial position is the weakest one in the square-pyramidal coordination of Cu(II), and thus the most natural place for the radical to be in. This was contrary to the accepted picture for the enzyme, but not in conflict with any experiment. In fact, model complex experiments[162] show that the radical is most likely located axially in the non-square-planar coordination of the copper. Also, Car−Parinello calculations by Rothlisberger and Carloni[163] on these model systems and on the GO active site confirm this fact. After the proton transfer, the radical is located at the equatorial tyrosine, implying that, simultaneously with the proton transfer, an electron is moved from the equatorial tyrosine to the axial one.

The second step in the proposed mechanism of GO is a hydrogen atom transfer from the substrate to the Tyr272 radical (step 2 in Scheme 23). Figure 21A shows the optimized transition state structure for this C−H activation step. The barrier was calculated to be 13.6 kcal/mol, which compares well with the known turnover numbers of the enzyme.[164] Hence, the calculations give very strong support to the proposed mechanism.

As seen in Figure 21A, the critical C−H bond has stretched to 1.36 Å at the transition state and the H−O bond to 1.24 Å. At the transition state, one spin is located at the copper (S = 0.49) and the other is shared by both the tyrosine and the substrate (S = 0.15 and S = 0.49, respectively). Consistently with the tyrosyl radical being a π-radical, we note that the hydrogen atom is transferred perpendicularly to the phenol ring plane. Stretching the phenol O−H bond in the plane of the ring would lead to a high-energy σ-radical.

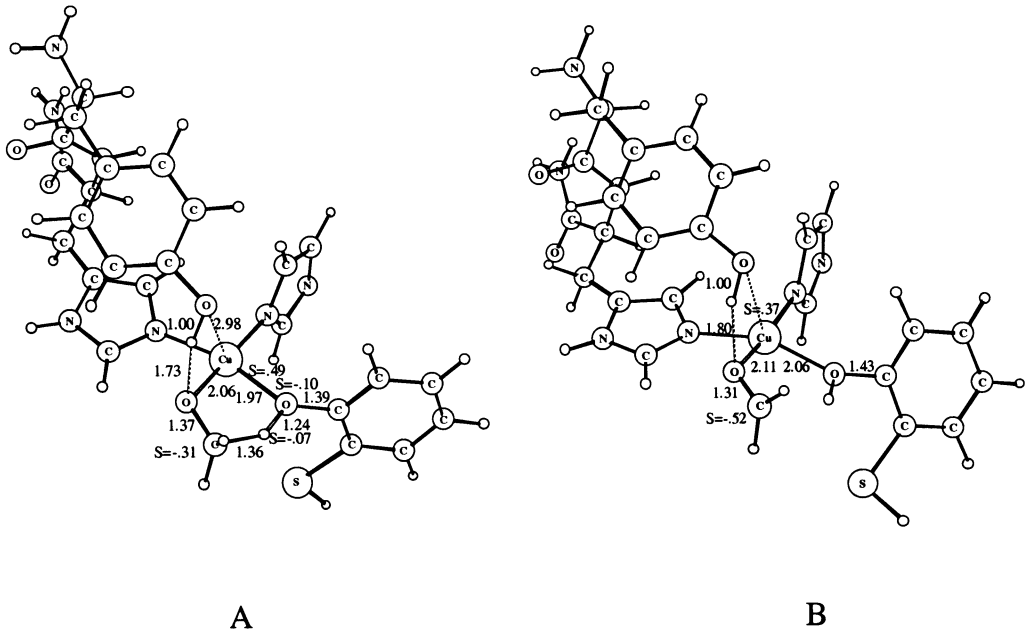

A B

Figure 21. Optimized geometries of (A) the transition state for the proposed rate-limiting hydrogen atom transfer of GO and (B) the ketyl radical intermediate (structure **3** in Scheme 23).

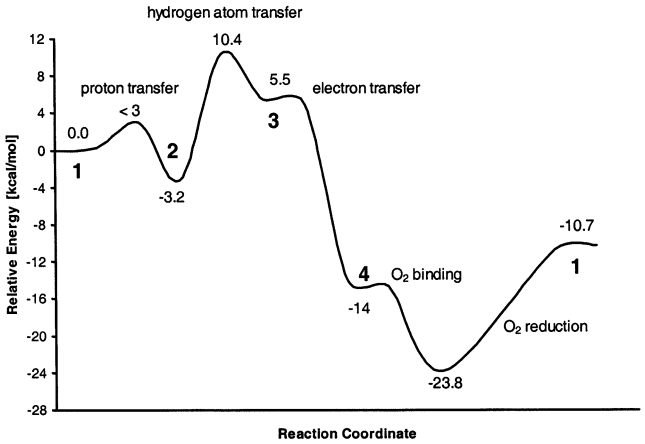

Figure 22. Calculated potential energy surface for the mechanism of galactose oxidase.

The hydrogen atom transfer is proposed to result in a substrate-derived ketyl radical (structure **3** in Scheme 23), which then would be oxidized through electron transfer to the copper center, yielding Cu(I) and the aldehyde product (structure **4** in Scheme 23). This proposed radical intermediate was localized (Figure 21B) at an energy 4.9 kcal/mol lower than the transition state, making the hydrogen atom transfer step endothermic by 8.7 kcal/mol. The intermediate is very unstable, with the barrier for its collapse to the closed shell Cu(I) and aldehyde product being very small. In practice, this radical intermediate is therefore probably impossible to detect.

The ketyl radical intermediate will readily reduce the copper center, yielding Cu(I) and aldehyde. The electron-transfer step was from the calculations estimated to be exothermic by ca. 5 kcal/mol. Energy is instead gained through the binding and one-electron reduction of dioxygen. Assuming the aldehyde product is released at this stage and that dioxygen occupies its coordination position, O_2^- is calculated to bind to copper by 20.6 kcal/mol more than the substrate alcoholate ($-OCH_3$). The calculated potential energy curve for the steps discussed above is displayed in Figure 22.

The role of the Tyr-Cys cross-link has also been studied theoretically. It has been suggested experimentally that this thioether bond is in part responsible for the 0.5−0.6 V lowering of the oxidation potential of this species compared to normal tyrosine.[165] The calculations on the catalytic mechanism were performed with and without the sulfur substitution and gave essentially the same potential energy curve, within ±1 kcal/mol, indicating that the cross-link has small electronic effect on the catalysis. The properties of the sulfur-substituted tyrosine, such as O−H BDE, pK_a, radical hyperfine coupling constants, and *g*-tensors, were also shown to be very similar to those of unsubstituted tyrosine.[166−170]

VIII. Amine Oxidase

Copper-containing amine oxidases (CAO's) form a family of redox-active enzymes that catalyze the oxidative deamination of primary amines by dioxygen to form aldehydes, ammonia, and hydrogen peroxide.[171] Catalysis requires a protein-based *o*-quinone cofactor, 2,4,5-trihydroxyphenylalaninequinone, referred to as topa quinone (TPQ). The crystal structure for yeast Hansenula polymorpha (HPAO) (among other CAO's) has been solved to 2.4 Å resolution.[172] At the active site a Cu atom is coordinated to the imidazole side chains of three histidines and to two water molecules, one equatorial and one axial in a distorted square-pyramidal geometry. The deeply buried TPQ cofactor and copper are in close proximity, but they are not coordinated to each other (see Figure 23). Early experimental studies on the mechanism of the oxidation of the reduced form of the cofactor gave indications for the intermediacy of a semiquinol radical form of the cofactor, and these enzymes have therefore been counted among the protein-radical-containing enzymes. However, the actual observation of the radical semiquinone as a stable intermediate in catalysis has not yet been made. Still, since the cofactor cycles between an oxidized and reduced form, the likelihood of a radical intermediate, more or less stable, is quite high. An advantage of a theoretical approach is that very unstable intermediates can be studied with equal ease as very stable ones. During the past years, several B3LYP studies have been performed on the mechanism of the CAO enzymes, ranging from the biogenesis of the TPQ cofactor[173] to the reductive[174] and oxidative[175] half-reactions. Some of the results obtained, with the emphasis on possible radical intermediates, will be described here.

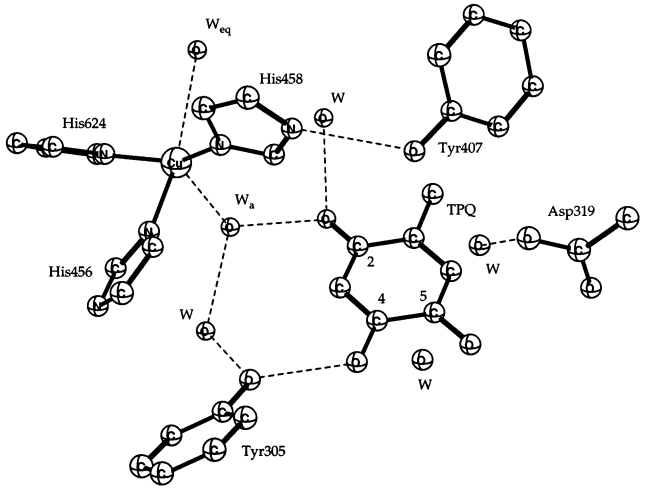

Figure 23. X-ray structure of the active site region of HPAO.

A. Biogenesis of TPQ

The recent B3LYP study of the mechanism for biogenesis of TPQ followed essentially a previously suggested scheme.[176] The starting point for this mechanism is a Cu(II) complex, a tyrosine, and dioxygen. When tyrosine and dioxygen bind to copper, tyrosine will lose a proton. Dioxygen will replace a water ligand and bind equatorially, while tyrosine will bind axially to the copper center. This structure is found to lead to a Cu(II) complex with a superoxo and a tyrosyl radical (see Figure 24). This step is estimated to be endergonic and this intermediate will

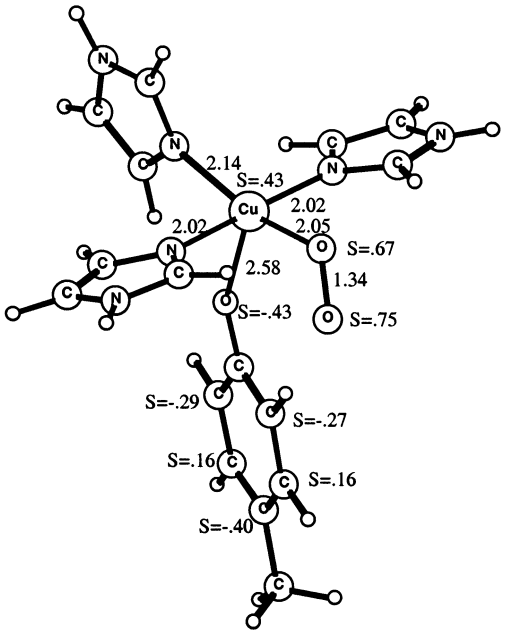

Figure 24. Optimized structure for the Cu(II) complex in copper-containing amine oxidase, for the situation where both tyrosine and dioxygen bind to copper.

therefore be difficult to locate. The axial tyrosyl ligation is quite similar to the one observed in galactose oxidase (see the separate section) and is probably quite general when tyrosine binds to a Cu(II) center. Cu(II)-TyrO•(rad) will in general be lower in energy than Cu(III)-TyrO$^-$. Similarly, Fe(III)-TyrO•(rad) will normally be lower than Fe(IV)-TyrO$^-$, and Mn(IV)-TyrO•(rad) lower than Mn(V)-TyrO$^-$. The spin distribution in Figure 24 shows that the spins on tyrosyl and copper are antiferromagnetically coupled, while the one on the superoxo radical is ferromagnetically coupled to the one on copper. The reverse type of coupling has a substantially higher energy. The reason for this is that the spin population on Cu(II) normally is around 0.5, the spin on tyrosyl 1.0, while the one on superoxo is between 1.2 and 1.7. To combine this to a total spin population of 1.0 is best achieved by the above spin-coupling scheme. The reverse spin-coupling, with an antiferromagnetic coupling between Cu(II) and superoxo, will lead to an unfavorably low spin population on the superoxo ligand.

In the second step of biogenesis, the superoxo ligand attacks the tyrosyl ring and forms a bridging peroxide bond between copper and the phenol. The barrier for this step is 8.4 kcal/mol. At this point the O−O bond cleavage can begin. The computed barrier is 16.7 kcal/mol. As usual in a heterolytic O−O bond cleavage this is accompanied by proton transfers, in this case from the sp^3 carbon of the phenol ring to one of the oxygens of the peroxide. An external water, the one originally bound to copper before O_2 took its place, assists in this proton transfer. At the TS there is only a proton motion and not yet any sign of O−O bond cleavage. This is due to an unusually large exothermicity of 46.0 kcal/mol for this step, which leads to a very early TS. Shortly after the TS is passed, when the proton has reached the peroxide oxygen, the O−O bond distance starts to increase and the reaction goes to the product without any additional barrier. In the next step of TPQ biogenesis, a water molecule attacks the quinone and the hydroxide group adds to the ring while the proton is transferred to one of the oxygens through a few conserved water molecules. A proton on the sp^3-carbon of the quinone is then transferred to the hydroxide on copper using the same water chain. In the final step, two protons and two electrons on the quinone are removed by adding O_2, forming H_2O_2 and TPQ.

B. Catalytic Mechanism

Experiments have shown that the CAO's utilize a two step, ping-pong type mechanism in their catalytic cycle.[177] The process can be formally divided into reductive and oxidative half-reactions, with the reductive half-reaction being

$$E_{ox} + RCH_2NH_2 \rightarrow E_{red} + RCHO$$

and with the oxidative half-reaction being

$$E_{red} + O_2 + H_2O \rightarrow E_{ox} + H_2O_2 + NH_3$$

The mechanism for the reductive half-reaction was studied using the B3LYP functional for the case of pea seedling amine oxidase (PSAO), and the reaction mechanism suggested by the calculations is shown in Scheme 24. It agrees on the most important points with the one suggested by experiments[178,179] but contains more details and energetics. As seen in this mechanism, there are no intermediates suggested with radical character. The proposed mechanism can be briefly described as going over eight steps. The first step is a thermoneutral addition of the amine substrate to the C5 carbon of TPQ, which occurs simultaneously as O5 becomes protonated by Asp300. There is a small barrier of 2.6 kcal/mol for this step. In the second step, there is a proton transfer from the substrate, over an external water and the O5 hydroxyl group to Asp300. This part is endothermic by 5.5 kcal/mol and goes over a barrier of 15.1 kcal/mol. In the third step, the O5 hydroxyl group of TPQ, formed in step one, becomes protonated to form a water molecule. This step goes over a barrier of 8.1 kcal/mol and is exothermic by 8.0 kcal/mol, leading to a product termed the substrate Schiff base, which has been observed experimentally.[180,181] The next steps of the reductive half-reaction are the most critical ones and they became rate-limiting in the model used, in agreement with experiments.[182] In the fourth step, a proton is transferred from Lys296 hydrogen bonded to O4 over to O2 using a hydrogen-bonded chain of two waters and one tyrosine, all of them observed at proper positions in the X-ray structures. This part is endothermic by 8.1 kcal/mol and goes over a barrier of 10.1 kcal/mol. In the fifth step, a C−H bond of the substrate is broken and the O4 of TPQ becomes protonated. The proton is suggested to be transferred over Lys296 in PSAO, while in other CAO's the role of lysine could be taken by a water molecule assisted by an asparagine. This step is strongly exothermic by 28.5 kcal/mol, which helps

Scheme 24. Theoretically Suggested Mechanism for the Reductive Half-Reaction of CAO

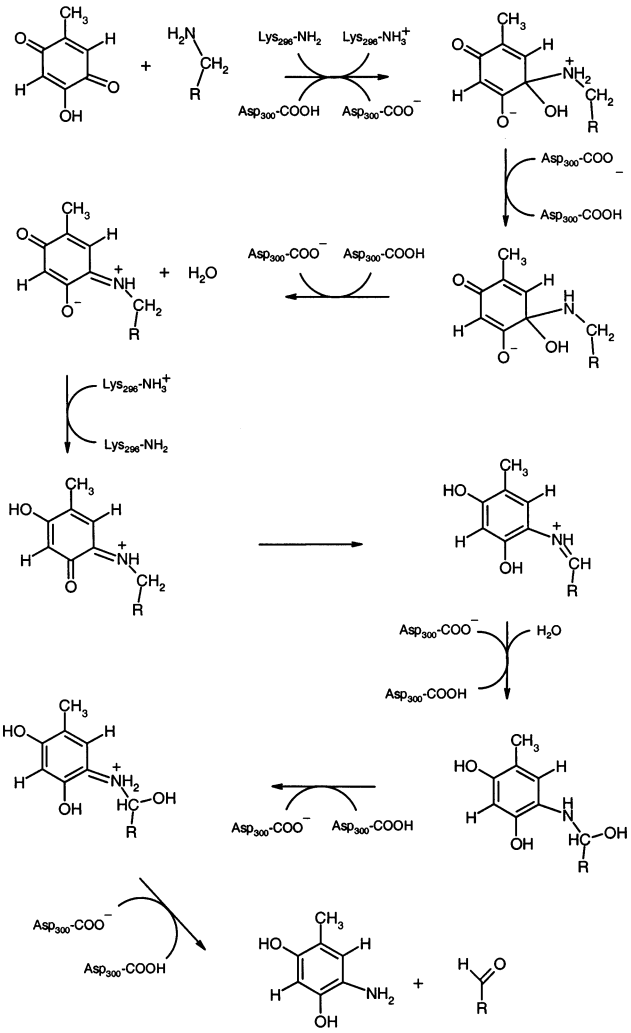

in overcoming the C−H bond cleavage barrier. A large part, 19 kcal/mol, of this exothermicity comes from the aromaticity introduced into the quinone ring. From the resting state, the barrier for C−H bond cleavage is 16.5 kcal/mol. The product is a second Schiff base, which has also been observed experimentally.[183,184] In the sixth step, the substrate is hydroxylated by the water molecule released in step three, and in step seven the substrate is protonated by Asp300. The barriers for step six of 11.8 kcal/mol and for step seven of 10.6 kcal/mol are substantially lower than for the rate-limiting step five. Finally, in step eight the aldehyde is released.

In contrast to the detailed knowledge of the reductive half-reaction, much less is known about the mechanism for the oxidative half-reaction.[185−189] The oxidative half-reaction uses molecular oxygen to recycle the reduced enzyme back to its oxidized resting state accompanied by the release of ammonia and hydrogen peroxide. This half-reaction was studied by B3LYP using similar models as for the reductive half-reaction.

It is in the first step of the oxidative reaction, where dioxygen is reduced, that the likelyhood of finding an intermediate radical is largest. This is also the part that has been most intensely studied experimentally. Of the experimentally suggested mechanisms[176,189] for the dioxygen reduction, the currently favored one[189] can be described as follows. First, dioxygen is suggested to bind at a site near the O2 position of TPQ. Dioxygen reduction is triggered by the first electron transfer from the reduced form of TPQ to the dioxygen, which leads to the formation of the superoxide ion, which may then form a bond to copper. This first electron transfer is suggested to be the rate-limiting step. This conclusion is supported by the negative redox potential of −0.16 V for the formation of the superoxide anion in relation to the estimated potential for TPQ_{sq}/TPQ_{red} of >0.1 V at pH 7.0.[189] Redox potentials of these species in solution suggest that this electron transfer is thermodynamically unfavorable, but the formation of superoxide is proposed to be stabilized by the positive charge on the ($TPQ_{sq}^{+\bullet}$), the neighboring hydrogen bonds and the cupric ion. The rate of electron tunneling from TPQ_{red} to O_2 should be controlled by the unfavorable driving force and the Franck−Condon barrier. This step is then followed by the successive transfers of the first proton, second electron, and second proton, which leads to the formation and release of H_2O_2. The O4 and O2 protons of the cofactor are suggested to be involved in this process.[190] Since an oxygen-18 isotope effect was found but no deuterium isotope effect, the reduction steps where the protons are transferred, are unlikely to be rate-limiting.

To address the role of copper in the dioxygen reduction, important experiments were performed replacing the active site copper by cobalt, nickel, and zinc.[191] Rather unexpectedly, the substitution of copper with cobalt did not change the rate of the reaction. This rules out the possibility that the metal undergoes a valence change from +2 to +1 during the reaction since the redox potential for Co(II) → Co(I) is very different from the one of copper.[192] Another possibility could be that cobalt in its resting state of the enzyme is Co(III) and undergoes a Co(III) → Co(II) valence change during the reaction. This possibility was also ruled out by EPR results, which showed that cobalt in the resting state of the enzyme is Co(II). The Ni(II)- and zinc-substituted enzymes were found to be almost inactive. These results indicate that the copper- and cobalt-containing enzymes use the same mechanism, but that in the catalytic cycle, no formal change in metal oxidation state takes place. The experiments suggest that the rate acceleration due to the metal could be several orders of magnitude.[191,193]

In the B3LYP study of the dioxygen reduction step,[194] an electron was found to be spontaneously transferred from TPQ to O_2 once dioxygen is placed close to O2, in sharp contrast to the experimental suggestion that this should be the rate-limiting step. However, if dioxygen first has to replace an additional water placed close to O2, the electron transfer step could be endergonic. Still, a rate-limiting electron transfer step appears difficult to rationalize from the model calculations. Another possible explanation for the experimental results was therefore suggested. It was pointed out that somewhere along the dioxygen reduction pathway there has to be a

Scheme 25. Theoretically Suggested Mechanism for the Oxidative Half-Reaction of CAO

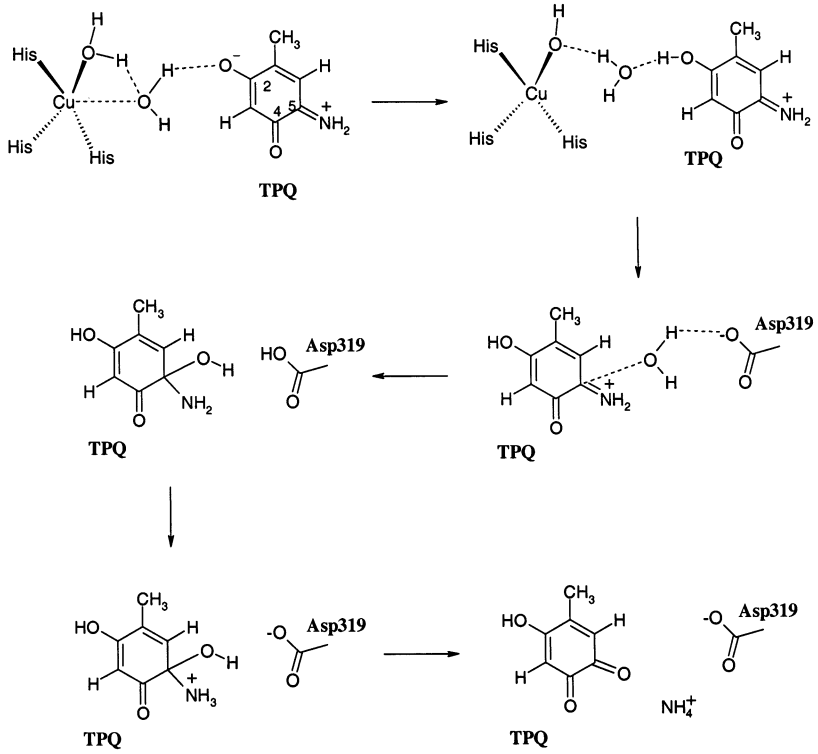

spin-transition, since dioxygen is a triplet and hydrogen peroxide a singlet. The suggestion made was therefore that the spin transition is actually rate-limiting, rather than the electron transfer. The strongest experimental evidence that this might be correct is the different results obtained using different metals as mentioned above. Both Cu(II) and Co(II), which both have a net spin, are active and the reaction rates are almost identical, despite different redox properties. On the other hand, Ni(II) and Zn(II), which lack spin, are both inactive. It therefore appears that the spin of the metal is critical, but not the charge or other redox properties. This is in line with a rate-limiting spin transition where the metal spin would catalyze the reaction by so-called spin catalysis, which is a well-known effect.

The following mechanism for dioxygen reduction in CAO was suggested by the B3LYP calculations.[194] In the first step dioxygen replaces the axial water (W_a) and binds between the O2 and O4 position of the cofactor TPQ. Dioxygen binding is accompanied by an electron transfer from the TPQ to dioxygen, which leads to the creation of a Cu(II)···O_2···M^+(rad) system, where M^+(rad) represents the semiquinol form of TPQ. This step is suggested to be slightly endergonic. After the electron-transfer step, the O_2^-(rad)···M^+(rad) radical pair produced is still in a triplet state. In the next step, the superoxide crosses over a barrier of 8.2 kcal/mol and binds to copper. This step is endothermic by 2.6 kcal/mol. Once the Cu−O_2^-(rad) bonded species is formed, a proton transfer from O2 and a hydrogen atom transfer from the O4 site of the cofactor take place in a concerted manner. This concerted $2H^+ + e^-$ transfer leads to the formation of singlet H_2O_2 and the triplet form of the cofactor TPQ. Due to the formation of the triplet TPQ, this step is quite endothermic by 12.9 kcal/mol. At this point a Cu(doublet)···TPQ(triplet) species is thus formed. After the formation of this species, a spin transition takes place, due to the weak exchange between Cu and TPQ, and singlet TPQ is formed. This step is calculated to be exothermic by 29.1 kcal/mol. On the basis of the model calculations and the above experimental observations, the presence of a paramagnetic metal can be implicated in the triplet to singlet spin transition in the cofactor TPQ, and this step is suggested to be the rate-limiting step of the entire oxidative half-reaction. Since the unbound O_2 state is the resting state for the rate-limiting spin transition, the large oxygen isotope effects found experimentally can be rationalized in terms of a large change of bond order.[189]

The remaining steps of the oxidative half-reaction are shown in Scheme 25 and can be described in the following way. In the first step, the TPQ cofactor is protonated at the O2 position by a water ligand on the copper complex. This step is endergonic by 1.8 kcal/mol and passes over a barrier of 5.4 kcal/mol. In the second step, an activation of a water molecule takes place, which is found to be endergonic by 6.1 kcal/mol and passes over a barrier of 14.4 kcal/mol. In the third step, a proton transfer from the O5 hydroxyl group to the NH_2 group at the O5 position of the TPQ leads to a covalently bound NH_3^+ group. This step has a barrier of 11.8 kcal/mol and is exergonic by 4.90 kcal/mol. Since this step follows two steps that together are endergonic by 7.9 kcal/mol, the overall barrier for this step is 19.7 kcal/mol. In the last step a proton abstraction by Asp319 triggers the release of the ammonium ion with a simultaneous formation of a neutral topaquinone and unprotonated Asp319. This step has a barrier of 6.0 kcal/mol and is exergonic by 7.5 kcal/mol.

Scheme 26. Catalytic Mechanism of CCP

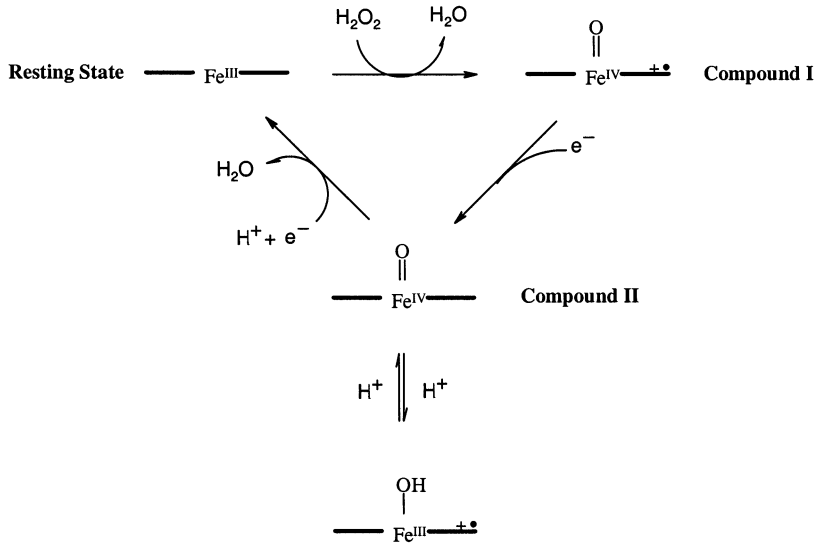

The conclusion from the B3LYP studies of the catalytic mechanism of CAO concerning the presence of intermediate radicals is that they only appear as unstable intermediates in the dioxygen reduction step and that they therefore probably will be difficult to detect.

IX. Cytochrome c Peroxidase

Heme-containing peroxidases are enzymes that can oxidize a variety of substrates by reacting with hydrogen peroxide. For most peroxidases the typical substrates are small aromatic molecules. An exception is cytochrome *c* peroxidase (CCP) found in the mitochondria electron transport chain, which has a protein, cytochrome *c*, as its redox partner. The mechanism for heme peroxidases is relatively well established (see Scheme 26) and was therefore a suitable target for the first study ever performed using DFT on an O−O bond cleavage in a redox-active enzyme.[195]

The first step of the catalytic cycle is the cleavage of the O−O bond of hydrogen peroxide and leads from the resting ferric state to an oxyferryl state with a simultaneous formation of a radical. For the majority of the peroxidases, the radical is located on the porphyrin of the heme, giving the intermediate known as compound I (see also the section on cytochrome P450s). However, in CCP the radical center has been determined to be Trp191, which is connected to the heme via the hydrogen-bonded His-Asp-Trp triad.[196] The reason for the positioning of the radical at this site rather than the porphyrin is not fully understood. Since CCP is an electron-transfer protein, it might have been expected that mutating Trp191 for a phenylalanine would make electron-transfer less efficient, but this did not turn out to be the case.[197]

The large similarities between the active sites of different heme peroxidases indicate a common reaction mechanism for O−O bond cleavage in these enzymes. The roles of the different amino acids around the heme have been studied using site-directed mutagenesis. For both CCP[198] and HRP (horseradish peroxidase)[199] it has been shown that in the distal region His52 is the most important residue and therefore needs to be included in a model of the O−O bond cleavage in CCP. The direct ligands to iron, the porphyrin, and the proximal histidine are obviously also needed in the model. It might be thought that the entire proximal His-Asp-Trp triad mentioned above must be included in the model, since a Trp radical is found after the reaction. However, a strong indication that the proximal tryptophan does not need to become oxidized in the actual O−O bond cleavage process is that the reaction rate for compound I formation in HRP has been found to be very similar to the rate obtained for CCP, even though HRP has a phenylalanine at the position for Trp191 of CCP. The O−O bond cleavage was therefore modeled without Asp235 and Trp191. In a second step of the modeling performed, the formation of the radical on Trp191 was studied using a model where the triad was included but without the distal histidine instead (see below).

The optimized transition state for O−O bond cleavage in CCP is shown in Figure 25 for a slightly larger model than the one used in the original study. The formation of this TS is preceded by a step where the proton on the hydrogen peroxide is transferred to the distal histidine forming an Fe(III)−OOH peroxide. The protonated histidine then moves slightly to be able to deliver the proton to the other oxygen of the peroxide during the O−O bond cleavage. This TS was obtained in the original study as a crossing between a doublet and a quartet potential surface. It is not obtained by an actual optimization using a Hessian, since this was not possible at the time. It has since then been shown that the two procedures lead to very similar transition states. For the larger model in the figure, the critical O−O and O−H distances were frozen from the smaller model and the rest of the structure was fully optimized.

The mechanism for O−O bond cleavage of hydrogen peroxide in heme peroxidases is very similar to the last two steps for the one of dioxygen in heme oxidases. The first part is obviously different, since

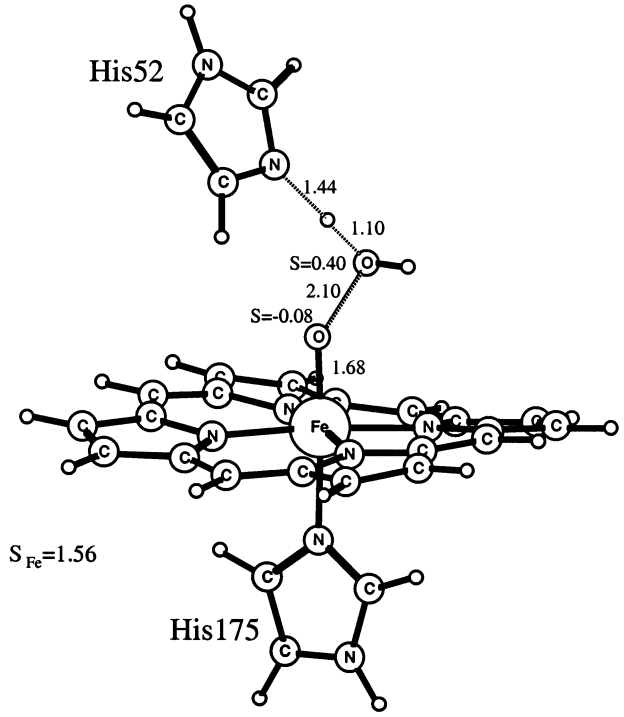

Figure 25. Approximate transition state for O−O bond cleavage in cytochrome *c* peroxidase (CCP).

only two electrons are needed to cleave the peroxide rather than four for dioxygen. This means that the oxidases have to start from Fe(II) rather than Fe(III) and that an additional electron is needed from the outside for the oxidases. For the cytochrome P450 enzymes a reductant outside the active site supplies the electron, while for cytochrome *c* oxidase this outside electron comes from Cu_B, which is also part of the bimetallic active site. One of the last two electrons needed for the O−O bond breaking comes from Fe(III) for both peroxidases and oxidases. The immediate source of the fourth electron is the porphyrin for both the peroxidases and for most oxidases. For CCP, the final position for the nonmetal radical is the Trp191, as mentioned above. The protons needed for the O−O bond cleavage in the heme peroxidases are supplied by the substrate hydrogen peroxide, while in the cytochrome P450 enzymes there is an outside proton source.

To get the proper spin distribution of compound I in CCP, a larger model than the one in Figure 25 was needed. Since the radical experimentally is found on Trp191, this residue is also needed in the model as well as His175 and Asp235, linking Trp191 to the heme group. On the other hand, the distal amino acids, important for the formation of compound I, are not likely to play any role for the spin distribution in the product. The final geometry obtained for the best model used for compound I is shown in Figure 26, together with important distances and spins. The structure was optimized for the quartet state, which is nearly degenerate with a doublet state. Two of the spins are in the Fe=O moiety, which has an electronic structure similar to the dioxygen molecule, with two unpaired spins in the antibonding π-orbitals. These two spins are weakly coupled to the third spin, which in the model is delocalized over the

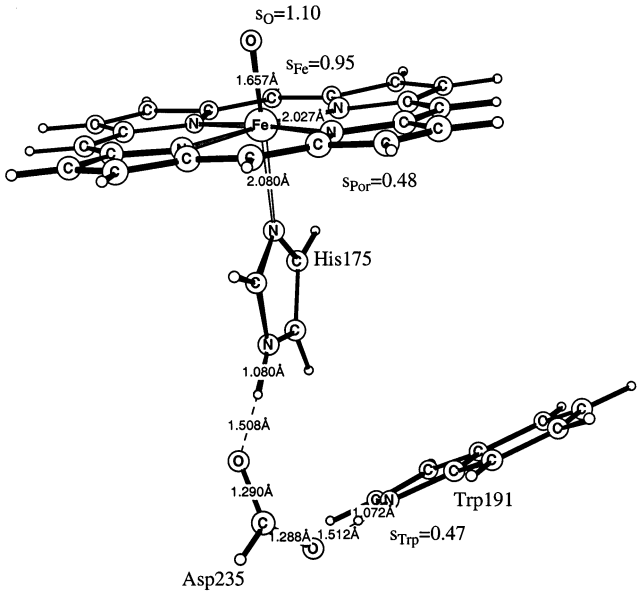

Figure 26. Optimized structure for compound I of cytochrome *c* peroxidase (CCP).

porphyrin and the tryptophan, with spins of 0.48 and 0.47, respectively. The result is thus at least partly in agreement with experiments, with spin on the tryptophan. However, the precise spin distribution is quite dependent on details of the models used, such as the presence of hydrogen bonds, exactly like in cytochrome P450, where the spin can be delocalized on the proximal cysteine.[200] This sensitivity means that the energy only depends weakly on the amount of spin delocalization, which also means that this property is not very significant for the chemistry, at least to the accuracy available from the B3LYP functional.

An interesting general question is whether the proton stays on the tryptophan radical. The result from the optimization was that the proton distance is 1.07 Å to the indole nitrogen and much longer, 1.51 Å, to the carboxylate group, which is in agreement with experiments that have indicated a cationic tryptophan radical.[15]

It could be argued that the determination of the position of a proton could be quite uncertain using the above gas-phase models, and that ideally a QM/MM model should have been used. However, in the present case where the gas-phase model favored the charge separated Asp^--Trp^+ system, the introduction of the protein is only expected to make this state even more stable. Instead, it is more important to use a model that correctly represents the resonance effects. These resonances are quite important, as can be seen on a comparison of the gas-phase proton affinities of the indole and pyrrole radicals, which differ by 8.7 kcal/mol in favor of the indole. It is furthermore of interest to note that the gas-phase phenol radical has a proton affinity that is 23.6 kcal/mol smaller than the one of indole, which explains why tyrosyl radicals are generally found to be neutral and tryptophan radicals cationic in enzymes.

X. Cytochrome P450s

Cytochrome P450s are an important class of heme iron enzymes that act as mono-oxygenases in steroid

Scheme 27. Rebound Mechanism for Alkane Hydroxylation by Cytochrome P450s

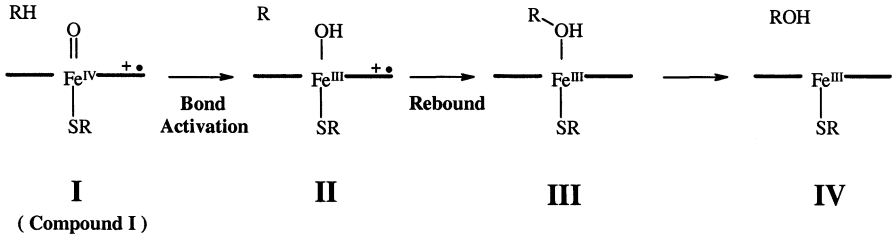

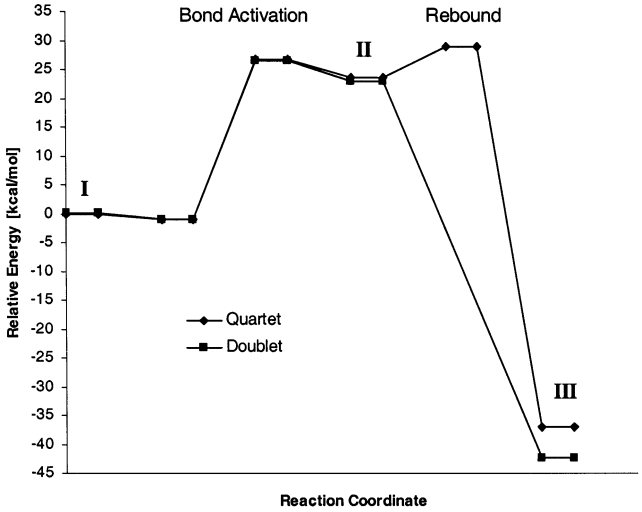

Figure 27. Calculated potential energy surfaces for the rebound mechanism of cytochrome P450s.[202,203]

biosynthesis and metabolism of toxic hydrocarbons.[201] Although not experimentally observed yet, the active oxidant in P450s is believed to be, as in cytochrome *c* peroxidase, the high-valent oxoiron(IV) compound I species (**I** in Scheme 27).

Various aspects of the electronic structure and reactivity of the P450 compound I have in the past few years been addressed computationally using density functional theory.[202−215] A very recent review by Shaik and co-workers describes this work.[200] Here, we briefly mention the most important energetic results concerning the alkane hydroxylation and alkene epoxidation mechanisms.

A. Alkane Hydroxylation

The most plausible mechanism for alkane hydroxylation is the so-called rebound mechanism proposed by Groves[216−219] (Scheme 27). In this mechanism, compound I first abstracts a hydrogen atom from the substrate, creating a substrate radical and a ferryl−hydroxo intermediate. This is followed by a rebound step, in which a ferric alcohol is formed. The alcohol product is then released, restoring the resting state.

Shaik and co-workers have in a number of studies used DFT techniques to examine various aspects of this alkane hydroxylation mechanism.[202,203]

The potential energy surface for the rebound mechanism with methane as a substrate was calculated for two spin states, the high-spin (HS) quartet state and the low-spin (LS) doublet state (See Figure 27). For the bond-activation step, the two spin states were shown to be nearly degenerate, with a calculated barrier of ca. 27 kcal/mol and endothermicity of ca. 24 kcal/mol. For the following rebound step the degeneracy is broken. The high-spin state was found to have a barrier for rebound of ca. 5 kcal/mol, while on the low-spin surface the rebound was found to be barrierless.

Yoshizawa and co-workers, using very similar methods, reported recently optimized rebound transition state structures for the HS quartet surface as well as the LS doublet surface, using ethane as a substrate.[215a] The barrier height from the intermediate was calculated to be ca. 5 kcal/mol, and the two spin states were found to be nearly degenerate along the whole reaction coordinate. However, using camphor as a substrate,[215b] the barriers dropped to 3.3 kcal/mol for the quartet state and 0.7 kcal/mol for the doublet state, but the quartet surface is now lower than the doublet surface.

This different behavior of the two spin surfaces obtained by Shaik and co-workers was proposed to explain recent ultrafast radical clock results by Newcomb and co-workers.[220]

The radical clock probes contain a cyclopropane ring with a methyl attached. On the fastest clocks a phenyl group is also attached to the ring. In a hydrogen atom abstraction scenario, a hydrogen atom on the methyl group should be easiest to abstract. When this happens, the cyclopropane ring will very quickly and irreversibly open, due to resonances in the ring. The amount of radical formation through hydrogen abstraction should therefore be mapped by the amount of products with open cyclopropane rings. In the case of P450, the product alcohols were found to have only a very low fraction (usually less than 5%) of open rings. The conclusion was therefore originally that a radical mechanism was ruled out for the majority of the reactions, which were considered to work by a concerted mechanism instead.[220] The model calculations by Shaik et al. suggest a somewhat different explanation. Their transition state for the first bond activation step is one of a pure hydrogen abstraction, thus leading to radical formation. However, since the barrier for the rebound step is zero, the reaction is suggested to proceed so fast that the cyclopropane ring would not have time to open. For the high-spin surface, on the other hand, the barrier is sufficiently high to actually lead to radicals stable enough to have time to open their cyclopropane rings before the rebound step. The reactions occurring on the high-spin surface would thus explain the presence of the small amount of ring-opened products. A key feature of the potential surfaces in this scenario is therefore the relative size of the barriers for the rebound step on the high- and low-spin surfaces.

Scheme 28. Mechanism for Alkene Epoxidation by Compound I in Cytochrome P450s

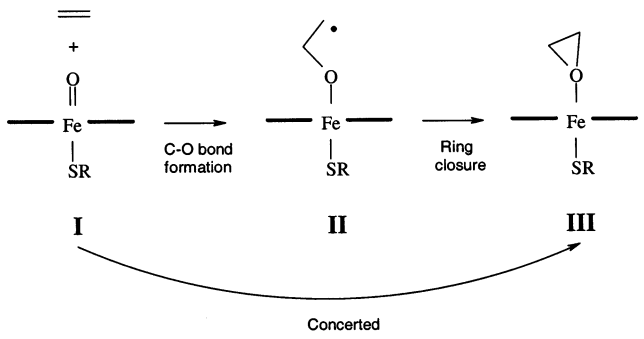

Another explanation for the radical clock results was suggested on the basis of a B3LYP study of methane monooxygenase,[8,221] for which radical clock experiments show a very similar picture as the one in P450. It was first shown that the radical clock probes have very low ionization potentials, which means that they can easily lose an electron to the highly oxidized iron center. This is therefore suggested to occur very early in the rebound step. If this happens, the ring-opened radical clock probes are no longer irreversibly ring-opened but can close again, as demonstrated by the calculations. With this mechanism, the amount of ring-opened products does therefore not depend on how fast the reaction is, unlike the mechanism of Shaik et al. Instead, the amount of ring-opened products should be determined by which atom on the radical probe is hydroxylated, which in turn will depend mainly on the dynamics but also to some extent on the charge distribution of the cationic clock probe after ionization. Dynamics will strongly favor the ring-closed products, since the methyl carbon will be very close to the hydroxyl group and the reaction is quite exothermic.

B. Olefin Epoxidation

Shaik and co-workers also studied the mechanism of ethene epoxidation performed by compound I (Scheme 28).[206−208] It was found that starting from either the HS or the LS states of compound I, the barrier for the C−O bond formation leading to the radical intermediate **II** is 14−15 kcal/mol in an almost thermoneutral step.[206] From there, the LS state forms the epoxide **III** without a barrier (<0.3 kcal/mol), while the HS state has a barrier of ca. 3 kcal/mol. The LS reaction is hence "effectively concerted", while the HS is stepwise. It was furthermore found that the true concerted reaction (**I → III**) has a barrier only ca. 4 kcal/mol higher than the stepwise reaction in the HS state.[207]

From **II**, a competing suicidal reaction, in which the carbon radical center reacts with a nitrogen atom of the heme, was identified.[208] The barrier for this was calculated to be less than 10 kcal/mol.

XI. Cytochrome c Oxidase

The enzyme that catalyzes respiratory oxygen reduction is cytochrome *c* oxidase (CcO), located in the mitochondrial or bacterial membrane in all aerobic organisms. Through the respiratory chain, electrons are transferred to a dimeric copper site (Cu_A) and then on to a low-spin heme (heme a). Transfer from heme a to the binuclear center, comprising a heme (heme a_3) and a copper complex (Cu_B), prepares the enzyme for O_2 reduction. Protons are available to the binuclear site from two channels, the K and the D channels. The exergonic reduction of O_2 is coupled to proton translocation across the membrane, resulting in a proton gradient, which is used to produce ATP. The overall reaction for the reduction of dioxygen is

$$O_2 + 4H^+ + 4e^- \rightarrow 2H_2O$$

indicating that it occurs in four separate steps, just like the formation of O_2 in PSII. At the same time four protons are translocated across the membrane in CcO.

Cytochrome *c* oxidase has not until recently been considered as a radical enzyme. However, the work of several groups have strongly implicated the presence of protein free radicals at the highest oxidation level of CcO.[222] The key experiment was one where no outside electrons were allowed to enter the binuclear site at the stage of the dioxygen cleavage process, by preparing the enzyme in a so-called mixed-valence state. The experiment showed that the O−O bond could still be cleaved. Three of the four electrons required for the cleavage are easy to identify. Two of them come from iron, which becomes oxidized from Fe(II) to Fe(IV), and a third one comes from copper, which is oxidized from Cu(I) to Cu(II). The two main alternatives for where the fourth electron comes from are the porphyrin and Tyr244 at the active site. A porphyrin is known to donate an electron in the O−O bond cleavage in P-450 and in some heme peroxidases, and a tyrosyl radical appears in PSII in the process of making the O_2 bond (see other sections). Since optical spectroscopy shows that the porphyrin is not ionized, the suggestion was that the fourth electron comes from the tyrosine.[222] A striking point in this context is that this tyrosine is cross-linked to a histidine bound to Cu_B, which suggests that radical chemistry has occurred.

In the B3LYP studies performed for the O−O bond cleavage in CcO, increasingly larger models have been used.[223−225] Only the most recent model will be discussed here. The starting points for these studies were the X-ray structures, which exist for both a mammalian[226] and a bacterial[227] cytochrome *c* oxidase. The optimized transition state for O−O bond cleavage in the largest model used is shown in Figure 28. There are two main results from the model studies. The first one is that a proton needs to be transferred to the peroxide to achieve a reasonable barrier. Second, and rather surprisingly, this proton cannot come from tyrosine. All attempts to transfer a proton from tyrosine before or during the O−O bond cleavage led to much too high barriers, of at least 25 kcal/mol. The experimental free energy barrier is only 12 kcal/mol (the lifetime of the peroxide is 200 μs).[228] This result essentially also rules out the tyrosine as the immediate electron donor in the O−O bond

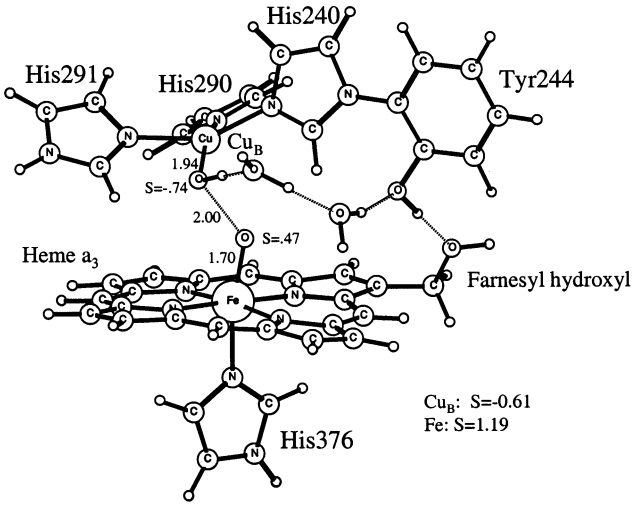

Figure 28. Approximate transition state for O−O bond cleavage in cytochrome *c* oxidase (CcO).

cleavage. Two main alternatives have then been considered for the origin of the peroxide proton. In the first alternative, leading to the transition state in the figure, the peroxide proton comes from one of the proton channels. On the basis of experiments, the K channel is the more likely channel. This channel enters the binuclear site at the farnesyl hydroxyl group on the porphyrin (see the figure). Due to strong resonance effects in the porphyrin ring, this position has a rather large pK_a. The proton should then travel via the tyrosine over a chain of water molecules to the peroxide. Since the protonated peroxide has not been observed, this proton transfer has to be assumed to be slightly endergonic. When the proton reaches the peroxide, the O−O bond cleavage starts. At the TS, the O−O bond length is about 2.0 Å. This geometry was reached both from complete optimizations (using Hessians) for smaller models and from a pointwise search using the large model. The spins on the oxygens at the TS are −0.74 and +0.47. The spins on iron and copper are 1.19 and −0.61, respectively, showing that these centers are antiferromagnetically coupled. To reach this TS, an electron from iron has been transferred to the O−O antibonding σ^* orbital of the peroxide. This electronic structure actually leads to a weak minimum shortly after the TS. At this point another electron is transferred to the O−O σ^* orbital to complete the bond cleavage. In the model shown in the figure, this electron comes from the porphyrin to create an initial product similar to compound I of P450 and some heme peroxidases (see other sections).

As a final step, it has been investigated using similar models whether an electron can move from the tyrosine to the porphyrin radical cation. The calculations support the possibility that the final product could be a tyrosyl radical, as proposed on the basis of experiments. However, the calculations also suggest that the tyrosyl radical is formed only after the O−O bond cleavage is completed, in contrast to previous proposals.

XII. Summary and Outlook

The present review has tried to cover most work performed so far using high-accuracy quantum chemical methods on mechanisms for radical-containing enzymes. Since these types of calculations hardly existed 5 years ago, the development has been quite rapid. Still, in terms of the development of chemical models to treat these reactions, this field has not settled and a continued progress at the same rate is to be expected. New programs containing new possibilities are constantly being produced, and computers are getting cheaper. One direction of the development of chemical models will undoubtedly be toward QM/MM models, where only the inner active site part of the enzyme is treated using quantum chemistry. A large part of the rest of the enzyme is then treated using molecular mechanics. Already a few QM/MM applications on redox-active enzymes have appeared.[213,229,230] However, it is highly unlikely that this methodology will take over entirely, since QM/MM applications require much longer computer times. It is also much more difficult to avoid mistakes and pitfalls in a QM/MM application than in the type of calculations described above. Much experience will be required to avoid falling into local minima and to learn how to optimally cut the enzyme into the QM and MM parts.

In terms of the electronic structure method being used in the applications, the situation appears much more settled. Almost all of the applications reviewed here have used DFT with the hybrid B3LYP functional. Although one could possibly foresee a better empirical parametrization of the hybrid functional, this is hardly going to have a major impact in this area. The problems encountered are seldom in terms of an insufficient accuracy of the quantum chemical treatment, but much more often in the choice of mechanism and chemical model. Pure ab initio type methods of coupled cluster type, for example, are still far too slow to be competitive in this area other than for benchmarking on small systems, and this will probably remain true for the next decade.

A pattern clearly seen in the applications performed so far, which is worth pointing out, is that finding the right enzyme mechanism will generally require several years of gradually refined computational modeling. Typical examples are photosystem II, cytochrome *c* oxidase, and ribonucleotide reductase, where model calculations have appeared stretching over the entire 5-year period from the first study until now. Even if the value of some of the results might be questioned, seen over the whole period there has been a remarkable progress.

XIII. Abbreviations

AA	arachadonic acid
AO	amine oxidase
ARNR	anaerobic ribonucleotide reductase
BDE	bond dissociation energy
BSS	benzylsuccinate synthase
CcO	cytochrome *c* oxidase
CCP	cytochrome *c* peroxidase
CoA	coenzyme A
DFT	density functional theory
EA	electron affinity
ENDOR	electron nuclear double resonance
EPR	electron paramagnetic resonance
ET	electron transfer

EXAFS	extended X-ray absorption fine structure
GO	galactose oxidase
HAT	hydrogen atom transfer
HPAO	hansenula polymorpha amine oxidase
HRP	horseradish peroxidase
HS	high spin
IMOMM	integrated molecular orbital/molecular mechanics
LS	low spin
MMO	methane monooxygenase
PES	potential energy surface
PFL	pyruvate formate lyase
PGG_2	prostaglandin endoperoxidase G_2
PGH_2	prostaglandin endoperoxidase H_2
PGHS	prostaglandin H synthase
PLP	pyridoxal 5′-phosphate
PSII	photosystem II
PT	proton transfer
PSAO	pea seedling amine oxidase
QM/MM	quantum mechanics/molecular mechanics
RNR	ribonucleotide reductase
TPQ	topa quinone
TS	transition state
WOC	water oxidizing complex

XIV. Acknowledgments

We thank the following persons for helpful discussions and for making manuscripts available prior to publication: Prof. Margareta Blomberg, Prof. Sason Shaik, Prof. Feliu Maseras, Prof. Leo Radom, Prof. Kazunari Yoshizawa, Rajeev Prabhakar, Vladimir Pelmenschikov, Kyung-Bin Cho, and Mattias Blomberg. The Wenner-Gen Foundations is acknowledged for financial support (F.H.).

XV. References

(1) Hohenberg, P.; Kohn, W. *Phys. Rev. B* **1964**, *136*, 864.
(2) Becke, A. D. *Phys. Rev.* **1988**, *A38*, 3098.
(3) Becke, A. D. *J. Chem. Phys.* **1992**, *96*, 2155.
(4) Becke, A. D. *J. Chem. Phys.* **1992**, *97*, 9173.
(5) Becke A. D. *J. Chem. Phys.* **1993**, *98*, 5648.
(6) Siegbahn, P. E. M.; Blomberg, M. R. A. *Annu. Rev. Phys. Chem.* **1999**, *50*, 221.
(7) Siegbahn, P. E. M.; Blomberg, M. R. A. *Chem. Rev.* **2000**, *100*, 421.
(8) Siegbahn, P. E. M.; Blomberg, M. R. A. *J. Phys. Chem. B* **2001**, *105*, 9375.
(9) Siegbahn, P. E. M. *Quart. Rev. Biophys.* **2003**, in press.
(10) Ehrenberg, A.; Reichard, P. *J. Biol. Chem.* **1972**, *247*, 3485.
(11) Voet, D.; Voet, J. G. *Biochemistry;* J. Wiley and Sons, Inc.: New York, 1995.
(12) Reichard, P. *Science* **1993**, *260*, 1773.
(13) Jordan, A.; Reichard, P. *Annu. Rev. Biochem.* **1998**, *67*, 71.
(14) Sjöberg, B.-M. *Struct. Bonding* **1997**, *88*, 139.
(15) Stubbe, J.; van der Donk, W. A. *Chem. Rev.* **1998**, *98*, 705.
(16) Nordlund, P.; Sjöberg, B.-M.; Eklund, H. *Nature* **1990**, *345*, 593.
(17) Uhlin, U.; Eklund, H. *Nature* **1994**, *370*, 533.
(18) Eriksson, M.; Uhlin, U.; Ramaswamy, S.; Ekberg, M.; Regnström, K.; Sjöberg, B.-M.; Eklund, H. *Structure* **1997**, *5*, 1077.
(19) Gräslund, A.; Sahlin M. *Annu. Rev. Biophys. Biomol. Struct.* **1996**, *25*, 259.
(20) Sturgeon, B. E.; Burdi, D.; Chen, S.; Huynh, B.-H.; Edmondson, D. E.; Stubbe, J.; Hoffman, B. M. *J. Am. Chem. Soc.* **1996**, *118*, 7551.
(21) Siegbahn, P. E. M. *J. Am. Chem. Soc.* **1998**, *120*, 8417.
(22) Siegbahn, P. E. M.; Blomberg, M. R. A.; Pavlov, M. *Chem. Phys. Lett.* **1998**, *292*, 421.
(23) Siegbahn, P. E. M.; Eriksson, L. A.; Himo, F.; Pavlov, M. *J. Phys. Chem. B* **1998**, *102*, 10622.
(24) Siegbahn, P. E. M. *J. Inorg. Chem.* **1999**, *38*, 2880.
(25) Himo, F.; Siegbahn, P. E. M. *J. Phys. Chem. B* **2000**, *104*, 7502.
(26) Siegbahn, P. E. M. *Chem. Phys. Lett.* **2002**, *351*, 311.
(27) Torrent, M.; Musaev, D. G.; Basch, H.; Morokuma, K. *J. Comput. Chem.* **2002**, *23*, 59.
(28) Stubbe, J. *Biol. Chem.* **1990**, *265*, 5330.
(29) Mao, S. S.; Holler, T. P.; Yu, G. X.; Bollinger, J. M.; Booker, S.; Johnston, M. I.; Stubbe, J. *Biochemistry* **1992**, *31*, 9733.
(30) Zipse, H. *J. Am. Chem. Soc.* **1995**, *117*, 11798.
(31) Stubbe, J. *Adv. Enzymol. Relat. Areas Mol. Biol.* **1990**, *63*, 349.
(32) Beckwith, A. L. J.; Crich, D.; Duggan, P. J.; Yao, Q. *Chem. Rev.* **1997**, *97*, 3273.
(33) Persson, A. L.; Eriksson, M.; Katterle, B.; Pötsch, S.; Sahlin, M.; Sjöberg, B.-M. *J. Biol. Chem.* **1997**, *272*, 31533.
(34) Pelmenschikov, V.; Siegbahn, P. E. M., in preparation.
(35) Cukier, R. I.; Nocera, D. G. *Annu. Rev. Phys. Chem.* **1998**, *49*, 337.
(36) Logan, D.; Andersson, J.; Sjöberg, B.-M.; Nordlund, P. *Science* **1999**, *283*, 1499.
(37) Cho, K.-B.; Himo, F.; Gräslund, A.; Siegbahn, P. E. M. *J. Phys. Chem. B* **2001**, *105*, 6445.
(38) Eklund, H.; Fontecave, M. *Structure* **1999**, *7*, 257.
(39) Andersson, J.; Westman, M.; Sahlin, M.; Sjöberg, B.-M. *J. Biol. Chem.* **2000**, *275*, 19449.
(40) Mulliez, E.; Ollagnier, S.; Fontecave, M.; Eliasson, R.; Reichard, P. *Proc. Natl. Acad. Sci. U.S.A.* **1995**, *92*, 8759.
(41) Liepinsh, E.; Otting, G. *Magn. Reson. Med.* **1996**, *35*, 30.
(42) Cho, K.-B.; Gräslund, A.; Siegbahn, P. E. M., in preparation.
(43) Andersson, J.; Bodevin, S.; Westman, M.; Sahlin, M.; Sjöberg, B.-M. *J. Biol. Chem.* **2001**, *276*, 40457.
(44) Sawers, G. *FEMS Microbiol. Rev.* **1999**, *22*, 543.
(45) Buckel, W.; Golding, B. *FEMS Microbiol. Rev.* **1999**, *22*, 523.
(46) Eklund, H.; Fontecave, M. *Structure* **1999**, *7*, R257.
(47) Knappe, J.; Neugebauer, F. A.; Blaschkowski, H. P.; Gänzler, M. *Proc. Natl. Acad. Sci. U.S.A.* **1984**, *81*, 1332.
(48) Wagner, A. F. V.; Frey, M.; Neugebauer, F. A.; Schafer, W.; Knappe, J. *Proc. Natl. Acad. Sci. U.S.A.* **1992**, *89*, 996.
(49) Sun, X.; Harder, J.; Krook, M.; Sjöberg, B.-M.; Reichard, P.*Proc. Natl. Acad. Sci. U.S.A.* **1993**, *90*, 577.
(50) Mulliez, E.; Fontecave, M.; Gaillard, J.; Reichard, P. *J. Biol. Chem.* **1993**, *268*, 2296.
(51) Sun, X.; Ollaigner, S.; Schmidt, P. P.; Atta, M.; Mulliez, E.; Lepape, L.; Eliasson, R.; Gräslund, A.; Fontecave, M.; Reichard, P.; Sjöberg, B.-M. *J. Biol. Chem.* **1996**, *271*, 6827.
(52) Young, P.; Andersson, J.; Sahlin, M.; Sjöberg, B.-M. *J. Biol. Chem.* **1996**, *271*, 20770.
(53) Krieger, C. J.; Roseboom, W.; Albracht, S. P. J.; Spormann, A. M. *J. Biol. Chem.* **2001**, *276*, 12924.
(54) Wong, K. K.; Kozarich, J. W. In *Metal Ions in Biological Systems, Metalloenzymes Involving Amino Acid-Residue and Related Radicals*, Eds. Sigel, H.; Sigel A.; Marcel Dekker: New York, 1994; Vol. 30, p 279.
(55) Vieche, H. G.; Merenyi, R.; Stella, L.; Zanousek, Z. *Angew. Chem., Int. Ed. Engl.* **1979**, *18*, 917.
(56) Vieche, H. G.; Zanousek, Z.; Merenyi, R.; Stella, L. *Acc. Chem. Res.* **1985**, *18*, 148.
(57) Stella, L.; Harvey, J. N. In *Radicals in Organic Synthesis, Volume 1: Basic Principles*, pp 360−380, Renaud, P., Sibi, M. P., Eds.; Wiley-VCH: New York, 2001.
(58) Armstrong, D. A.; Yu, D.; Rauk, A. *Can. J. Chem.* **1996**, *74*, 1192.
(59) Rauk, A.; Yu, D.; Taylor, J.; Shustov, G. V.; Block, D. A.; Armstrong, D. A. *Biochemistry* **1999**, *38*, 9089.
(60) Himo, F. *Chem. Phys. Lett.* **2000**, *328*, 270.
(61) Himo, F.; Eriksson, L. A. *J. Chem. Soc., Perkin Trans. 2* **1998**, *2*, 305.
(62) Barone, V.; Adamo, C.; Grand, A.; Brunel, Y.; Subra, R. *J. Am. Chem. Soc.* **1995**, *117*, 1083.
(63) Barone, V.; Adamo, C.; Grand, A.; Subra, R. *Chem. Phys. Lett.* **1995**, *242*, 351.
(64) Barone, V.; Adamo, C.; Grand, A.; Jolibois, F.; Brunel, Y.; Subra, R. *J. Am. Chem. Soc.* **1995**, *117*, 12618.
(65) Reddy, S. G.; Wong, K. K.; Parast, C. V.; Peisach, J.; Magliozzo, R. S.; Kozarich, J. W. *Biochemsitry* **1998**, *37*, 558.
(66) Zhang, W.; Wong, K. K.; Magliozzo, R. S.; Kozarich, J. W. *Biochemsitry* **2001**, *40*, 4123.
(67) Gauld, J. W.; Eriksson, L. A. *J. Am. Chem. Soc.* **2000**, *122*, 2035.
(68) Leppänen, V.-M.; Merckel, M. C.; Ollis, D. L.; Wong, K. K.; Kozarich, J. W.; Goldman, A. *Structure* **1999**, *7*, 733.
(69) Becker, A.; Fritz-Wolf, K.; Kabsch, W.; Knappe, J.; Schultz, S.; Wagner, A. F. V. *Nature Struct. Biol.* **1999**, *6*, 969.
(70) Brush, E. J.; Lipsett, K. A.; Kozarich, J. W. *Biochemistry* **1988**, *27*, 2217.
(71) Parast, C. V.; Wong, K. K.; Lewisch, S. A.; Kozarich, J. W.; Peisach, J.; Magliozzo, R. S. *Biochemistry* **1995**, *34*, 4 (8), 2393.
(72) Himo, F. and Eriksson, L. A. *J. Am. Chem. Soc.* **1998**, *120*, 11449.
(73) Leuthner, B.; Leutwein, C.; Schulz, H.; Hörth, P.; Haehnel, W.; Schilz, E.; Schägger, H.; Heider, J. *Mol. Microbiol.* **1998**, *28*, 615.
(74) Beller, H. R.; Spormann, A. M. *FEMS Microbiol. Lett.* **1999**, *178*, 147.
(75) Beller, H. R.; Spormann, A. M. *Appl. Environ. Microbiol.* **1997**, *63*, 3729.
(76) Beller, H. R.; Spormann, A. M. *J. Bacteriol.* **1997**, *179*, 670.
(77) Beller, H. R.; Spormann, A. M. *J. Bacteriol.* **1998**, *180*, 5454.
(78) Coschigano, P. W.; Wehrman, T. S.; Young, L. Y. *Appl. Envirnon. Microbiol.* **1988**, *64*, 1650.

(79) Himo, F. *J. Phys. Chem. B.* **2002**, *106*, 7688.
(80) Herschman, H. R. *Biochim. Biophys. Acta* **1996**, *1299*, 125.
(81) Blomberg, M. I.; Blomberg, M. R. A.; Siegbahn, P. E. M.; van der Donk, W. A.; Tsai, A.-L. *J. Phys. Chem. B* **2003**, *107*, 3297.
(82) Kulmacz, R. J.; et al. *J. Biol. Chem.* **1987**, *262*, 10524.
(83) Karthein, R.; et al. *Eur. J. Biochem.* **1988**, *171*, 313.
(84) Hsi, L. C.; et al. *Biochem. Biophys. Res. Commun.* **1994**, *202*, 1592.
(85) Xiao, G.; et al. *Biochemistry* **1997**, *36*, 1836.
(86) Hamberg, M.; Samuelsson B. *J. Biol. Chem.* **1967**, *242*, 5336.
(87) Malkowski, M. G.; Ginell, S. L.; Smith, W. L.; Garavito, R. M. *Science* **2000**, *289*, 1933.
(88) Picot, D.; Loll, P. J.; Garavito, M. R. *Nature* **1994**, *367*, 243.
(89) Luong, C.; et al. *Nature Struct. Biol.* **1996**, *3*, 927.
(90) Kurumbail, R. G.; Stevens, A. M.; Gierse, J. K, McDonald, J. J.; Stegeman, R. A.; Pak, J. Y.; Gildehaus, D.; Miyashiro, J. M.; Penning, T. D.; Seibert, K.; Isakson, P. C.; Stallings W. C. *Nature* **1996**, *384*, 644.
(91) Bhattacharyya, D. P.; Lecomte, M.; Rieke, C. J.; Garavito, M. R.; Smith, W. L. *J. Biol. Chem.* **1996**, *271*, 2179.
(92) Ludwig, M. L.; Matthews, R. G. *Annu. Rev. Biochem.* **1997**, *66*, 269.
(93) Banerjee, R. *Biochemistry* **2001**, *40*, 6191.
(94) Eggerer, H.; Stadtman, E. R.; Overath, P.; Lynen, F. *Biochem. Z.* **1960**, *333*, 1.
(95) Golding, B. T.; Radom, L. *J. Am. Chem. Soc.* **1976**, *98*, 6331.
(96) Babior, B. M. *Acc. Chem. Res.* **1975**, *8*, 376.
(97) Rétey, J. *Recent Adv. Phytochem.* **1979**, *13*, 1.
(98) Golding, B. T. *B12*; Dolphin, D., Ed.; J. Wiley & Sons: New York, 1982, Vol. 1, p 543.
(99) Finke, R. G.; Schiraldi, D. A.; Mayer, B. J. *Coord. Chem. Rev.* **1984**, *54*, 1.
(100) Halpern, J. *Science* **1985**, *227*, 869.
(101) Hay, B. P.; Finke, R. G. *J. Am. Chem. Soc.* **1986**, *108*, 4820.
(102) Hay, B. P.; Finke, R. G. *J. Am. Chem. Soc.* **1987**, *109*, 8012.
(103) Finke, R. G.; Martin, B. D. *Inorg. Chem.* **1990**, *29*, 19.
(104) Garr, C. D.; Sirovatka, J. M.; Finke, R. G. *J. Am. Chem. Soc.* **1996**, *118*, 11142.
(105) Sirovatka, J. M.; Finke, R. G. *J. Am. Chem. Soc.* **1997**, *119*, 3057.
(106) Hansen, L. M.; Kumar, P. N. V. P.; Marynick, D. S. *Inorg. Chem.* **1994**, *33*, 728.
(107) Hansen, L. M.; Derecskei-Kovacs, A.; Marynick, D. S. *J. Mol. Struct. (THEOCHEM)* **1998**, *431*, 53.
(108) Andruniow, T.; Zgierski, M. Z.; Kozlowski, P. M. *J. Phys. Chem. B* **2000**, *104*, 10921.
(109) Andruniow, T.; Zgierski, M. Z.; Kozlowski, P. M. *Chem. Phys. Lett.* **2000**, *331*, 509.
(110) Andruniow, T.; Zgierski, M. Z.; Kozlowski, P. M. *J. Am. Chem. Soc.* **2001**, *123*, 2679.
(111) Jensen, K. P.; Sauer, S. P. A.; Liljefors T.; Norrby, P.-O. *Organometallics* **2001**, *20*, 550.
(112) Jensen, K. P.; Ryde, U. *J. Mol. Struct. (THEOCHEM)* **2002**, *585*, 239.
(113) Dölker, N.; Maseras, F. Lledós, A. *J. Phys. Chem. B* **2001**, *105*, 7564.
(114) Dölker, N.; Maseras, F. Lledós, A., submitted for publication.
(115) Rovira, C.; Kunc, K.; Hutter, J.; Parinello, M. *Inorg. Chem.* **2001**, *40*, 11.
(116) Kozlowski, P. M. *Curr. Op. Chem. Biol.* **2001**, *5*, 736.
(117) Wetmore, S. D.; Smith, D. M.; Radom, L. *ChemBioChem* **2001**, *2*, 919.
(118) Smith, D. M.; Golding, B. T.; Radom, L. *J. Am. Chem. Soc.* **1999**, *121*, 9388.
(119) Smith, D. M.; Golding, B. T.; Radom, L. *J. Am. Chem. Soc.* **1999**, *121*, 1, 1383.
(120) Beatrix, B.; Zelder, O.; Kroll, F. K.; Orlygsson, G.; Golding, B. T.; Buckel, W. *Angew. Chem., Int. Ed. Engl.* **1995**, *34*, 2398.
(121) Golding, B. T.; Radom, L. *Am. Chem. Soc.* **1976**, *98*, 6331.
(122) Smith, D. M.; Golding, B. T.; Radom, L. *J. Am. Chem. Soc.* **1999**, *121*, 1037.
(123) Wetmore, S. D.; Smith, D. M.; Radom, L. *J. Am. Chem. Soc.* **2001**, *123*, 7963.
(124) Wetmore, S. D.; Smith, D. M.; Radom, L. *J. Am. Chem. Soc.* **2001**, *122*, 10208.
(125) Wetmore, S. D.; Smith, D. M.; Radom, L. *J. Am. Chem. Soc.* **2001**, 123, 8678.
(126) (a) George, P.; Glusker, J. P.; Bock, C. W. *J. Am. Chem. Soc.* **1995**, *117*, 10131. (b) George, P.; Glusker, J. P.; Bock, C. W. *J. Am. Chem. Soc.* **1997**, *119*, 7065.
(127) Smith, D. M.; Golding, B. T.; Radom, L. *J. Am. Chem. Soc.* **1999**, *121*, 5700.
(128) Smith, D. M.; Golding, B. T.; Radom, L. *J. Am. Chem. Soc.* **2001**, *123*, 1664.
(129) George, P.; Siegbahn, P. E. M.; Glusker, J. P.; Bock, C. W. *J. Phys. Chem. B* **1999**, *103*, 7531.
(130) Semialjac, M.; Schwarz, H. *J. Am. Chem. Soc.* **2002**, *124*, 8974.
(131) Barry, B. A.; Babcock, G. T. *Proc. Natl. Acad. Sci. U.S.A.* **1987**, *84*, 7099.
(132) Yachandra, V. K.; Sauer, K.; Klein, M. P. *Chem. Rev.* **1996**, *96*, 2927.
(133) Siegbahn, P. E. M.; Crabtree, R. H. *J. Am. Chem. Soc.* **1999**, *121*, 117.
(134) Zouni, A.; Witt, H.-T.; Kern, J.; Fromme, P.; Krauss, N.; Saenger, W.; Orth, P. *Nature* **2001**, *409*, 739.
(135) Hoganson, C. W.; Lydakis-Simantiris, N.; Tang, X.-S.; Tommos, C.; Warncke, K.; Babcock, G. T.; Diner, B. A.; McCracken, J.; Styring, S. *Photosynth. Res.* **1995**, *46*, 177.
(136) Babcock, G. T. In *Photosynthesis from Light to Biosphere*; Mathis, P., Ed.; Kluwer: Dordrecht, 1995; Vol 2, p 209.
(137) Tommos, C.; Tang, X.-S.; Warncke, K.; Hoganson, C. W.; Styring, S.; McCracken, J.; Diner, B. A.; Babcock, G. T. *J. Am. Chem. Soc.* **1995**, *117*, 10325.
(138) Haumann, M.; Bögershausen, O.; Cherepanov, D.; Ahlbrink, R.; Junge, W. *Photosynth. Res.* **1997**, *51*, 193.
(139) Ahlbrink, R.; Haumann, M.; Cherepanov, D.; Bögershausen, O.; Mulkidjanian, A.; Junge, W. *Biochemistry* **1998**, *37*, 1131.
(140) Haumann, M.; Junge, W. *Biochim. Biophys. Acta* **1999**, *1411*, 86.
(141) Haumann, M.; Mulkidjanian, A.; Junge, W. *Biochemistry* **1999**, *38*, 1258.
(142) Blomberg, M. R. A.; Siegbahn, P. E. M. *Mol. Phys.* **2003**, *101*, 323.
(143) Westphal, K. L.; Tommos, C.; Cukier, R. I.; Babcock, G. T. *Curr. Opinion Plant Biol.* **2000**, *3*, 236.
(144) Styring, S. A.; Rutherford, A. W. *Biochemistry* **1988**, *27*, 4915.
(145) Sharp, R. R. In *Manganese Redox Enzymes*; Pecoraro, V. L., Ed.; VCH: New York, 1992, pp 177−196.
(146) Iuzzolini, L.; Dittmer, J.; Dörner, W.; Meyer-Klaucke, W.; Dau, H. *Biochemistry* **1998**, *37*, 17112.
(147) Siegbahn, P. E. M. *J. Inorg. Chem.* **2000**, *39*, 2923.
(148) Siegbahn, P.E. M. In *Molecular Modeling and Dynamics of Bioinorganic Systems*; Comba, P., Banci, L., Eds.; Kluwer Academic Publishers: Norwell, MA, 1997, pp 233−253.
(149) Siegbahn, P. E. M. *Curr. Opin. Chem. Biol.* **2002**, *6*, 227.
(150) Ito, N.; Phillips, S. E. V.; Stevens, C.; Ogel, Z. B.; McPherson, M. J.; Keen, J. N.; Yadav, K. D. S.; Knowles, P. F. *Nature* **1991**, *350*, 87.
(151) Whittaker, M. M.; Whittaker, J. W. *J. Biol. Chem.* **1988**, *263*, 6074.
(152) Branchaud, B. P.; Montague-Smith, M. P.; Kosman, D. J.; McLaren, F. R. *J. Am. Chem. Soc.* **1993**, *115*, 798.
(153) Whittaker, M. M.; Whittaker, J. W. *Biophys. J.* **1993**, *64*, 762.
(154) Wachter, R. M.; Branchaud, B. P. *J. Am. Chem. Soc.* **1996**, *118*, 2782.
(155) Wachter, R. M.; Branchaud, B. P. *Biochemistry* **1996**, *35*, 14425.
(156) Wachter, R. M.; Montague-Smith, M. P.; Branchaud, B. P. *J. Am. Chem. Soc.* **1997**, *119*, 7743.
(157) Himo, F.; Eriksson, L. A.; Maseras, F.; Siegbahn P. E. M. *J. Am. Chem. Soc.* **2000**, *122*, 8031.
(158) Maseras, F.; Morokuma K. *J. Comput. Chem.* **1995**, *16*, 1170.
(159) Maseras, F. *Top. Organomet. Chem.* **1999**, *4*, 165.
(160) Ujaque, G.; Maseras, F.; Lledos, A. *J. Am. Chem. Soc.* **1999**, *121*, 1317.
(161) Maseras, F.; Eisenstein, O. *New J. Chem.* **1998**, *22*, 5.
(162) a) Wang, Y.; Stack, T. D. P. *J. Am. Chem. Soc.* **1996**, *118*, 13097. (b) Wang, Y.; DuBois, J. L.; Hedman, B.; Hodgson, K. O.; Stack, T. D. P. *Science* **1998**, *279*, 537.
(163) Rothlisberger, U. and Carloni, P. *Int. J. Quantum Chem.* **1999**, *73*, 209.
(164) Wachter, R. M.; Branchaud, B. P. *Biochim. Biophys. Acta* **1998**, *1384*, 43.
(165) Itoh, S.; Hirano, K.; Furuta, A.; Komatsu, M.; Ohshiro, Y.; Ishida, A.; Takamuku, S.; Kohzuma, T.; Nakamura, N.; Suzuki, S. *Chem. Lett.* **1993**, 2099.
(166) Himo, F.; Eriksson, L. A.; Blomberg, M. R. A.; Siegbahn, P. E. M. *Int. J. Quantum Chem.* **2000**, *76*, 714.
(167) Himo, F.; Babcock, G. T.; Eriksson, L. A. *Chem. Phys. Lett.* **1999**, *313*, 374.
(168) Wise, E. W.; Pate, J. B.; Wheeler, R. A. *J. Phys. Chem. B* **1999**, *103*, 4772.
(169) Engström, M.; Himo, F.; Ågren, H. *Chem. Phys. Lett.* **2000**, *319*, 191.
(170) Himo, F.; Noodleman, L.; Blomberg, M. R. A.; Siegbahn, P. E. M. *J. Phys. Chem. A.* **2002**, *106*, 8757.
(171) Klinman, J. P. *Chem. Rev.* **1996**, *96*, 2541.
(172) Li, R.; Chen, L.; Cai, D.; Klinman, J. P.; Mathews, F. S. *Crystallogr., Sect. D* **1997**, *53*, 364.
(173) Prabhakar, R.; Siegbahn, P. E. M., 2003, submitted.
(174) (a) Prabhakar, R.; Siegbahn, P.E. M. *J. Phys. Chem. B* **2001**, *105*, 4400. (b) Prabhakar, R.; Siegbahn, P.E. M. *J. Comput. Chem.* **2003**, in press.
(175) Prabhakar, R.; Siegbahn, P. E. M. *J. Phys. Chem. B* **2003**, in press.
(176) Dooley, D. M. *J. Biol. Inorg. Chem.* **1999**, *4*, 1.
(177) Klinman, J. P.; Mu, D. *Annu. Rev. Biochem.* **1994**, 63, 299.
(178) Hartmann, C.; Klinman, J. P. *Biochemistry* **1991**, *30*, 4605.

(179) Bellelli, A.; Finnazi-Agro, A.; Floris, G.; Brunori, M. J. *J. Biol. Chem.* **1991**, *266*, 20654.
(180) Wilmot, C. M.; Murray, J. M.; Gordon, A.; Parsons, M. R.; Convery, M. A.; Blakeley, V.; Corner, A. S.; Palcic, M. M.; Knowles, P. F.; McPherson, M. J.; Phillips, S. E. V. *Biochemistry* **1997**, *36*, 1608.
(181) Brown, D.E.; McGuirl, M. A.; Dooley, D. M.; Janes, S. M.; Mu, D.; Klinman, J. P. *J. Biol. Chem.* **1991**, *266*, 4049.
(182) Hartmann, C.; Brzovic, P.; Klinman, J. P. *Biochemistry* **1993**, *32*, 2234.
(183) Cai, D.; Dove, J.; Nakamura, N.; Sanders-Loehr, J.; Klinman, J. P. *Biochemistry* **1997**, *36*, 11472.
(184) Klinman, J. P. *J. Biol. Chem.* **1996**, *271*, 27189.
(185) Dooley, D. M.; Cote, C. E.; Golnik, K. C. *J. Mol. Catal.* **1984**, *23*, 243.
(186) Suzuki, S.; Sakurai, T.; Nakahara, A.; Manabe, T.; Okuyama, T. *Biochemistry* **1983**, *22*, 1630.
(187) Dooley, D. M.; McGuirl M. A.; Brown, D. E.; Turowski, P. N.; McIntire, W. S.; Knowles, P. F. *Nature* **1991**, *349*, 262.
(188) Turowski, P. N.; McGuirl M. A.; Dooley, D. M. *J. Biol. Chem.* **1993**, *268*, 17680.
(189) Qiaojuan, S.; Klinman, J. P. *Biochemistry* **1998**, *37*, 12513.
(190) Farnum, M.; Palcic, M. M.; Klinman, J. P. *Biochemistry* **1986**, *25*, 1898.
(191) Mills, S. A.; Klinman, J. P. *J Am Chem Soc.* **2000**, *122*, 9897.
(192) Drummond, J. T.; Matthews, R. G. *Biochemistry* **1994**, *33*, 3732.
(193) Mure, M.; Klinman, J. P. *J. Am. Chem. Soc.* **1993**, *115*, 7117.
(194) Prabhakar, R.; Siegbahn, P. E. M.; Minaev, B. F.; Ågren, H., to be published.
(195) Wirstam, M.; Blomberg, M. R. A.; Siegbahn, P. E. M. *J. Am. Chem. Soc.* **1999**, *121*, 10178.
(196) Finzel, B. C.; Poulus, T. L.; Kraut, J. *J. Biol. Chem.* **1984**, *259*, 13027.
(197) Choudhury, K.; Sundaramoorthy, M.; Mauro, J. M.; Poulus, T. L. *J. Biol. Chem.* **1992**, *267*, 25656.
(198) Erman, J. E.; Vitello, L. B. *J. Am. Chem. Soc.* **1992**, *114*, 6592.
(199) Rodriguez-Lopez, J. N.; Smith, A. T.; Thorneley, R. N. F. *J. Biol. Inorg. Chem.* **1996**, *1*, 136.
(200) Shaik, S.; de Visser, S. P.; Ogliaro, F.; Schwarz, H.; Schröder, D. *Curr. Opin. Chem. Bio.* **2002**, *6*, 556.
(201) Ortiz de Montellano, P. R., Ed. *Cytochrome P450: Structure, Mechanism and Biochemistry*, 2nd ed.; Plenum Press: New York, 1995.
(202) Ogliaro, F.; Harris, N.; Cohen, S.; Filatov, M.; de Visser, S. P.; Shaik, S. *J. Am. Chem. Soc.* **2000**, *122*, 8977.
(203) Harris, N.; Cohen, S.; Filatov, M.; Ogliaro, F.; Shaik, S. *Angew. Chem., Int. Ed.* **2000**, *39*, 2003.
(204) Ogliaro, F.; Cohen, S.; de Visser, S. P.; Shaik, S. *J. Am. Chem. Soc.* **2000**, *122*, 12892.
(205) Ogliaro, F.; Cohen, S.; Filatov, M.; Harris, N.; Shaik, S. *Angew. Chem., Int. Ed.* **2000**, *39*, 3851.
(206) de Visser, S. P.; Ogliaro, F.; Harris, N.; Shaik, S. *J. Am. Chem. Soc.* **2001**, *123*, 3037.
(207) de Visser, S. P.; Ogliaro, F.; Shaik, S. *Chem. Commun.* **2001**, 2322.
(208) de Visser, S. P.; Ogliaro, F.; Shaik, S. *Angew. Chem., Int. Ed.* **2001**, *40*, 2871.
(209) de Visser, S. P.; Ogliaro, F.; Gross, Z.; Shaik, S. *Chem. Eur. J.* **2001**, *7*, 4954.
(210) Ogliaro, F.; de Visser, S. P.; Cohen, S.; Kaneti, J.; Shaik, S. *Chembiochem* **2001**, *3*, 848.
(211) Ogliaro, F.; de Visser, S. P.; Groves, J. T.; Shaik, S. *Angew. Chem., Int. Ed.* **2001**, *40*, 2874.
(212) Ogliaro, F.; de Visser, S. P.; Cohen, S.; Sharma, P. K.; Shaik, S. *J. Am. Chem. Soc.* **2002**, *124*, 2806.
(213) Schoneboom, J. C.; Lin, H.; Reuter, N.; Thiel, W.; Cohen, S.; Ogliaro, F.; Shaik, S. *J. Am. Chem. Soc.* **2002**, *124*, 8142.
(214) Yoshizawa, K.; Kagawa, Y.; Shiota, Y. *J. Phys. Chem. B.* **2000**, *104*, 12365.
(215) (a) Yoshizawa, K.; Kamachi, T.; Shiota, Y. *J. Am. Chem. Soc.* **2001**, *123*, 9806. (b) Kamachi, T.; Yoshizawa, K. *J. Am. Chem. Soc.* **2003**, in press.
(216) Groves, J. T.; McClusky, G. A. *J. Am. Chem. Soc.* **1976**, *98*, 859.
(217) Groves, J. T.; van der Puym M. *J. Am. Chem. Soc.* **1976**, *98*, 5290.
(218) Groves, J. T.; Subramanian, D. V. *J. Am. Chem. Soc.* **1984**, *106*, 2177.
(219) Groves, J. T. *J. Chem. Educ.* **1985**, *62*, 928.
(220) Toy, P. H.; Newcomb, M.; Hollenberg, P. F. *J. Am. Chem. Soc.* **1998**, *120*, 7719.
(221) Siegbahn, P. E. M. *J. Biol. Inorg. Chem.* **2001**, *6*, 27.
(222) Proshlyakov, D. A.; Pressler, M. A.; Babcock, G. T. *Proc. Natl. Acad. Sci. U.S.A.* **1998**, 95, 8020.
(223) Blomberg, M. R. A.; Siegbahn, P. E. M.; Babcock, G. T.; Wikström, M. *J. Inorg. Biochem.* **2000**, *80*, 261.
(224) Blomberg, M. R. A.; Siegbahn, P. E. M.; Babcock, G. T.; Wikström, M. *J. Am. Chem. Soc.* **2000**, *122*, 12848.
(225) Blomberg, M. R. A.; Siegbahn, P. E. M.; Wikström, M. *Inorg. Chem.* **2003**, in press.
(226) Yoshikawa, S.; Shinzawa-Itoh, K.; Nakashima, R.; Yaono, R.; Yamashita, E.; Inoue, N.; Yao, M.; Fei, M. J.; Libeu, C. P.; Mizushima, T.; Yamaguchi, H.; Tomizaki, T.; Tsukihara, T. *Science* **1998**, *280*, 1723.
(227) Ostermeier, C.; Harrenga, A.; Ermler, U.; Michel, H. *Proc. Natl. Acad. Sci. U.S.A.* **1997**, *94*, 10547.
(228) Karpefors, M.; Ädelroth, P.; Namslauer, A.; Zhen, Y.; Brzezinski, P. *Biochemistry* **2000**, *39*, 14664.
(229) Rothlisberger, U.; Carloni, P.; Doclo, K.; Parinello, M. *J. Biol. Inorg. Chem.* **2000**, *5*, 236.
(230) Guallar, V.; Gherman, B. F.; Lippard, S. J.; Friesner, R. A. *Curr. Opin. Chem. Biol.* **2002**, *6*, 236.

CR020436S